

# **B. TECH. PROJECT REPORT**

**On**

## **Design Development and Aerodynamic Analysis of an Ornithopter**

**BY**

**Yash Sarda**



**DEPARTMENT OF MECHANICAL ENGINEERING  
INDIAN INSTITUTE OF TECHNOLOGY INDORE**

**May 2022**



# Design, Development and Aerodynamic Analysis of an Ornithopter

PROJECT REPORT

*Submitted in partial fulfillment of the requirements  
for the award of the degrees*

*of*

**BACHELOR OF TECHNOLOGY**

**in**

**MECHANICAL ENGINEERING**

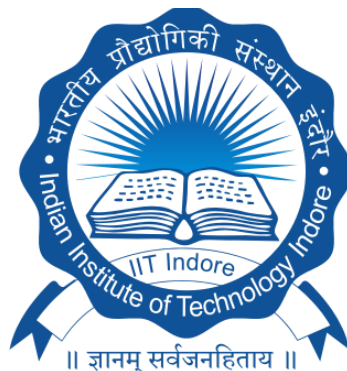
*Submitted by:*

**Yash Sarda**

**Department of Mechanical Engineering**

*Guided by:*

**Dr. Devendra Deshmukh (IIT Indore)**



**INDIAN INSTITUTE OF TECHNOLOGY INDORE**

**May 2022**



## **CANDIDATE’S DECLARATION**

I hereby declare that the project entitled “**Design, Development and Aerodynamic Analysis of an Ornithopter**” submitted in partial fulfillment for the award of the degree of Bachelor of Technology in ‘Mechanical Engineering’ completed under the supervision of **Dr. Devendra Deshmukh**, Associate Professor, Discipline of Mechanical Engineering, IIT Indore is an authentic work.

Further, I declare that I have not submitted this work for the award of any other degree elsewhere.



**Yash Sarda**

**Roll no. 180003066**

---

## **CERTIFICATE by BTP Guide(s)**

It is certified that the above statement made by the students is correct to the best of my/our knowledge.



**Dr. Devendra Deshmukh,**  
**Associate Professor,**  
**Department of Mechanical Engineering,**  
**IIT Indore.**



## **ACKNOWLEDGEMENTS**

I wish to thank Dr. Devendra Deshmukh for his kind support and valuable guidance. He motivated me to pursue the project of my interest and redirected me whenever I got lost. I am really grateful for the opportunities I received under his tutelage.

I would also like to thank members of Spray and Combustion Lab for their constant guidance and suggestions, especially Mr. Arpit Joglekar and Mr. Devashish Chorey. Without their support this report would not have been possible.

I am also thankful for facilities provided by Discipline of Mechanical Engineering, IIT Indore, at each step.

**Yash Sarda**

B.Tech. IV Year

Discipline of Mechanical Engineering

IIT Indore



## **PREFACE**

This report on ‘Design, Development and Aerodynamic Analysis of an Ornithopter’ is prepared under the guidance of Dr. Devendra Deshmukh.

Through this report, I have attempted to explain the design and analysis of a large scale Ornithopter that I built during my senior year at IIT Indore. This report aims to elaborate the design and development process of special class of vehicles called Ornithopters. This involves three major aspects; flapping mechanisms, mechanical design and manufacturing, and derivation of mathematical model of flapping flight. All three aspects are explained in detailed manner. Some problems encountered in manufacturing are also given, along with possible alternatives. The Ornithopter model designed in this report has provision for implementing a control system. While main objective of my work was developing a working prototype of an ornithopter, the project can be continued in various dimensions as explained at the end of the report.

Through this thesis, efforts have been made to present the methodology, experimental results and conclusions of the study in a lucid and comprehensible manner through this report. Figures, charts, CAD models and tables have been included to make the reading easier. This report can serve as a guidebook for all those who wish to develop their own ornithopter.

**Yash Sarda**  
**B.Tech. IV Year**  
**Department of Mechanical Engineering**  
**IIT Indore**



## **ABSTRACT**

In recent years the theme of flying vehicles propelled by flapping wings, often known as ornithopters, has attracted researchers because of its various applications in surveillance, monitoring and transport. Even with state-of-the-art FAVs (Flapping Aerial Vehicles), we are far away from achieving control and manoeuvrability of real insects and birds. Understanding the aerodynamics of flapping flight and structural patterns of birds' wings is essential for developing robust and high-performance flapping-wing aerial robots.

The objective for this project is to design an ornithopter from scratch. Complete development procedure is described in the report so that the final product can be replicated easily. The development process includes analysis and evaluation of flapping mechanisms, theoretical model of flapping flight and prototype design.

Forces and moments due to some critical unsteady aerodynamic mechanisms as well as static and dynamic stability of aircraft are studied to derive the vehicle's equations of motion under the symmetric flapping assumption. The aerodynamic model should accommodate most types of flapping mechanisms encountered in literature with slight modification in the code.

The Ornithopter's design focuses on increasing its kinematic similarity to an actual bird by evaluating the feasibility and effectiveness of several flapping mechanisms. For this purpose, makeshift prototypes were made. The overall evaluation of the mechanism is based on ease of manufacturing, compactness, its bilateral symmetry, and kinematics involved with it.

**Keywords:** Ornithopter, Flapping Flight, Mechanical Design, Aerodynamics



# Table of Contents

Candidate’s Declaration	i
Supervisor’s Certificate	i
Acknowledgement	iii
Preface	v
Abstract	vii
List of Figures	xi
List of Tables	xv

## **Chapter 1. Introduction**

1.1 Flapping Flight.....	1
1.2 Ornithopters.....	2
1.3 Thesis Overview.....	3

## **Chapter 2. Literature Review**

2.1 Flapping Mechanisms.....	5
2.2 Previously Designed models.....	8
2.3 Aerodynamics of flapping flight.....	9
2.4 Adopted results.....	12

## **Chapter 3. Flapping Mechanisms**

3.1 Wing Kinematics of birds.....	13
3.2 Procedure of Selection.....	16
3.3 Single Crank Mechanism.....	19
3.4 Dual Shaft Mechanism.....	24
3.5 Dual Crank Mechanism.....	26
3.6 Summary of observations.....	30

## **Chapter 4. Mechanical Design and Analysis**

4.1 Preliminary design.....	31
4.2 Specifics of Dual crank Mechanism.....	34
4.3 Gearbox design.....	35
4.4 Wings.....	39

4.5 Tail Mechanism.....	39
4.6 Overall Weight estimation.....	40
<b>Chapter 5. Construction and Assembly</b>	
5.1 Gearbox.....	41
5.2 Wings.....	44
5.3 Tail Assembly.....	46
5.4 Complete Model.....	47
<b>Chapter 6. Electronics</b>	
6.1 Actuators.....	49
6.2 Electronic Speed controller (ESC).....	50
6.3 Power Supply.....	51
6.4 Computer (Arduino Nano).....	52
6.5 Inertial measurement unit (MPU6050).....	52
6.6 Radio communications.....	53
6.7 Manual system.....	54
6.8 Automatic system.....	54
<b>Chapter 7. Aerodynamic model of flapping flight</b>	
7.1 Definitions and Nomenclature.....	56
7.2 Mathematical Model.....	56
7.3 Simulink model.....	60
7.4 Simulation Results.....	66
<b>Chapter 8. Results &amp; Discussions</b>	
<b>Chapter 9. Conclusion &amp; scope for Further Investigations</b>	
9.1 Future Scope.....	73
9.2 Applications.....	74
9.3 Conclusion.....	74

References

# List of Figures

Figure 1.1: Wingtip paths relative to body for variety of flyers indicated by arrows. .....	1
Figure 1.2: Various Ornithopter Models ( <a href="#">Link1</a> , <a href="#">Link2</a> , <a href="#">Link3</a> , <a href="#">Link4</a> ) .....	2
Figure 2.1: elevation-depression: Flapping motion; pronation-supination: Pitching motion.....	5
Figure 2.2: (d) and (e) only flapping motion, (f) flapping and pitching motion, (g) flapping and folding motion.....	6
Figure 2.3: (a) only flapping motion; (g) flapping and folding motion.....	7
Figure 2.4: A: Leading Edge Suction; B: Flow separation and reattachment.....	10
Figure 2.5: Size of flyers vs Reynolds Number.....	12
Figure 3.1: Structural similarity between bird wing (a) and human arm (b).....	13
Figure 3.2: Wing motions of a bird.....	14
Figure 3.3: Graphs of Flapping Angle, folding angle and lead-lag angle.....	15
Figure 3.4: Four bar mechanism.....	17
Figure 3.5: Range of flapping angle.....	18
Figure 3.6: Single Crank mechanism test model.....	20
Figure 3.7: Linkage Simulation.....	20
Figure 3.8: Graphs of Kinematic Parameters: Single Crank Mechanism.....	22
Figure 3.9: Asymmetry in flapping angles of Single Crank Mechanism.....	23
Figure 3.10: Various Four-bar flapping mechanisms.....	23
Figure 3.11: Dual Shaft mechanism test model.....	24
Figure 3.12: Solidworks Simulation.....	24
Figure 3.13: Dual Crank mechanism test model.....	26
Figure 3.14: Solution of optimization problem: Dual Crank Mechanism.....	26
Figure 3.15: Graphs of Kinematic Parameters: Dual Crank Mechanism.....	28
Figure 3.16: Six bar mechanism: Flapping + Folding Motion.....	29
Figure 4.1: Aspect Ratio and Wing loading of various birds.....	32
Figure 4.2: Opensource Ornithopter Design ( <a href="#">Link5</a> ).....	33
Figure 4.3: Terminal Position of flapping Mechanism.....	34

Figure 4.4: Linkage software model.....	35
Figure 4.5: Gears.....	36
Figure 4.6: Gear Train.....	37
Figure 4.7: Variables of the mechanism.....	38
Figure 4.8: Tail mechanism.....	40
Figure 4.9: Solidworks Mass Properties.....	40
Figure 5.1: Mounting1: Isometric View, Front View, Side View.....	41
Figure 5.2: Mounting2: Isometric View, Front View, Side View.....	42
Figure 5.3: Mounting3: Isometric View, Front View, Side View.....	42
Figure 5.4: Complete Gear assembly.....	43
Figure 5.5: compound gear assembled through square shaft.....	44
Figure 5.6: Dimensions of the wing.....	45
Figure 5.7: CAD Model and assembly of wingspar.....	45
Figure 5.8: finely knit cotton fabric vs polythene plastic.....	46
Figure 5.9: Tail Assembly.....	47
Figure 5.10: Complete CAD model.....	47
Figure 5.11: Completed Ornithopter.....	48
Figure 6.1: Tower Pro SG90 servo and BLDC motor.....	50
Figure 6.2: Simonk 30A.....	50
Figure 6.3: Bonka Ultra Light U2 Series Lipo Battery.....	51
Figure 6.4: Arduino nano V3.0.....	52
Figure 6.5: MPU6050.....	52
Figure 6.6: Radio Frequency Modules.....	53
Figure 6.7: Manual System.....	54
Figure 6.8: Schematic of automatic system.....	54
Figure 7.1: Frame of references used in aircraft dynamics.....	55
Figure 7.2: Frames of Reference.....	57
Figure 7.3: 3-2-1 convention of Euler angles.....	58
Figure 7.4: Convention for Tail angles.....	59
Figure 7.5: Simulink Model.....	60
Figure 7.6: Definition of flapping angle.....	60

Figure 7.7: Definition of pitching angle.....	61
Figure 7.8: Tail Angles.....	62
Figure 7.9: Modified Strip theory: breaking wing into chordwise elements.....	63
Figure 7.10: Forces on Airfoil.....	63
Figure 7.11: NACA 0012 Aerodynamic Coefficients ( <a href="#">Link6</a> ).....	64
()	
Figure 7.12: Total Force and Moment at Centre of Mass (CoM).....	65
Figure 7.13: Gliding angles and different control parameters.....	67
Figure 7.14: Safe zone charts.....	67
Figure 7.15: Snippets of video simulation.....	68

Link1: <https://robots.ieee.org/robots/smartbird/Photos/SD/smartbird-photo1-full.jpg>

Link2:<https://3dprint.com/wp-content/uploads/2014/08/robirds.png>

Link3:<https://www.youtube.com/watch?v=OfwX6X4Nx20>

Link4:[https://www.festo.com/media/cms/central/media/editorial/img/cc/bionics-bionicswift-00249-festo\\_h820.webp](https://www.festo.com/media/cms/central/media/editorial/img/cc/bionics-bionicswift-00249-festo_h820.webp)

Link5:<https://content.instructables.com/ORIG/F85/20IB/JUCY84HC/F8520IBJUCY84HC.png>

Link6:<https://www.researchgate.net/publication/273218999/figure/fig1/AS:393455999176707@1470818628612/NACA-0012-polar-for-360-deg-incidence-range-So-it-is-proposed-that-the-lift-coefficient.png>



# List of Tables

Table 2.1: Pros and Cons of four-bar flapping mechanisms.....	7
Table 3.1: Four-bar linkage configurations.....	19
Table 3.2: Optimisation Problem conditions: Single Crank Mechanism.....	21
Table 3.3: Specification of makeshift dual shaft mechanism.....	25
Table 3.4: Optimisation Problem conditions: Dual Crank Mechanism.....	27
Table 3.5: Summary of observations.....	30
Table 4.1: Preliminary Design Parameters.....	34
Table 4.2: Reduction Ratios.....	36
Table 4.3: Possible Gear Ratios.....	37
Table 6.1: Servo and Motor specifications.....	49
Table 7.1: Important terms and their definitions.....	56
Table 7.2: Model Specific Parameters.....	66
Table 8.1: Summary of results of chapter 3.....	71



# Chapter 1

## Introduction

### 1.1 Flapping Flight

Natural fliers like birds and insects have captivated the human minds through history. The ease and grace with which they move in the air significantly surpasses the state of the art in aircraft and their control systems. Flapping flight is more complicated than flight with fixed wings because of the structural movement and the resulting unsteady fluid dynamics. The main aerodynamic difference between birds and fixed-wing aircraft is that the birds do not have separate actuators to produce thrust. Their wings must produce both the lift and the thrust required to sustain the flight.

In general, wing kinematics of birds involve tucking in the wing on the upstroke, instantaneously changing the airfoil camber, and using non-sinusoidal, stroke patterns such as carving out a figure-of-eight pattern with the wing tip. These motions modify the air flow around wings to generate lift and thrust. Researchers have been able to identify few of these aerodynamic effects, yet we are far from completely understanding those phenomena. Hence, the development of comprehensive aerodynamic theory for flapping still remains an outstanding research problem in aerospace engineering.

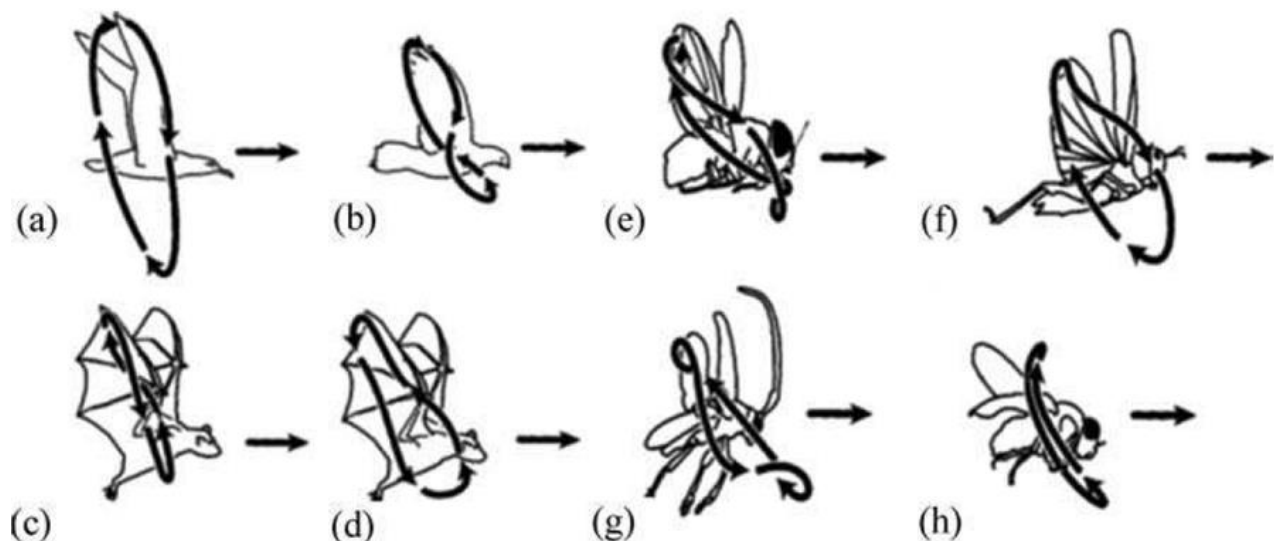


Figure 1.1: Wingtip paths relative to body for variety of flyers indicated by arrows.[1]

- (a) albatross, fast gait; (b) pigeon, slow gait; (c) horseshoe bat, fast flight; (d) horseshoe bat, slow gait;  
(e) blowfly; (f) locust; (g) June beetle; (h) fruitfly

## 1.2 Ornithopters

As demonstrated by birds and insects, flapping wings offer potential advantages in manoeuvrability and energy savings compared with fixed-wing aircraft, as well as potentially vertical take-off and landing. In recent years the subject of flying vehicles propelled by flapping wings, also known as ornithopters has been popular among researchers because of its varied applications in Surveillance, Environmental monitoring, search and rescue missions and transport. Many models have been designed by researchers and hobbyist with novelties in different areas such as mechanical design, material, electronics and control system as well as power source which are being used for different purposes. For example, Festo Smartbird [2] has implemented active wing morphing and it is capable of take-off and land without assist. Aerium's Robird [3] is focused on biomimicry. It imitates the hawk and currently being used on airports to scare away flocks of birds on runways. Bionic swift by Festo [4] uses artificial feathers in their novel wing design. Also, few models based on bats are fabricated in research organisations. Caltech's bat robot B2 [5] and Brown University's Ro-bat [6] constructed novel mechanism with more degrees of freedom. Another example in line is Festo's Flying Fox [4]. These advances in ornithopter research shows its potential for futuristic applications.

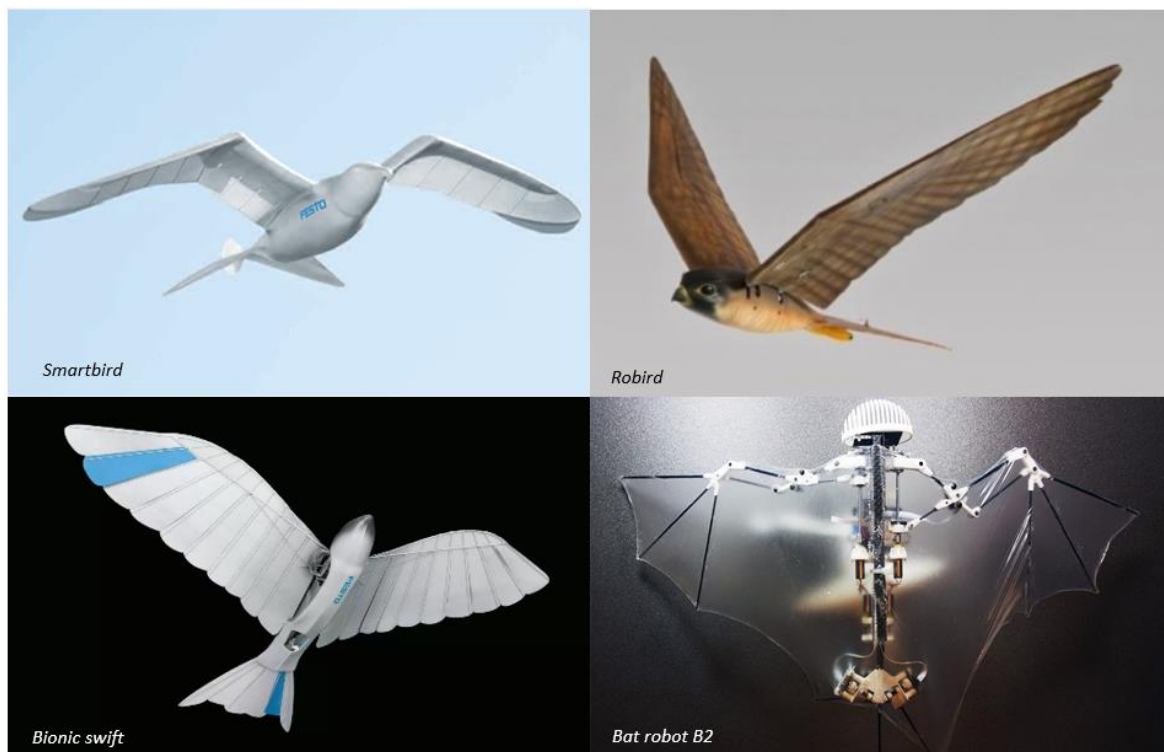


Figure 1.2: Various Ornithopter Models.

Ornithopter based products designed for specific purpose like surveillance or biomimicry are becoming popular. The need to develop a basic ornithopter model is essential for research in various areas such as control and aerodynamics, and also for commercial product development. There are very few opensource ornithopters models available today. Many of them do not describe the development process nor do they provide detailed instructions to replicate them. For these reasons, the main motive behind this project is to elaborate design and development of a large scale ornithopter including detailed analysis of mechanisms, aerodynamic models and construction procedure.

The main objective is to design a working prototype of a large scale ornithopter. Other supplementary objectives would be to create basic aerodynamic model of flapping flight, reviewing literature and previously built ornithopters and analysing various flapping mechanisms. Also, the observations and experimental findings will be reported to provide insight to the reader.

### **1.3 Thesis Overview**

This thesis is organized in multiple chapters, each chapter having its own objectives and conclusions.

#### ***Chapter 2 Literature Review***

The Literature review is divided into three different sections: flapping mechanisms, previously built models and the aerodynamics of flapping flight.

#### ***Chapter 3 Flapping Mechanisms***

This chapter elaborates on kinematics of birds' wings. Three flapping mechanisms were analysed and the best one was selected for implementation in the final model.

#### ***Chapter 4 Design and analysis***

Preliminary design parameters of the final prototype are determined in this section. Design of gearbox is explained in depth and dimensions of overall design are described.

#### ***Chapter 5 Construction and Assembly***

This chapter presents the selection of material and manufacturing method for several designed parts. The assembling process along with CAD models are given in this section.

### ***Chapter 6 Electronics***

Electronic system of ornithopter, reasoning behind choosing specifications of electronic components and alternatives are discussed in this chapter.

### ***Chapter 7 Aerodynamic model and simulations***

This chapter presents mathematical model of flapping flight along with its implementation in Simulink. The results of simulation and observations are explained.

### ***Chapter 8 Results and Discussion***

This chapter summarises the previous chapters' work and lists the obtained results.

### ***Chapter 9 Conclusions and scope for further investigations***

Scope of future research stemming from this report is given. Along with this application of the ornithopters are discussed.

## Chapter 2

# Literature Review

The Literature review is divided into three different sections: flapping mechanisms, previously built models and the aerodynamics of flapping flight. The literature referred here includes research papers, thesis, engineering reports, patents as well as some documentaries or infographics from YouTube. At the end, a summary of results which we will directly adopt from literature is given.

### 2.1 Flapping Mechanisms

To begin the review of mechanisms, firstly we need to understand the motion of birds' wings. The birds' wing kinematics are generally classified into four types of motion from an ornithopter engineer's point of view. These motions are flapping, pitching, lead-lag (or sometimes referred as fore and aft motion of the wing) and folding motion. Different literature sources have used their own terminology, yet there is significant similarity in their classification of wing kinematics. For example, the effects of phase difference between flapping motion and pitching motion are described in [7]. In [8], the kinematic data of three large scale birds (seagull, goose and crane) was described by simple two-jointed arm model using three characteristic angles corresponding to flapping, folding and lead-lag motion. [9] defined the flapping motion in more general sense by introducing a new parameter called stroke plane angle. Except lead-lag, we can see all the motions given in this reference.

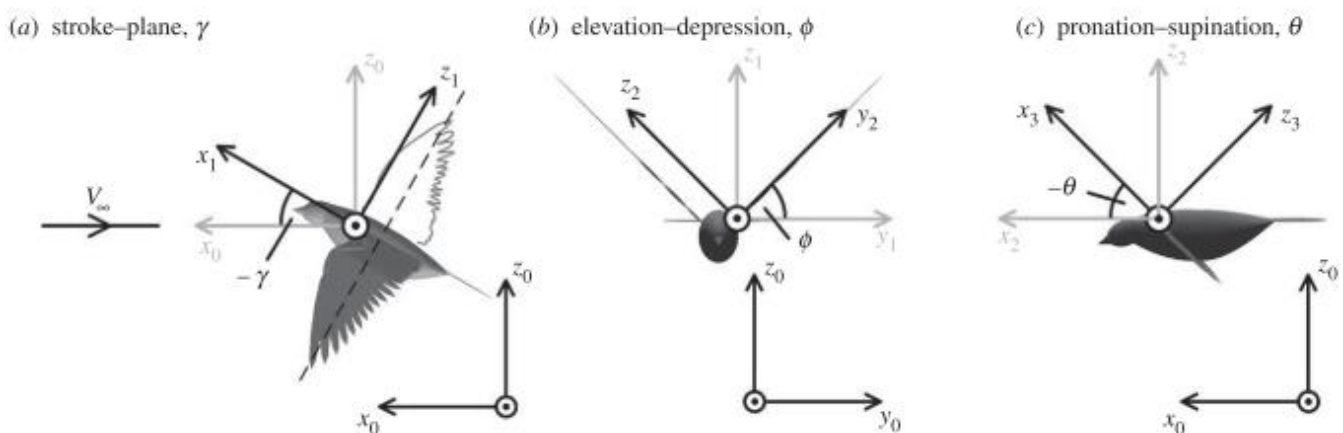


Figure 2.1: elevation-depression : Flapping motion; pronation-supination: Pitching motion [9]

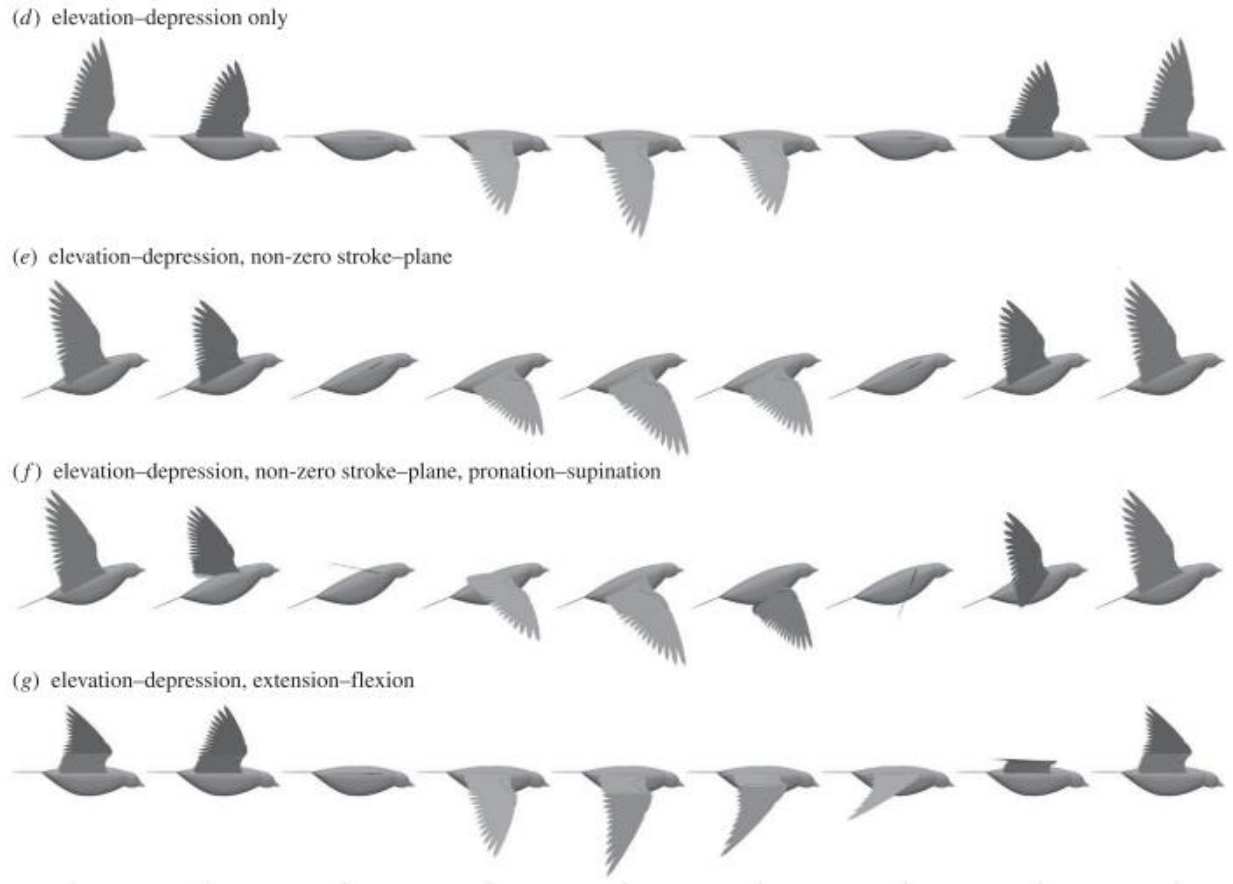


Figure 2.2: (d) and (e) only flapping motion, (f) flapping and pitching motion, (g) flapping and folding motion. [9]

The flapping, lead-lag and pitching motions are experimentally verified in [10] via motion capture technique that tracks the position of retroreflective markers place on wing of an model ornithopter. The kinematic data acquired in this paper, provides justification for assuming above classification.

The next part is reviewing the mechanisms which are built for imitating above motions. [11] has presented an excellent review on mechanisms which could imitate flapping motion. The five mechanisms presented in this paper (figure 3.10) are analysed on various grounds such as kinematics, dynamics, flapping symmetry and manufacturability. According to this paper, the conditions required for smooth operation of a four-bar mechanism includes that transmission angle should be around  $90^{\circ}$  and coupler motion should be near harmonic. The conclusions about four-bar mechanism from this study are given in Table 2.1.

Mechanism Type	Advantages	Drawbacks
Single crank	Simplest and lightest	Neither completely symmetrical nor harmonic flapping wing motion
Single crank with offset	Simple, light weight, symmetrical motion, and little phase difference between the flapping of the two half wings	Crossing each other of the rockers when they are in the same vertical plane
Slider crank	Symmetrical flapping motion	Frictional losses and difficulty in fabrication
Double crank	Symmetrical flapping motion	Complexity, high weight, and out of phase motion
Alternate configuration	Providing the same flapping motion	Cannot be used by biplane flapping wing, and non-symmetrical shape

Table 2.1: Pros and Cons of four-bar flapping mechanisms [11]

[12] and [13] have discussed the problem of asymmetric flapping in single crank mechanism. Even though, this mechanism can never achieve the ideal symmetric flapping, it was shown that optimum condition can be reached where the slight asymmetry in motion can be compensated by the simple and lightweight design of this particular mechanism. [14] presents flapping mechanisms of three existing successful flapping wing MAVs with hovering and actively stable flight performances. These mechanisms were designed due to problems like desynchronized motion of both wings, less mechanical efficiency, insufficient flapping amplitude to generate lift and lack of symmetry in mass distribution of mechanism leading to unequal loading on wings occurring in traditional four-bar mechanisms. [15] introduced a novel six-bar mechanism which could perform three modes of motion: flapping, lead-lag and pitching. Even though this mechanism is controlled by a single actuator, the overall mechanism is too bulky. For the implementing folding motion, usually four-bar mechanism is modified by adding two extra links which couples the flapping and folding motion together. This concept was implemented in Festo's Smartbird [2] and also used in [16], [17] and [18]. This concept is illustrated in figure 3.3.

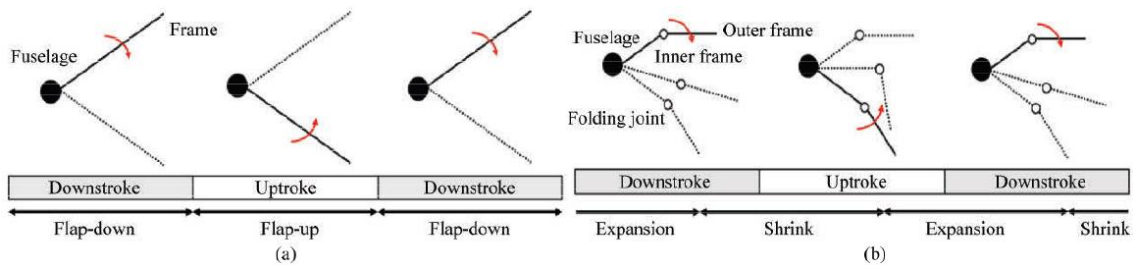


Figure 3.3: (a) only flapping motion; (g) flapping and folding motion [16]

## 2.2 Previously Designed models

This section of literature review, highlights few successful benchmark ornithopter models which are still being referred by ornithopter research community. The reference data and insights provided by those models is used in next chapters.

Phoenix model from Massachusetts Institute of Technology was developed by Zachary John Jackowski [19] and it was inspired from the commercially available model Kestrel [20]. The thesis describes the development process of Phoenix and reasoning behind determining preliminary design parameters such as wingspan, overall mass, etc. Phoenix was designed for carrying payload of sensors and electronics. So, it was made much more durable and sturdier. It uses dual shaft mechanism which is described in following chapters.

The Festo's Smartbird and bionic swift are two ornithopters developed by its Bionic Learning Network division [4]. The bionic swift has mimicked the wings of actual birds as closely as possible. It uses ultralight foam feathers which are connected to a carbon quill, joined to the actual hand and arm wings as in the natural model. During the wing upstroke, the individual lamellae fan out so that air can flow through the wing. This means that the birds need less force to pull the wing up. During the downstroke, the lamellae close up so that the birds can generate more power to fly. Due to this close-to-nature replica of the wings, the Bionic Swifts have a better flight profile than previous wing-beating drives.

Smartbird is an ultralight but powerful flight model with exceptional aerodynamic qualities and agility. This ornithopter, which is inspired by the herring gull, can start, fly and land autonomously – with no additional drive mechanism. Its wings not only beat up and down, but also twist at specific angles. So along with flapping motion it can also actively control pitching motion. This is made possible by an active articulated torsional drive, which in conjunction with a complex control system makes for unprecedented flying efficiency.

The commercially available model called Robird [3] is being used to scare away the birds from different scenarios. Robird is AERIUM's proprietary Wildlife Management and bird-strike mitigation tool. This model is based on predatory bird species so it can act as a scarecrow. The tail mechanism of Robird consist of split tail, where each left and right parts are controlled independently by servos. More information about these models can be found on (<https://www.youtube.com/watch?v=w6VLzKACnS8>).

By examining real feathers, the Stanford researchers discovered that adjacent feathers stick to each other to resist sliding in one direction only using micron-scale features that the researchers describe as “directional Velcro”. This concept is referred while creating the PigeonBot [21]. With the real feathers elastically connected to a pair of robotic bird wings with wrist and finger joints that can be actuated individually, PigeonBot relies on its biohybrid systems for manoeuvrings, while thrust and a bit of additional stabilizing control comes from a propeller and a conventional tail. The interesting point mentioned in the article is that PigeonBot’s roll could be controlled with just the movement of the finger joint on the wing, and that this technique is inherently much more stable than the aileron roll used by conventional aircraft.

The bat bot B2, developed by researchers at Caltech and the University of Illinois at Urbana-Champaign (UIUC) has very complex driving mechanism which is used for altering its wing shape by flexing, extending, and twisting at its shoulders, elbows, wrists, and legs. It weighs only 93 grams and has approximate wingspan of 1 foot. The researchers have used a special elastic, 56 microns thick, silicon membrane for the wings to match the morphology of the bat. More about this model can be found in [5] .

### **2.3 Aerodynamics of flapping flight**

Various aerodynamic theories and models were given to mathematically explain the flapping flight. This includes modified strip theory, lifting line theory, blade element theory etc. the most influential aerodynamic model was given by professor Delaurier in in 1993 [22] which is still being used today. This designed oriented model is has been developed using modified strip theory (MST) approach. The given model assumed high aspect ratio for the wing, an requirement of modified strip theory and the finite span unsteady-wake effects are accounted for by modified Theodorsen functions. Partial leading-edge suction and effects of camber of wing were also include in this model. Stall modelling is done by combining two sets of equations. When the attached flow range is exceeded or in the post-stall range, totally separated flow is assumed to abruptly occur, for which all chordwise aerodynamic forces area modelled as negligible.

Various aerodynamic effects have been explained in [1], [23]–[28] and their precedents. Few effects are more profound in case of insect flight; however, these effects can be applied to bird flight if the dimensionless parameters are in appropriate range. These effects are discussed below:

### ***Leading Edge Suction:***

As the wing increases its angle of attack, the fluid stream passing over the wing separates as it crosses the leading edge but rejoins before reaching the trailing edge. In such instances, a leading-edge vortex occupies the separation zone above the wing. Because the flow reattaches, the fluid continues to flow smoothly from the trailing edge and the Kutta condition is maintained. Because the wing is translating at a high angle of attack, the fluid is given more downward motion, resulting in a significant increase in lift. As shown in figure 2.4 (left), The dark blue arrow represents the leading edge suction force.

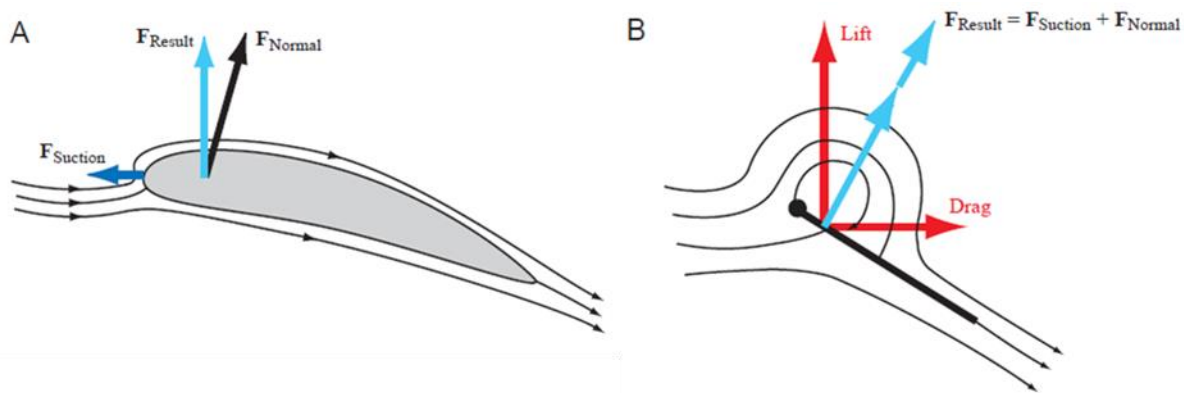


Figure 2.4: A: Leading Edge Suction; B: Flow separation and reattachment [23]

### ***Added mass effect:***

The added mass effect is a non-circulatory contribution related to the acceleration of the wing. Because of this acceleration, the air around the wing is pushed or pulled creating a pressure difference around the wings. The suction created behind the wing is low pressure zone whereas the pushing surface creates high pressure zone. To account for this extra force, we include the mass of the air in the mass of wing.

### ***Rotational Forces:***

When a flapping wing rotates span-wise (pitching motion) while translating at the same time, fluid flow around the wing deviates from the Kutta condition and the stagnation region moves away from the trailing edge. This initiates a sharp, dynamic gradient at the trailing edge, leading to shear. Resistance occurs due to fluid viscosity, and additional circulation must be generated around the wing to re-establish the Kutta condition at the trailing edge. That is, the wing generates

a rotational circulation in the fluid to counteract the effects of rotation. The re-establishment of Kutta condition is not immediate, and requires a finite amount of time. If, in this time, the wing continues to rotate rapidly, then the Kutta condition may never be actually observed at any given instant of time during the rotation but the tendency of the fluid to counteract the rotation nevertheless causes the extra circulation. Thus, the extra circulation proportional to the angular velocity of rotation continues to be generated until smooth, tangential flow can be established at the trailing edge. Depending on the direction of rotation, this additional circulation causes rotational forces that either add to or subtract from the net force due to translation. This effect is also often called the ‘Kramer effect’.

### ***Wake Capture:***

During the flapping motion of wings, sometimes vortices may form if the flow is not laminar. Due to complex kinematics of the wing, it may hit its own wake and capture its energy; thus, resulting in greater lift, called wake capture. The details can be found in the literature related to insect flapping. The effect of wake capture is very difficult to model analytically and is generally neglected during modelling process.

Nondimensional parameters can define the type of flapping flight and the relative contribution of various aerodynamic effects presented above. These numbers are explained below from [28].

The Strouhal number, defined as  $St = Af/U$ , represents the ratio of the amplitude, A, to the distance travelled in one stroke (the forward velocity, U, divided by the frequency, f). A bird operating at a high  $St$  would have a very large amplitude or a fast frequency compared to its forward velocity.  $St$  can be also thought of as the non-dimensional amplitude. In the study of natural flyers and swimmers in cruising condition it is found that the Strouhal number, is often within a narrow region of  $0.2 < St < 0.4$ . [1]

The reduced frequency, defined as  $k = \pi f / U$ , gives the ratio between the chord length, and the distance travelled in one stroke, independent of flapping amplitude. Hence it can determine the relative influence of unsteady vortex wake.  $k$  can be thought of as the non-dimensional flapping frequency. [1] suggests that, in fast forward flight, the reduced frequency and the tend to be low, whereas in slow forward flight, reduced frequency tend to be high, resulting in highly unsteady flow structures.

The Reynolds number is the ratio of inertial forces to viscous forces within a fluid. Given reference length  $L_{ref}$  and reference velocity  $U_{ref}$ , Reynolds number is defined as

$$Re = \frac{U_{ref} L_{ref}}{\nu}$$

Where  $\nu$  is kinematic viscosity.

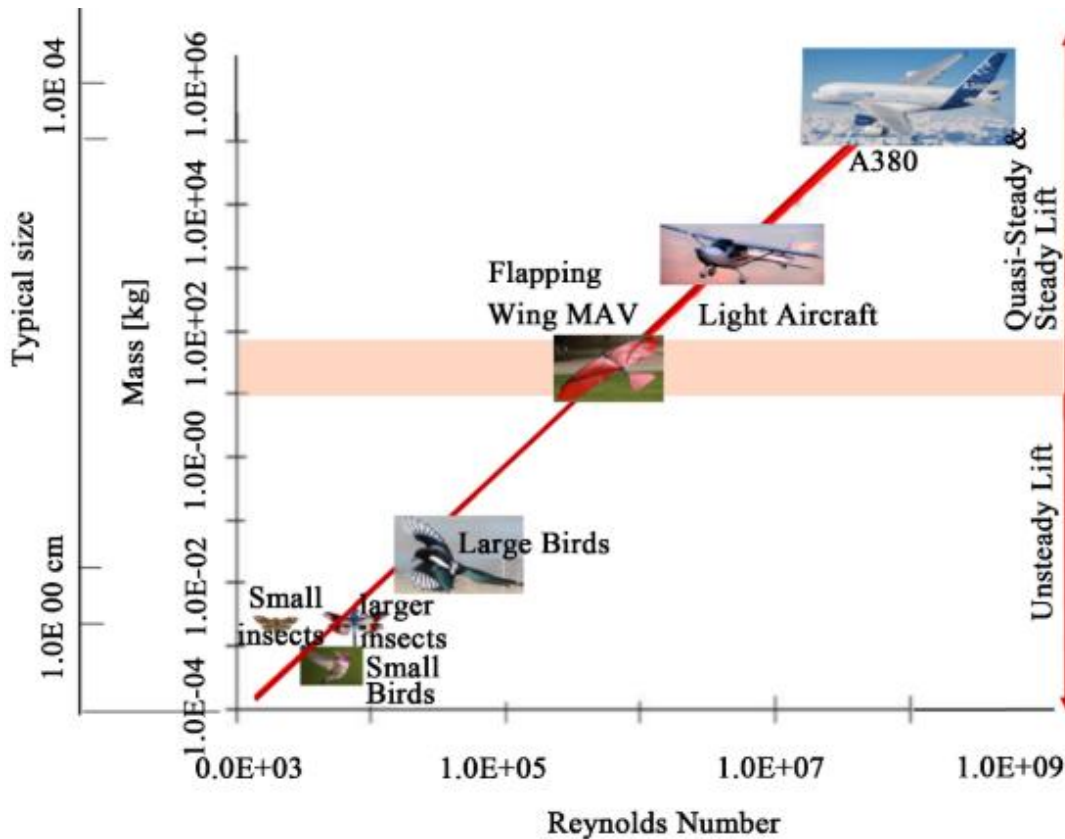


Figure 2.5: Size of flyers vs Reynolds Number [26]

## 2.4 Adopted results

Following results are directly adopted from literature:

- 1) The transmission angle in four-bar flapping mechanism should be around  $90^\circ$  for smooth operation. [11]
- 2) The flapping and pitching motion are generally out of phase. [29]
- 3) In general, increase in flapping amplitude implies increase in lift.[16]
- 4) At high angle of attacks, the aerodynamic coefficients are modelled proportional to  $\sin 2\alpha$  instead of  $\sin \alpha$ . This is generally seen in insect flight dynamics.[30],[25]

## Chapter 3

# Flapping Mechanisms

### 3.1 Wing Kinematics of birds

While flapping, birds systematically twist, extend and deform their wings to produce multiple aerodynamic effects, which contribute to their ultimate manoeuvrability. For a bird to be able to deform and twist its wings, an adaptation in the skeletal and muscular systems is required. The key features that seem desirable are modification of camber and flexing of the wing planform between upstroke and downstroke, twisting, area expansion and contraction, and transverse bending [1]. To perform these functions, birds have a bone structure in their wings similar to the one in a human arm as shown in figure 3.1.

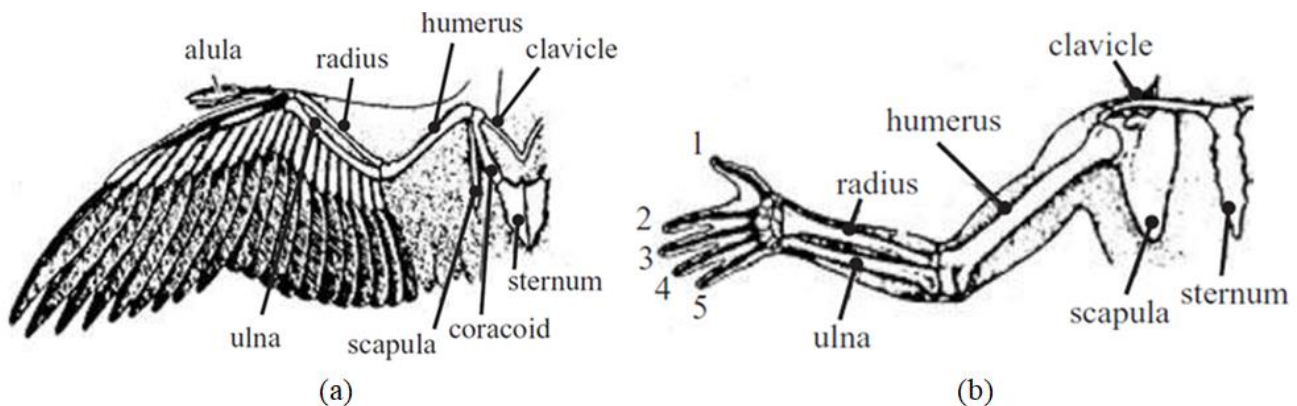


Figure 3.1: Structural similarity between bird wing (a) and human arm (b)[1]

The wing movements of birds are very complex. Directly imitation of these movements would lead to complex, heavy mechanisms. Therefore, before starting designing process, we need simplify and approximately quantify these motions. From previous studies [9], [7] and [17], we can model overall movement of the wing in four different motions as shown in figure 3.2:

- a) **Flapping Motion:** is up and down plunging motion of the wing about root chord.
- b) **Pitching Motion:** is the pitching motion of wing and can vary along the span.
- c) **Lead-lag Motion:** (or fore-and-aft oscillation), which is in-plane lateral movement of wing.

d) **Folding Motion**: which is commonly shown by large birds, is bending motion of wing planform.

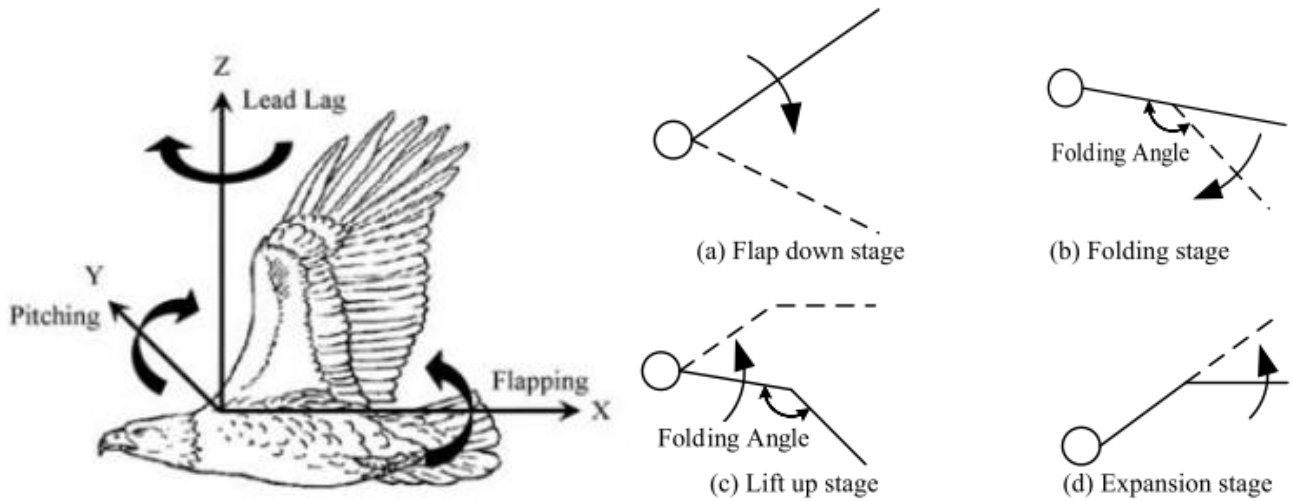


Figure 3.2: Wing motions of a bird [17][7]

Each of these motions contribute for generating lift according to [28], but only flapping motion is absolutely necessary to generate sufficient lift. [15] attempted to design a flapping wing mechanism with flapping-pitching–Lead-Lag motion with single actuator, whereas Smartbird from Festo Corporation has implemented active pitching movement by adding another actuator in the wings. Considering available manufacturing facilities and complexity of these mechanisms, we will only focus on flapping motion with passive pitching.

The pitching motion is passive for flexible wing as the aerodynamic forces generated due to other motions, deform the wing planform. We can achieve desired pitching motion by altering the material and structure of the wing.

[8] has quantified these motions from videos of flying Seagull, Crane and Goose. A two-jointed arm model is used to approximate the profile of the quarter-chord line of a wing. The characteristics angles of this model are given in the form of Fourier series. The plots this data is shown in figure 3.3. Flapping Angle, folding angle and lead-lag angle are shown by  $\psi_1$ ,  $\psi_2$  and  $\phi_2$ .

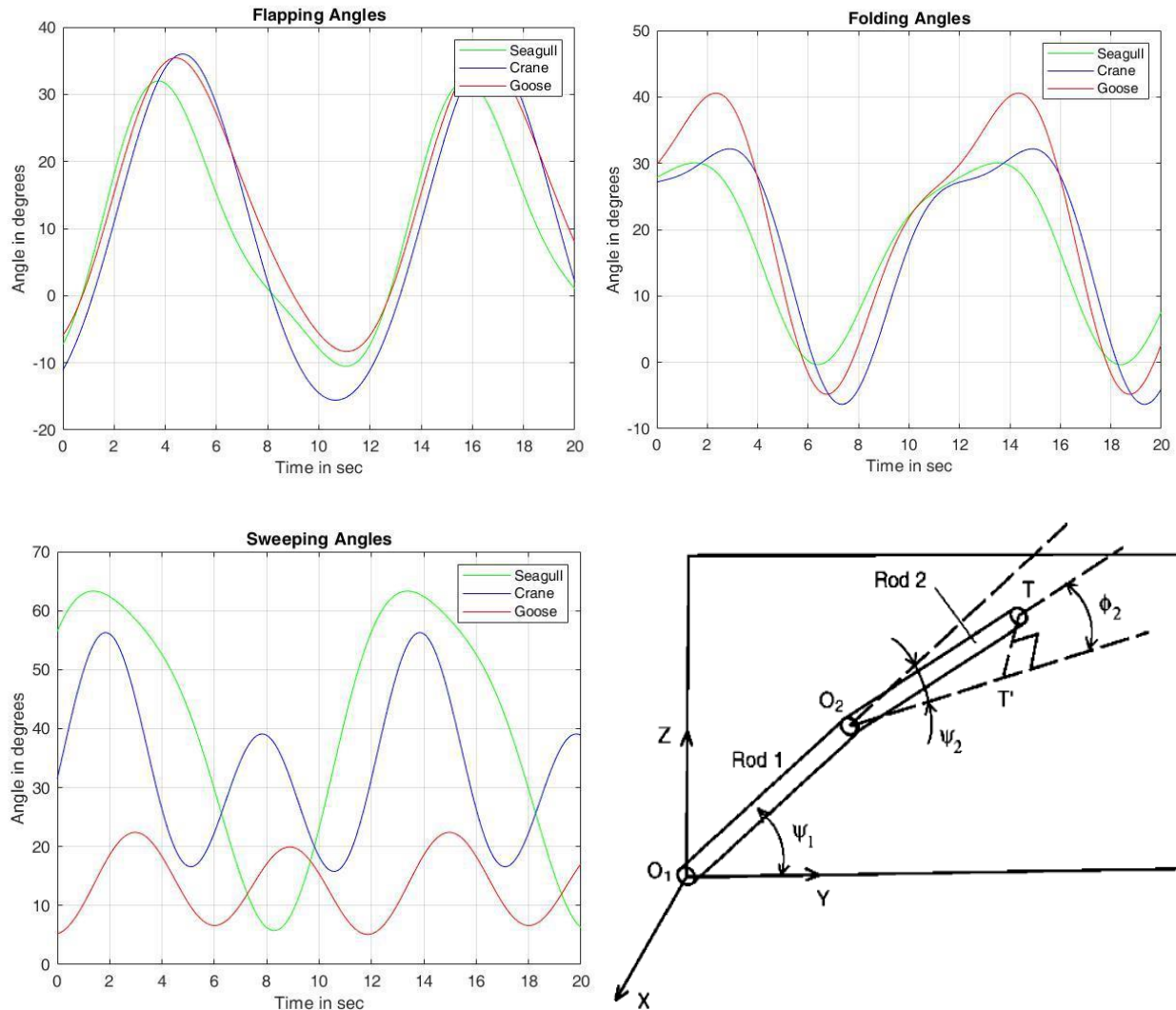


Figure 3.3: Graphs of Flapping Angle, folding angle and lead-lag angle [8]

Observations from the graphs:

- Flapping and Folding angles are interlinked and occur in similar pattern for different birds. Therefore, linking both angles to same actuator is justified.
- Sweeping angle is dependent on bird species so it will require independent actuator.
- Ratio of flapping angle above horizontal to flapping angle below horizontal is between 3 and 6. i.e.,  $6 > \phi_{up}/\phi_{down} > 3$
- Average flapping amplitude is 50 degrees.

## 3.2 Procedure of Selection

There are various mechanisms well documented in literature for flapping. Each of these mechanisms has some advantages and disadvantages. This chapter presents the analysis of those mechanisms, both theoretically and experimentally. In conclusion the best suited mechanism for the project was selected.

As noted in literature review, most of the flapping mechanisms are modified versions of standard four bars mechanism in crank-Rocker configuration. Three of those mechanisms namely *Single Crank Mechanism*, which is widely used for rubber band powered toy ornithopters, *Dual Shaft Mechanism* which has been implemented in Well-known models such as MIT's Phoenix and Kestrel by Kinkade [20] and *Dual crank mechanism* from Festo's Smartbird are analysed.

Performance of these mechanisms will be compared in following aspects:

➤ *Loading on the structure:*

To examine the load on linkages and actuators, we draw conclusions from makeshift mechanisms.

➤ *Design compatibility and ease of manufacturing:*

Bilateral symmetry of mechanism, symmetry in motion of both wings, types of joint required to manufacture will be considered in this section.

➤ *Range of motion:*

The maximum flapping angle produced by each mechanism, constrained with limitations on transmission angle and Grashof criteria is considered.

### 3.2.1 Four Bar Mechanism Terminology and Basic results:

For purpose of analysis, general terms associated with four bar mechanism in crank-rocker configuration are explained. The rotating link directly receiving power from actuator is termed as ***Crank***. The oscillating link is called as ***Rocker***. The stationary link is called ***Base or fixed link***. The link joining Crank and Rocker is called as ***Connector***. The angle between Rocker and Connector is called as ***Transmission Angle***. The directed angle from base to Crank is called as

**Crank Angle.** ( $\alpha$  in figure 3.4) The directed angle from rocker to base is called as **Rocker Angle**. ( $\beta$  in figure 3.4)

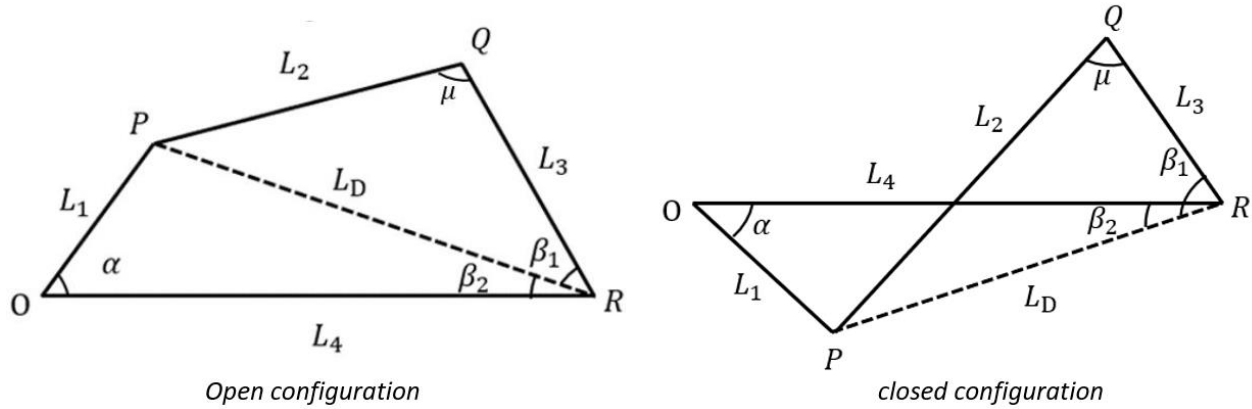


Figure 3.4: Four bar mechanism

When connector crosses the fixed link, the mechanism is said to be in *closed configuration*. If connector does not cross the fixed link, the mechanism is said to be in *open configuration*.

For Standard four bar mechanisms, rocker angle  $\beta$  can be defined as:

$$\beta = \beta_1 + M\beta_2$$

Where  $M$  is defined as,

$$M = \begin{cases} 1, & 0 \leq \alpha \leq \pi \\ -1, & \pi < \alpha \leq 2\pi \end{cases}$$

Therefore, output angle is,

$$\beta = \cos^{-1} \left( \frac{L_3^2 + (L_1^2 + L_4^2 - 2L_1L_4 \cos \alpha) - L_2^2}{2L_3\sqrt{L_1^2 + L_4^2 - 2L_1L_4 \cos \alpha}} \right) + M \cos^{-1} \left( \frac{L_4^2 + (L_1^2 + L_4^2 - 2L_1L_4 \cos \alpha) - L_1^2}{2L_4\sqrt{L_1^2 + L_4^2 - 2L_1L_4 \cos \alpha}} \right)$$

Also, the transmission angle is given by,

$$\mu = \cos^{-1} \left( \frac{L_2^2 + L_3^2 - (L_1^2 + L_4^2 - 2L_1L_4 \cos \alpha)}{2L_2L_3} \right)$$

For smooth operation of mechanism,

the transmission angle is generally taken in the range of  $90^\circ \pm 50^\circ$ .

When four-bar mechanism is used for flapping, we need to define a new variable  $\theta$ , which is angle between the vertical and the fixed link. Therefore, flapping angles can be formulated as shown:

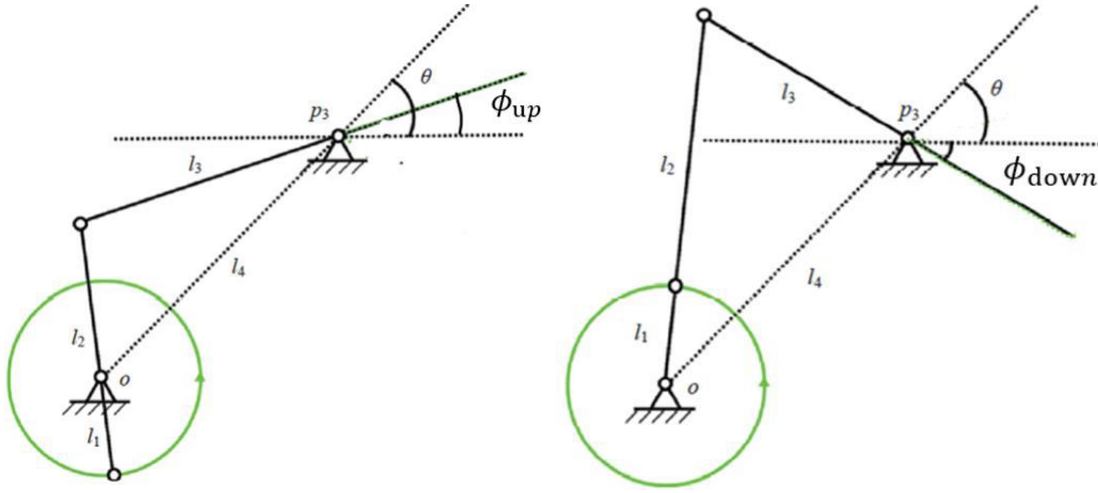


Figure 3.5: Range of flapping angle

$$\phi_{up} = \theta - \cos^{-1} \left( \frac{L_4^2 + L_3^2 - (L_2 - L_1)^2}{2L_4L_3} \right)$$

$$\phi_{down} = \cos^{-1} \left( \frac{L_4^2 + L_3^2 - (L_2 + L_1)^2}{2L_4L_3} \right) + \theta$$

$$\text{Range of Flapping} = \phi_{up} + \phi_{down}$$

As we can see, the variable of interest which is range of flapping, depends on  $L_1, L_2, L_3, L_4$  and  $\theta$ . It is clear that all angles between linkages only depends on relative ratios of  $L_1, L_2, L_3, L_4$  and not on their individual lengths. Therefore, while optimising for such target variables, it is necessary to normalise the lengths of linkages. We will use the following in further analysis:

$$\widetilde{L}_1 = 1; \widetilde{L}_2 = \frac{L_2}{L_1}; \widetilde{L}_3 = \frac{L_3}{L_1}; \widetilde{L}_4 = \frac{L_4}{L_1}$$

The Grashof condition for a four-bar linkage states: If the sum of the shortest and longest link of a planar four-bar linkage is less than or equal to the sum of the remaining two links, then the shortest link can rotate fully with respect to a neighboring link. In other words, the condition is satisfied if:

$$s + l < p + q$$

Where  $s$  is the shortest link,  $l$  is the longest, and rest links are denoted by  $p$  and  $q$ .

The movement of a four-bar linkage can be classified into eight cases based on the dimensions of its four links. Let  $a$ ,  $b$ ,  $g$  and  $h$  denote the lengths of the input crank, the output crank, the ground link and coupling link, respectively. Then, we can construct the three terms  $T_1$ ,  $T_2$  and  $T_3$  as shown in the table:

$$T_1 = g + h - a - b;$$

$$T_2 = b + g - a - h;$$

$$T_3 = b + h - a - g;$$

$T_1$	$T_2$	$T_3$	Grashof condition	Input link	Output link
-	-	+	Grashof	Crank	Crank
+	+	+	Grashof	Crank	Rocker
+	-	-	Grashof	Rocker	Crank
-	+	-	Grashof	Rocker	Rocker
-	-	-	Non-Grashof	0-Rocker	0-Rocker
-	+	+	Non-Grashof	$\pi$ -Rocker	$\pi$ -Rocker
+	-	+	Non-Grashof	$\pi$ -Rocker	0-Rocker
+	+	-	Non-Grashof	0-Rocker	$\pi$ -Rocker

Table 3.1: Four-bar linkage configurations

Hence, lengths of links should be chosen such that  $T_1$ ,  $T_2$  and  $T_3$  becomes positive. These conditions are equivalent to:

- A) The shortest link is input crank and the longest link is either fixed link or coupling link.
- B) Grashof criteria is followed. i.e., Sum of shortest and longest link is less than sum of the other two.

### 3.3 Single Crank Mechanism

In the figure 3.6, each wingspar is a rocker of a four-bar mechanism with shared crank.

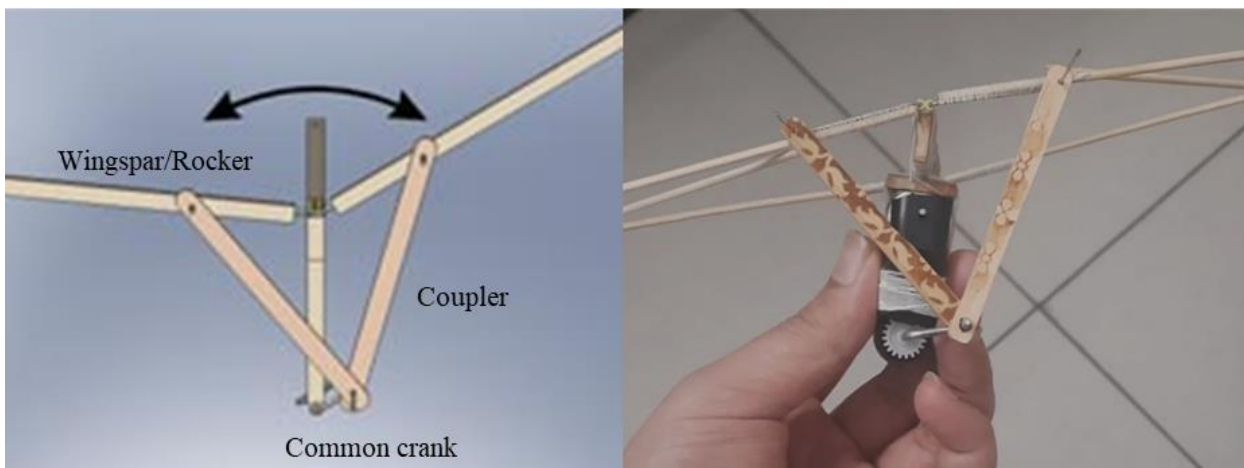


Figure 3.6: Single Crank mechanism test model

The total range of flapping angle is determined by several constraints applied to above mechanism including Grashof criteria, conditions on transmission angle and application specific geometric constraints.

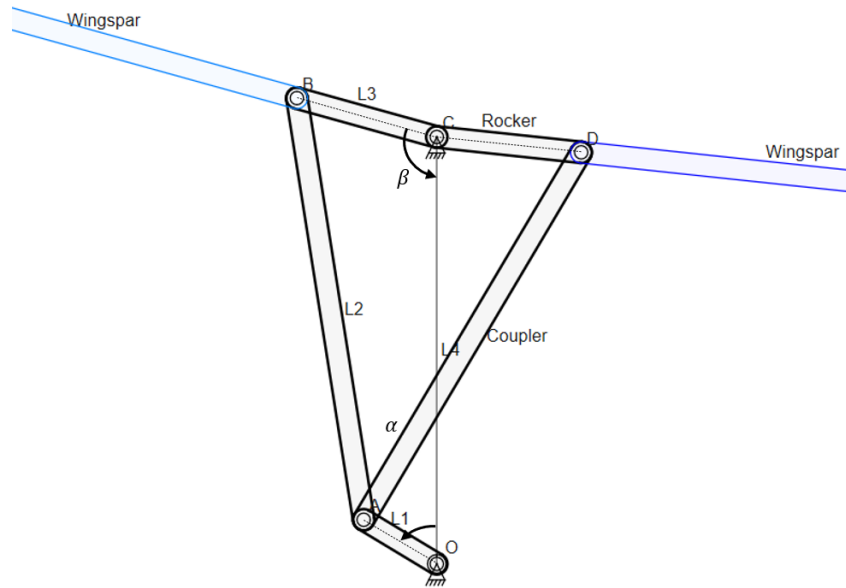


Figure 3.7: Linkage Simulation

Since we need maximum flapping angle under those constraints, we can formulate optimization problem to get relative lengths of the linkages. Let L1, L2, L3 and L4 denote lengths of crank, coupler, rocker and base respectively as shown in figure 3.7.

Hence, we need to maximize, range of flapping angle, subject to following conditions:

Condition	Remarks
$\theta = 0^0$	As shown in figure 3.7, base is parallel to vertical.
$L_2 > \max(L_1, L_3, L_4)$	Coupler is assumed to be largest link for this specific application.
$L_1 < \min(L_2, L_3, L_4)$	Crank is the smallest link.
$L_1 + L_2 < L_3 + L_4$	Grashof condition for crank-rocker configuration.
$40^0 < \mu < 140^0$	Transmission angle should around ideal $90^0$ , so the mechanism do not lock up.

Table 3.2: Optimisation Problem conditions: Single Crank Mechanism

As shown earlier, we need to find only  $\widetilde{L}_2$ ,  $\widetilde{L}_3$  and  $\widetilde{L}_4$ , as  $\theta$  is already fixed. These values are found by searching through equally spaced points in multivariable space. In this case there are three variables  $\widetilde{L}_2$ ,  $\widetilde{L}_3$  and  $\widetilde{L}_4$ . After carefully evaluating the obtained solutions and crossing of extreme cases, following solution is chosen for implementation.

$$(\widetilde{L}_2, \widetilde{L}_3, \widetilde{L}_4) = (4.9230, 2.3846, 4.4615)$$

for makeshift prototype we used scaled up parameters given by

$$L_1 = 13 \text{ mm}, L_2 = 64 \text{ mm}, L_3 = 31 \text{ mm} \text{ and } L_4 = 58 \text{ mm}.$$

### Range of Motion:

Maximum flapping angle for above parameters can be determined as follows:

$$\phi_{up} = \cos^{-1} \left( \frac{L_4^2 + L_3^2 - (L_2 + L_1)^2}{2L_4L_3} \right) - 90^0 = 26.4906^0$$

$$\phi_{down} = -\cos^{-1} \left( \frac{L_4^2 + L_3^2 - (L_2 - L_1)^2}{2L_4L_3} \right) + 90^0 = 28.6476^0$$

$$\text{Range of Flapping} = \phi_{up} + \phi_{down} \approx 55^0$$

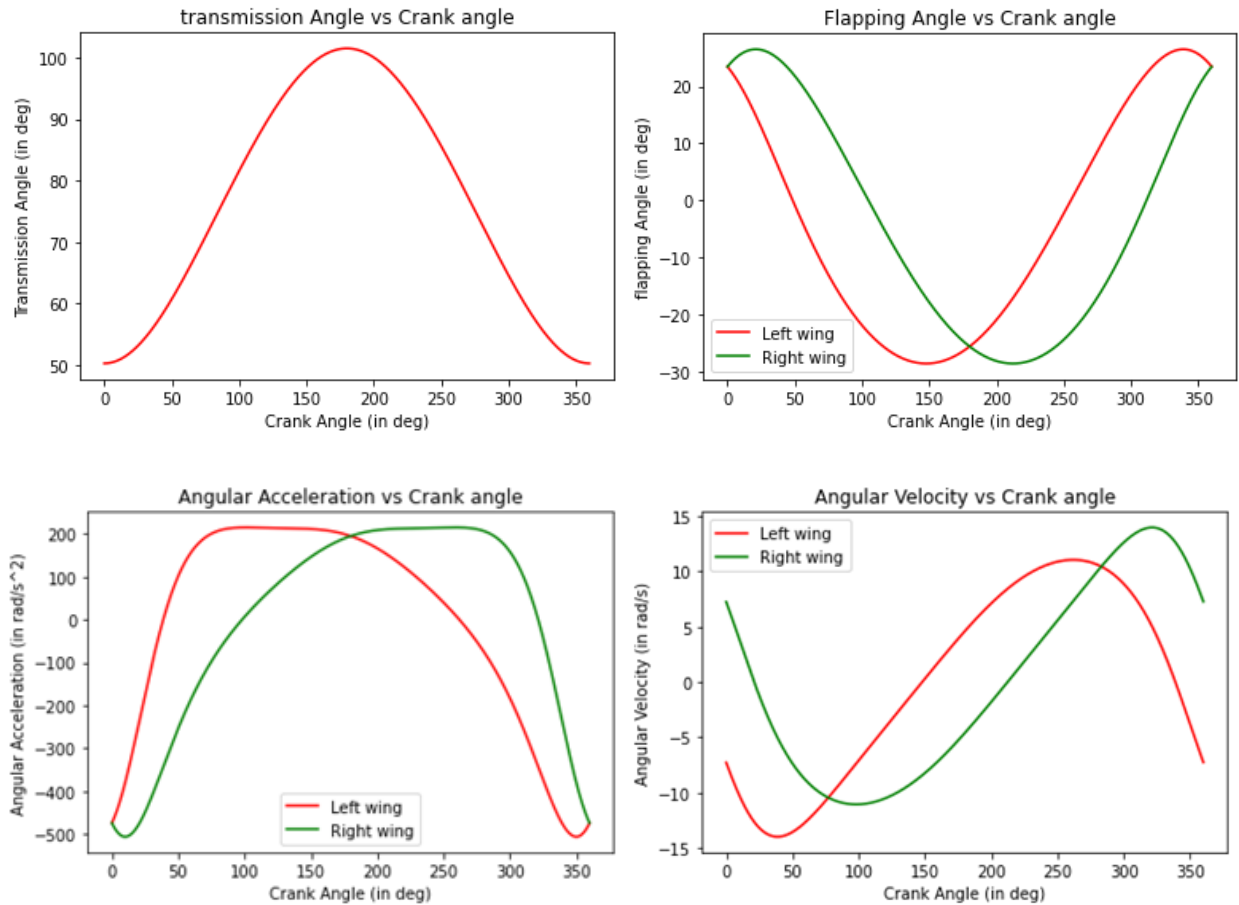


Figure 3.8: Graphs of Kinematic Parameters: Single Crank Mechanism

### Loading:

The force on wingspar can be modelled as sum of inertial force, resistive force and due to the weight of the wing. The inertial force is proportional to acceleration or angular acceleration of the wingspar and acts along the direction of angular acceleration ( $\alpha$ ). Whereas resistive force is proportional to square of the angular velocity and acts in opposite direction of angular velocity ( $\omega$ ). The weight of the wing applies almost constant torque in same direction throughout flapping cycle. Based on makeshift model, we draw following conclusions:

- There is a locking point during flapping cycle, which needs the highest amount of torque from actuator. At very low RPM the mechanism locks at that point.
- The load on motor is inversely proportional to length of rocker link (L3) and directly proportional to length of crank (L1). So, adjustments can be made accordingly if actuator is unable take the load.

### Design compatibility and ease of manufacturing:

Although the mechanism is very simple and easy to manufacture, it lacks in symmetry. Both rockers should be in unison for ideal flapping motion. The makeshift model built on this mechanism had inherent tendency to turn. Even offsetting the tail was not enough to balance the model. The difference of angle between left and right wingspar is plotted below.

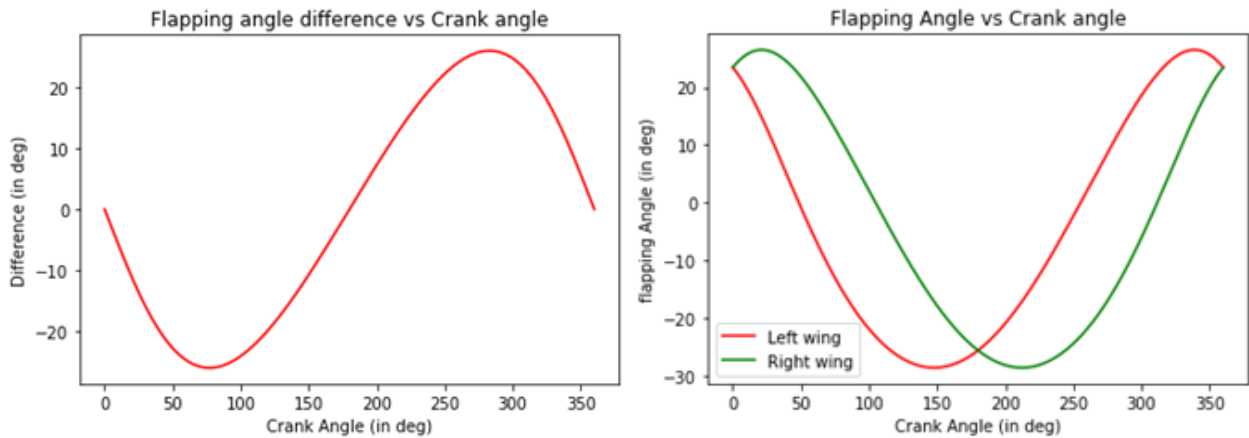


Figure 3.9: Asymmetry in flapping angles of Single Crank Mechanism

Some modifications in mechanism can yield more symmetric motion. For example, adding a bent crank or separating the hinge point of wingspars as shown in (b) and (e) in figure 3.10 respectively. The optimisation of these modified mechanisms is discussed in literature review.

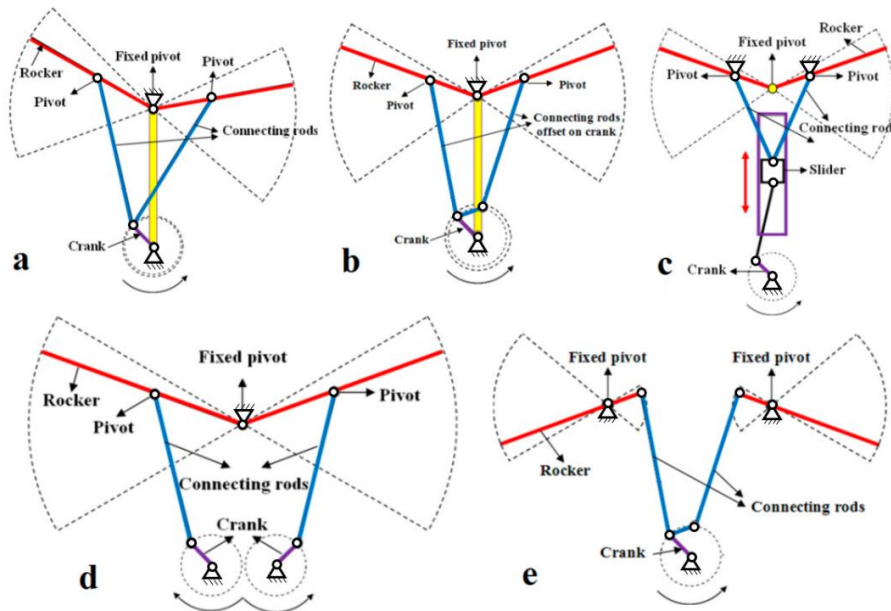


Figure 3.10: Various Four-bar flapping mechanisms

### 3.4 Dual Shaft Mechanism

As shown in the figure 3.11, both cranks are attached on dual shaft. These cranks are further connected to wingspars by couplers.

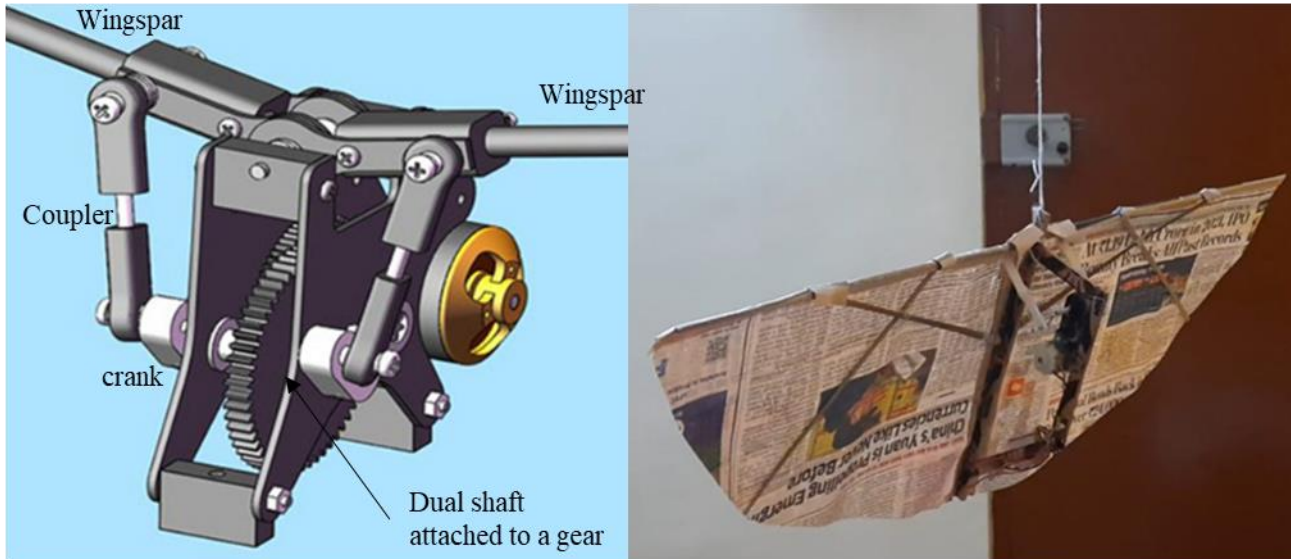


Figure 3.11: Dual Shaft mechanism test model

Dual shaft mechanism is not planar. Ideally the coupler joints are not revolute joints with one degree of freedom. However, for sake of simplicity and easy manufacturing, we will consider the planar approximation of this mechanism. In figure 3.12, the actual trajectory of circled point on wingspar is showed by red line and approximated trajectory is showed red dashed line.

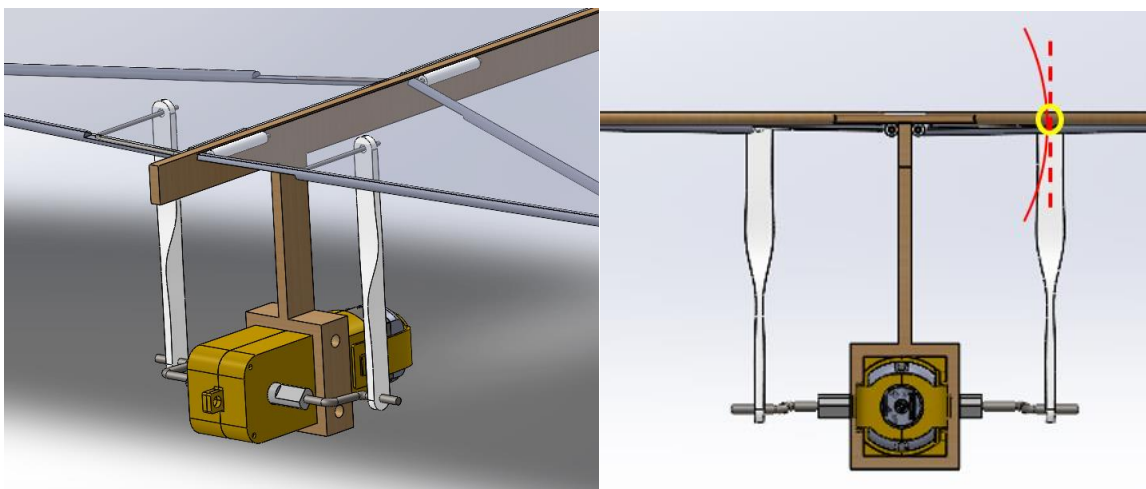


Figure 3.12: Solidworks Simulation

### Range of Motion:

Here the range of motion can be as large as possible in theory. So, we cannot set an optimisation problem based on some theoretical results. However, by experimenting again and again with makeshift model shown in figure 3.11 (right) helped me to determine the lengths of support rods and crank, very close to optimum solution. The final lengths and flapping angle are tabulated below.

Crank Radius	11 mm
Shaft Length	25 mm
Connecting rods	64 mm
Maximum Flap-up angle	34 <sup>0</sup>
Maximum Flap-down angle	19 <sup>0</sup>
Maximum flapping amplitude	53 <sup>0</sup>

Table 3.3: Specification of makeshift dual shaft mechanism

### Load on Motor:

Similar to previous loading analysis the force on wingspar can be modelled as sum of inertial force, resistive force and due to the weight of the wing. observations drawn from makeshift mechanism:

- Since the links were joined by revolute joint in makeshift model, the links were sliding out of the joint. Some stoppers were needed to lock the joints. From this we can conclude that there are some forces were acting perpendicular to plane of mechanism.
- The flap down position is locking point for this mechanism. Without sufficient RPM, the mechanism does not work.

### Design compatibility and ease of manufacturing:

Dual shaft mechanism is yielding perfectly symmetric flapping. Although the bilateral symmetry of mechanism is lost due to positioning of motor/actuator. A worm gear can be used to keep bilateral symmetry as shown below; however, it will change the flapping frequency and make it more difficult to manufacture.

On the other hand, assuming this mechanism as planar allow us to use revolute joints for linkages. However, it significantly reduces the range of flapping motion. One way to overcome this is to use ball and socket joints for coupler. Using ball and socket joints will increase the complexity as well as overall weight of the mechanism.

### 3.5 Dual Crank Mechanism

As shown in the figure 3.13, the pivot point of wingspars/rockers is separated. Also, gears are used to exactly mirror the motion of cranks, hence this mechanism is capable of executing perfectly symmetric flapping motion.

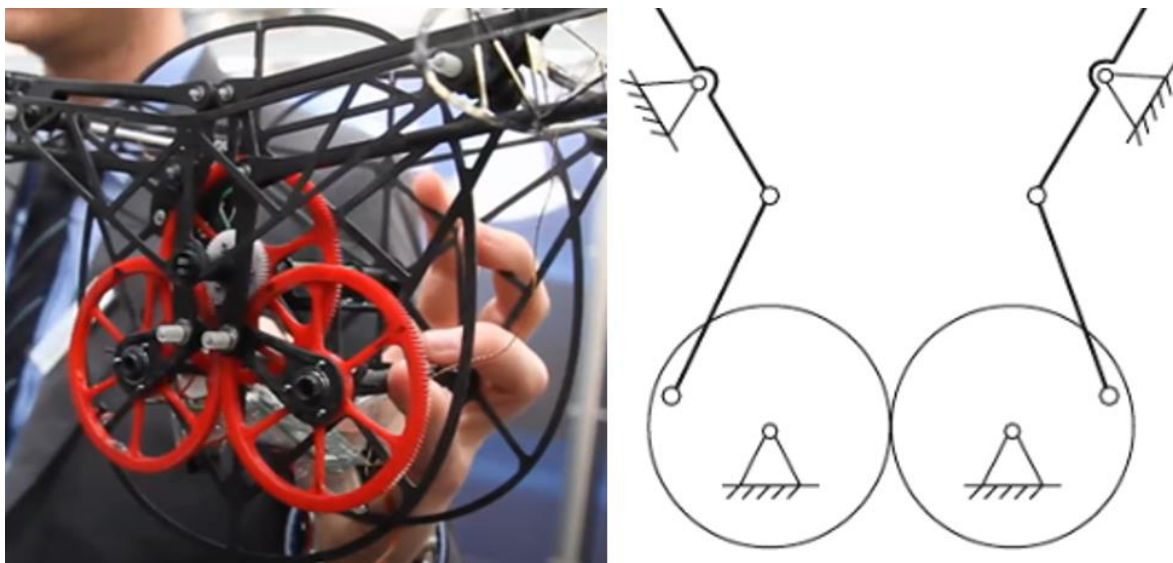


Figure 3.13: Dual Crank mechanism test model [2]

Crank	Coupler	Rocker	Base	Angle between Base and horizontal ( $\theta$ )
15 mm	29 mm	30 mm	42 mm	$67^\circ$

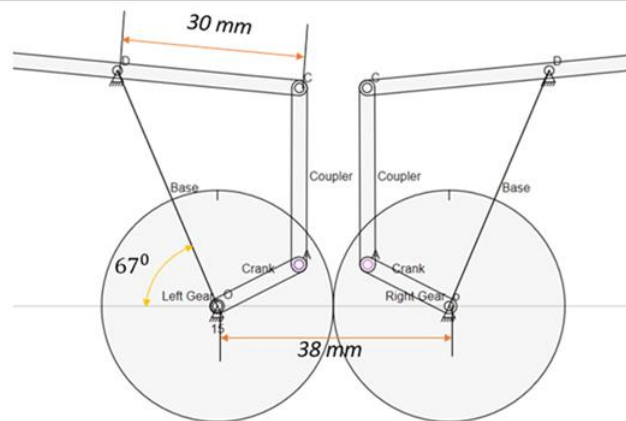


Figure 3.14: Solution of optimization problem: Dual Crank Mechanism

Similar to previous analysis, the total range of flapping angle is determined by several constrains. Since we need maximum flapping angle range under those constrains, we can formulate optimization problem. Therefore, maximize range of flapping angle, subject to:

Condition	Remarks
$L_4 > \max(L_1, L_2, L_3)$	Fixed link is assumed to be the longest link for this specific application.
$L_1 < \min(L_2, L_3, L_4)$	Crank is the smallest link.
$L_1 + L_2 < L_3 + L_4$	Grashof condition for crank-rocker configuration.
$40^\circ < \mu < 140^\circ$	Transmission angle should around ideal $90^\circ$ , so the mechanism do not lock up.
$L_4 \cos \theta > L_3$	sum of both rocker links should be less than distance between wingspar pivots to avoid clashing of both rocker links.

Table 3.4: Optimisation Problem conditions: Dual Crank Mechanism

The optimisation problem is solved by previously described method. After carefully evaluating the obtained solutions and crossing of extreme cases, following solution is chosen for implementation.

$$(\widetilde{L}_2, \widetilde{L}_3, \widetilde{L}_4, \theta) = (1.96, 2.04, 2.85)$$

Therefore,  $L_1 = 15$  mm,  $L_2 = 29$  mm,  $L_3 = 30$  mm and  $L_4 = 42$  mm.  $\theta = 67^\circ$

### Range of Motion:

Maximum flapping angle under above conditions is

$$\phi_{up} = \theta - \cos^{-1} \left( \frac{L_4^2 + L_3^2 - (L_2 - L_1)^2}{2L_4L_3} \right) = 67 - 11.66 = 55.34$$

$$\phi_{down} = \cos^{-1} \left( \frac{L_4^2 + L_3^2 - (L_2 + L_1)^2}{2L_4L_3} \right) - \theta = 73.20 - 67 = 6.20$$

$$\text{Range of Flapping} = \phi_{up} + \phi_{down} = 55.34 + 6.20 = 61.54$$

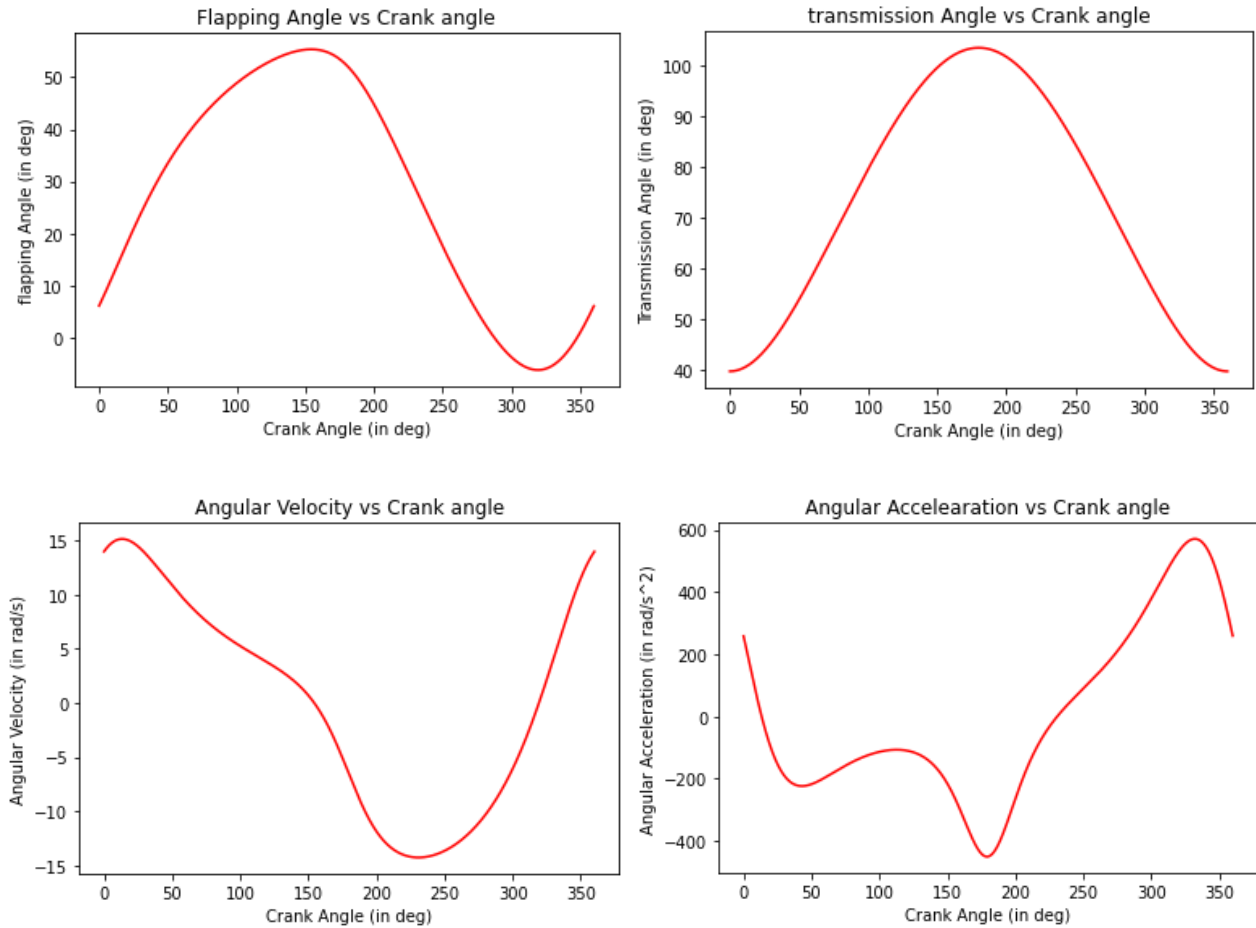


Figure 3.15: Graphs of Kinematic Parameters: Dual Crank Mechanism

The crank Angle shown in above graphs is measured from base to crank with reference to figure 3.14.

### Load on Motor:

Even though this mechanism is based on four-bar linkage, it performed a lot better than the single crank mechanism. Some observations made from makeshift model:

- Separating pivots of each wingspar by some distance, improved the performance. It also helps to avoid clashing of rocker linkages. (See condition 5 in optimisation problem).
- The mechanism did not lock even with very low RPM.

### Design compatibility and ease of manufacturing:

This mechanism is more complex and heavier than the single crank mechanism, but it has added benefits of perfectly symmetric flapping motion as well as bilateral symmetry. Moreover, with slight modifications, folding motion can be added as shown below. Festo Smartbird and [17] have demonstrated this modification.

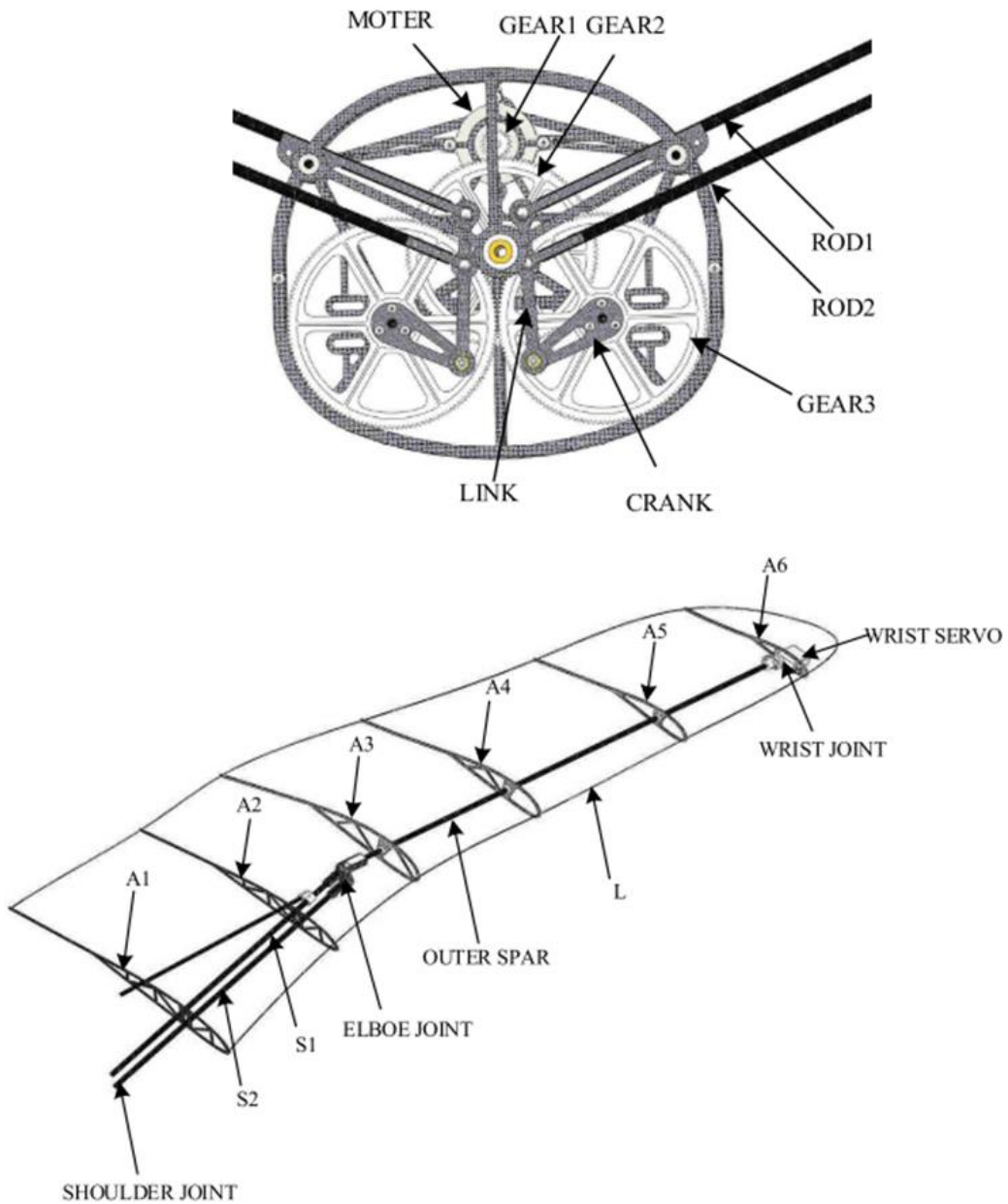


Figure 3.16: Six bar mechanism : Flapping + Folding Motion [17]

### 3.6 Summary of observations

Below is the summary of observations made in this chapter. Based on them and recommendations received from supervisor, Dual Crank Mechanism was selected to be implemented in main model. The most significant point favouring this mechanism is the provision of adding more complex kinematics of flapping plus folding motion.

Different Aspects	Flapping Mechanisms		
	Single Crank	Dual Shaft	Dual Crank
Flapping Symmetry	Almost Symmetric	Exact Symmetric	Exact Symmetric with provision of folding motion
Bilateral Symmetry	Yes	*No	Yes
Weight	Lightweight	Heavy	Heavy
Complexity and ease of manufacturing	Simple	Complex	Complex
Loading	Locks up on low RPM	Locks up on low RPM	Do not lock

Table 3.5: Summary of observations

## Chapter 4

# Mechanical Design and Analysis

The design process for the ornithopter began by studying previously developed ornithopters. It was found that overall mass of ornithopter was the most influential parameter in the design process. Due to stringent constrain on mass of the components, designing a small scale ornithopter (mass < 50 gm), requires very specific actuators and electronics system. moreover, smaller ornithopters are much difficult to control than their bigger counterpart. For these reasons, we decided to design a large scale ornithopter resembling an owl or a crow.

The preliminary design parameters like wingspan, length of body, flapping frequency, overall mass, wing area are estimated based on empirical relations and by referring previous models. Instead of fixing the exact value of these parameters, their range was calculated. This flexibility was helpful for iterative design process.

### 4.1 Preliminary design

As we have decided to build a large scale ornithopter, wingspan is assumed to be in range of 1 - 1.2 m. Often, when flapping animals are studied, parameters of interest are related to the body mass  $m$  of the animal. Using the dimensional argument method, assuming geometric similarity for the animals considered, one can determine a relation between the wingspan and the mass. [1] suggests that, over a large range of the weight, birds and aircraft basically, follow the power law:

$$L = 1.704 m^{1/3} \text{ (For birds).}$$

Considering length of each wing 50 cm and width of fuselage around 10 cm, we can estimate overall mass of the model to be approx. 400 gm.

In general, the agility and ability to manoeuver improves with a smaller Aspect Ratio (AR). On the other hand, with a large AR, the lift-to-drag ratio  $L/D$ , or the so-called glide ratio, increases with an increasing AR. Among bird wings, aspect ratios vary from about 1.5 to as high as about 18. According to [31], Aspect ratio and wing loading of birds are closely related to their flight style. We can see in figure 4.1, that our reference birds (owls and crows) have low aspect ratio as well as low wing loading.

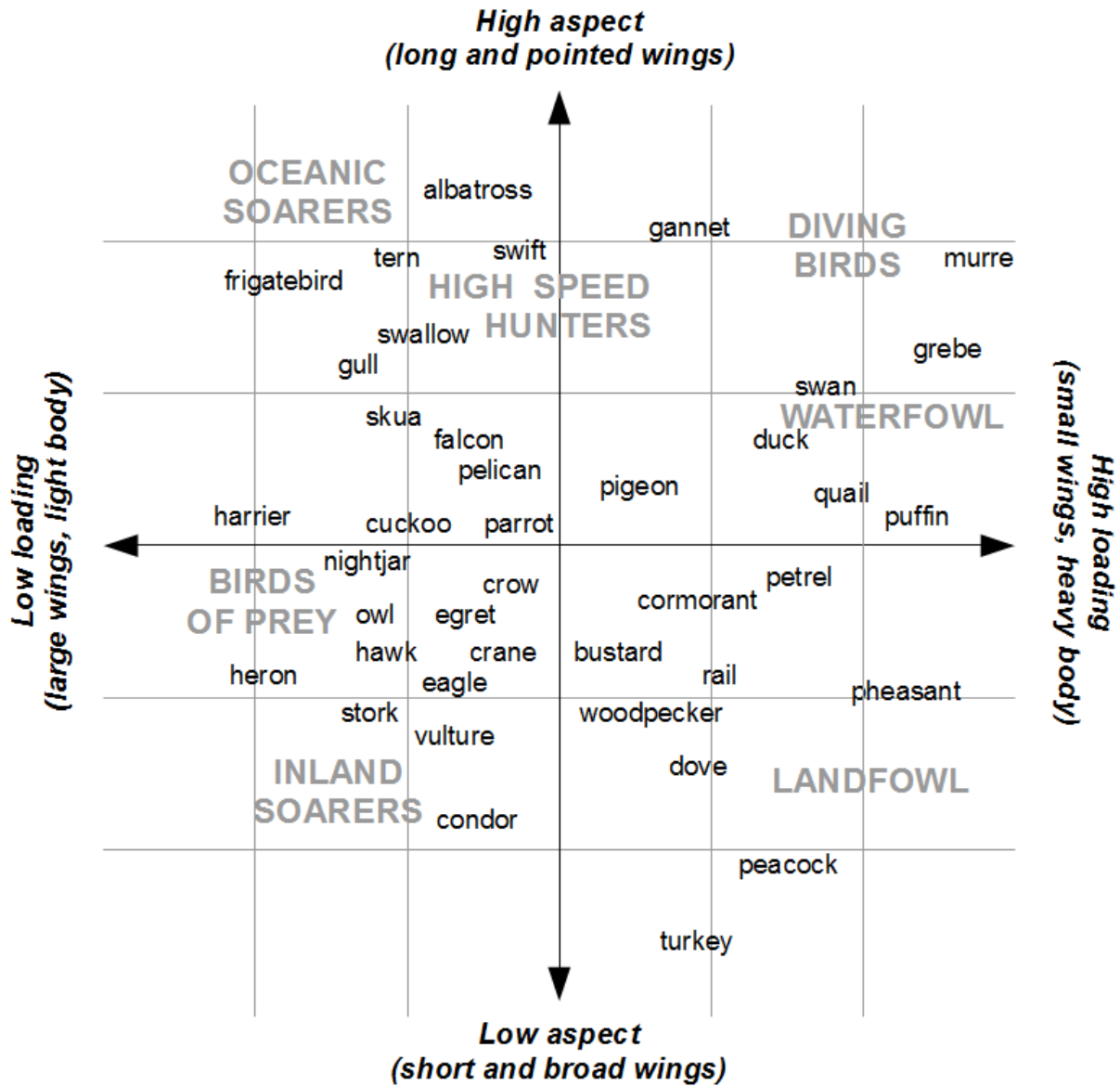


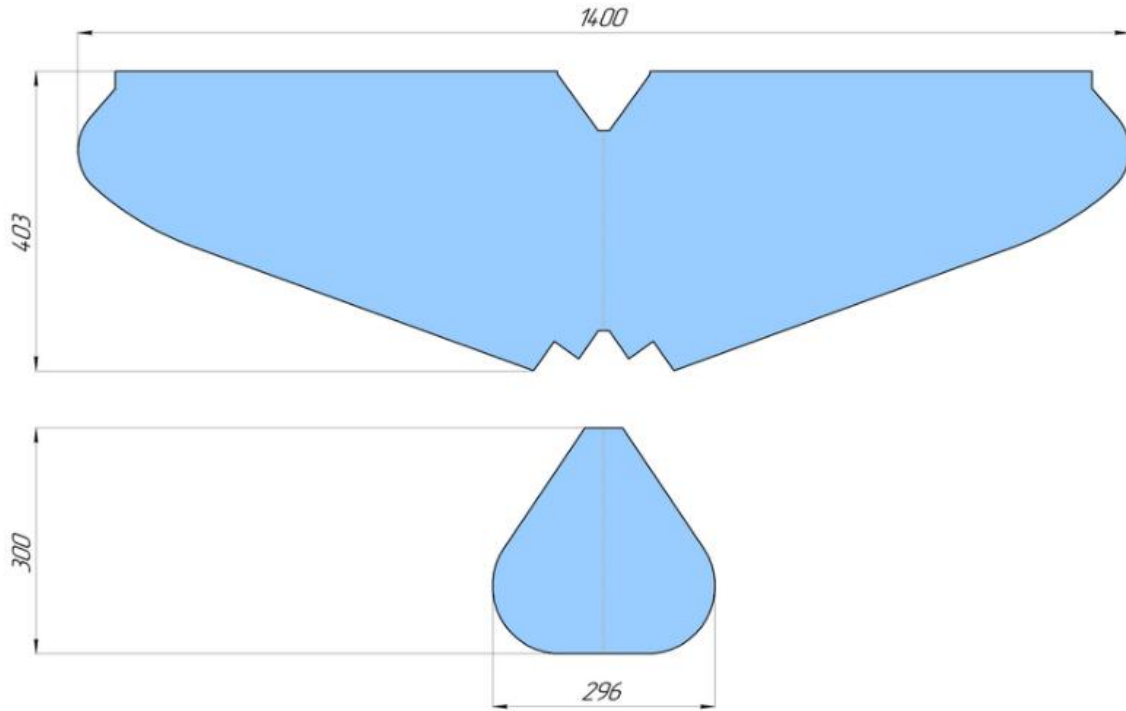
Figure 4.1: Aspect Ratio and Wing loading of various birds [31]

Figure 4.2 shows schematic of an opensource ornithopter with wingspan of 1.4 m. assuming elliptical wings we can calculate its aspect ratio.

$$\text{Wing length} = 1.4/2 = 0.7 \text{ m}$$

$$\text{Wing area} = 0.25\pi a b = 0.25 \pi \times 0.7 \times 0.403 = 0.2215 \text{ m}^2$$

$$\text{Aspect Ratio} = \frac{(\text{Wing Length})^2}{\text{Wing Area}} = (0.7)^2 / 0.2215 = 2.212$$



*Wing and tail outline*

Figure 4.2: Opensource Ornithopter Design

Using above reference value, we can estimate root chord length of our model as well as it's area.

$$\text{Wing Area} = (\text{Wing Length})^2 / \text{Aspect Ratio} = (0.55)^2 / 2.2 \sim 0.1375 \text{ m}^2$$

Assuming elliptical wings,

$$\text{Wing Area} = 0.25 \pi \times \text{Wing Length} \times \text{Root Chord Length}$$

$$\text{Root Chord Length} = 0.1375 / (0.25 \pi \times 0.55) = 0.32 \text{ m}$$

Flapping frequency is calculated using empirical relations obtained from []. The relation is given by:

$$f = 3.98 \text{ m}^{-0.27} \text{ (For birds except hummingbirds).}$$

$$f = 3.98 * (0.400)^{-0.27} \sim 5 \text{ Hz}$$

As flapping frequency is sensitive parameter, we use broader range of frequency from 2-10 Hz so it can be tuned later. Tail angle and Tail dimensions are determined by applying geometric similarity to figure 4.2. The tail angle is taken to be  $60^{\circ}$  degrees or  $\pi/3$  radians. This value is also used in few DIY tutorials on the YouTube for hobby ornithopters. Following table presents preliminary values calculated above.

Parameter Name	Range	Calculated Value
Wingspan	1 – 1.2 m	1.1 m
Aspect Ratio	2.212	2.212
Root chord length	30 – 34 cm	32 cm
Mass	350 – 450 gm	400 gm
Flapping Frequency	2-10 Hz	5 Hz
Tail Length	22-26 cm	24 cm
Max. Tail width	26-29 cm	27.7 cm
Tail angle	$55^{\circ}$ - $65^{\circ}$	$60^{\circ}$

Table 4.1: Preliminary Design Parameters

## 4.2 Specifics of Dual crank Mechanism

In previous chapter, the flapping mechanism and lengths of linkages were determined. The specifications are showed below. Figure 4.3 show terminal positions.

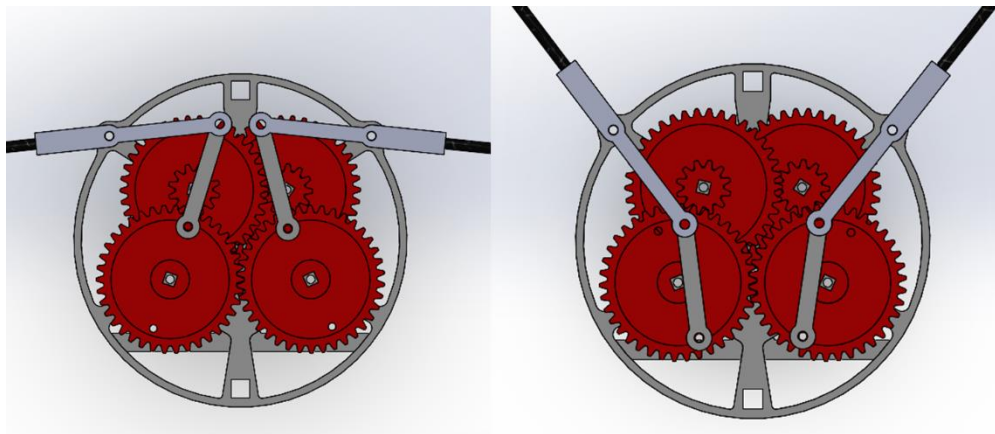


Figure 4.3: Terminal Position of flapping Mechanism

Crank	Coupler	Rocker	Base	Angle between Base and horizontal ( $\theta$ )
15 mm	29 mm	30 mm	42 mm	$67^\circ$

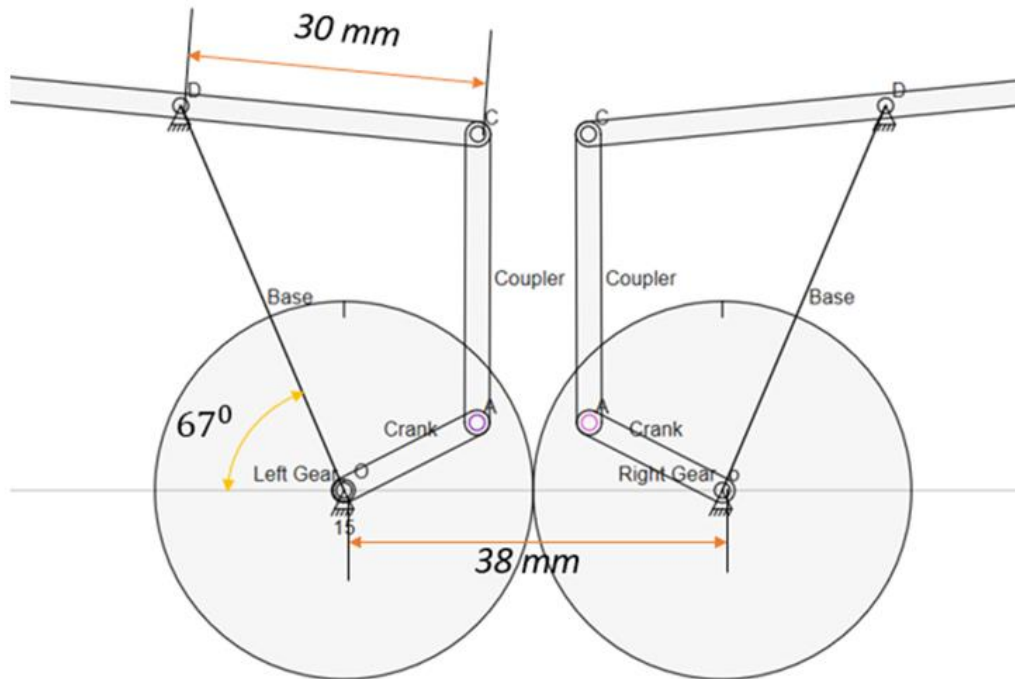


Figure 4.4: Linkage software model

### 4.3 Gearbox design

The most important part of the ornithopter is its gearbox. As per seen in above section, we need rotary motion of two meshed gears at 5 Hz frequency or 300 rpm. Considering the approximate power required to drive the mechanism, brushless drone motors with Lithium-Polymer rechargeable battery is the best available option in market. While designing our objective were as follows:

- Gearbox parts should be easy to manufacture. Preferably by 3D printing.
- Overall mass of the gearbox should be minimum.
- Individual components should be easily replaceable.
- Design should be as compact as possible.

Keeping these points in mind, we tested several designs and modified them accordingly to arrive at the final gearbox design. During manufacturing it was found out that 3D printed gears were

not precise enough to be used in model. Hence old designs were scrapped and new design was made according to commercially available plastic gears.

### 4.3.1 Gear Reduction

After surveying commercially available gears, we selected few gears compatible with each other, which are shown below.

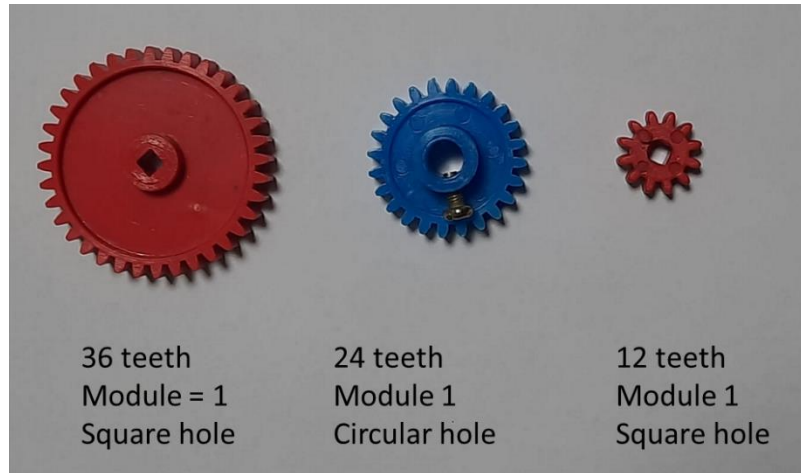


Figure 4.5: Gears

Using these gears, following pairs of gears are possible.

Gear 1	Gear 2	Reduction Ratio
36 Teeth	24 Teeth	1.5
36 Teeth	12 Teeth	3
24 Teeth	12 Teeth	2

Table 4.2: Reduction Ratio

So, any gear train made by these gears should have reduction ratio as multiple of 1.5, 3 and 2.

The BLDC motor used in the model have multiple variants with different RPM ratings. The available motors in the market were 1000 KV, 1400 KV, and 2100 KV.

Along with this, Lithium Polymer battery used in the model has maximum output voltage of 11.5 volts. Since we need flapping frequency range around 2-10 Hz, we can calculate required gear reduction as follows:

Maximum Flapping Frequency = 10 Hz = 600 rpm

Gear Reduction Ratio = Maximum RPM of Motor / Maximum flapping frequency

Motor Ratings in KV	Maximum RPM	Gear Reduction Ratio	Closest possible reduction Ratio
1000	11500 rpm	19.16667	18
1400	16100 rpm	26.8333	27
2100	24150 rpm	40.25	42

Table 4.3: Possible Gear Ratios

Gear Reduction ratio 27 was chosen because it was closest to actual requirement and the resulting gearbox becomes symmetric.

### 4.3.2 Gear Train arrangement

For achieving gear reduction of 27, total 5 gears were used. One pinion gear with 12 teeth was attached to motor shaft. Two compound gears with 36 and 12 teeth and two spur gears with 36 teeth were utilized.

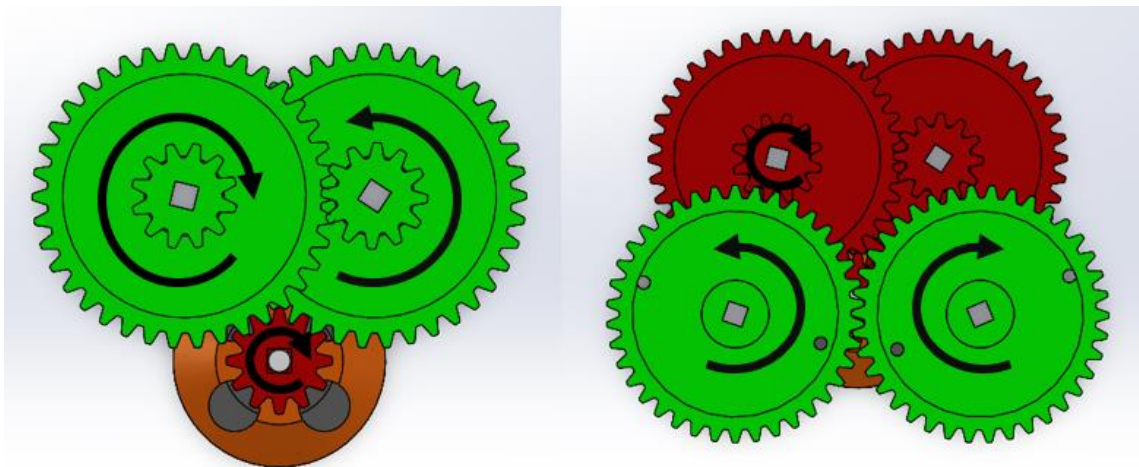


Figure 4.6: Gear Train

As shown in figure 4.6, two compound gears are meshed in series with pinion gear mounted on motor as shown in figure 4.6 (left). Two spur gears are meshed with each other and one of them is connected to the remaining train as shown in figure 4.6 (right).

The holes on spur gears are meant for attaching coupler link. Hence the spur gears at the end of the gear train are cranks for our mechanism. Note that, for supporting these gears, we will be using cantilever shafts which will be supported on mountings. The exact design and assembly will be explained in next chapter.

### 4.3.3 Loading Analysis

Because of gear reduction of 27, the speed of shaft reduces 27 folds and the torque applied on wingspars is multiplied by 27. Suppose the motor supplies torque  $\tau_{motor}$ . The final torque on each gear containing the crank link is  $\frac{27}{2}\tau_{motor}$ . Following snippet defines the linkages and crank angle  $\alpha$ .

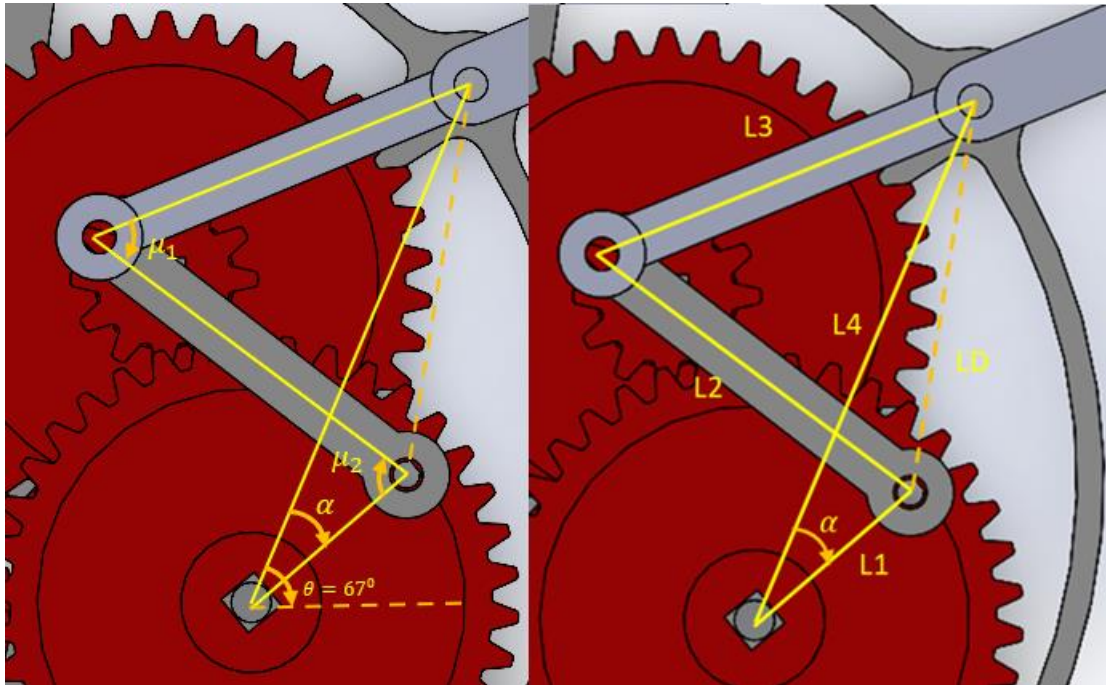


Figure 4.7: Variables of the mechanism

The magnitude of torque on wingspar is given by,

$$\tau_{wingspar} = \frac{27}{2} \tau_{motor} \frac{L_1}{L_2} \sin \mu_1 \sin \mu_2$$

Where  $\mu_2$  is transmission angle between links  $L_1$  and  $L_2$ . Similarly,  $\mu_1$  is transmission angle between link  $L_3$  and  $L_2$ . We can model the  $\tau_{wingspar}$  according to inertial and resistive forces as well as weight of the wing to get torque required by motor. We elaborate above equation by including directional sense to it.

The upstroke begins when  $\alpha = -23^\circ$  and  $\mu_2 = 180^\circ$  and ends when  $\alpha = -23^\circ + 180^\circ = 157^\circ$  and  $\mu_2 = 0^\circ$ . These are terminal positions where links  $L_1$  and  $L_2$  overlap. Assuming clockwise rotation of gear attached to the crank, during the upstroke the link  $L_3$  is pulled by link  $L_2$  and during downstroke the link  $L_3$  is pushed by link  $L_2$ . From this we can conclude:

$$\tau_{wingspar} = \begin{cases} -\frac{27}{2} \tau_{motor} \frac{L_1}{L_2} \sin \mu_1 \sin \mu_2, & -23^\circ < \alpha < 157^\circ; \text{Upstroke} \\ +\frac{27}{2} \tau_{motor} \frac{L_1}{L_2} \sin \mu_1 \sin \mu_2, & -23^\circ > \alpha > -203^\circ; \text{Downstroke} \end{cases}$$

#### 4.4 Wings

The wing design chosen is based on wing designs used in previous ornithopters developed by Zachary John Jackowski and Kinkade. The wings have a triangular support structure made from carbon rods. A main spar runs along the leading edge of the wing and a strut connects from the rear of the ornithopter's body to a point near the tip of the main spar. The exact schematic is given in figure 5.6 in the next chapter.

#### 4.5 Tail Mechanism

Different types of tail mechanism have been validated by previous ornithopter models. Here we are again referring the designs of kestrel ornithopter. The tail section of the ornithopter is responsible for controlling the direction of motion as well as orientation of ornithopter. The tail is directly connected to a servo which controls the tail-roll angle. This whole assembly is attached to main body frame by a revolute joint, where another servo controls the tail-elevation angle via separate linkage (shown in circle in figure 4.8). More details can be found in next chapter.



Figure 4.8: Tail mechanism

The tail-elevation angle controls the pitching movement of the vehicle whereas tail-roll angle controls roll and yaw motion. Note that the functional relationship of roll-pitch-yaw motions and tail angles is very convoluted. Care must be taken while designing the control system based on these angles.

#### 4.6 Overall Weight estimation

The overall estimated mass was calculated by Solidworks software. It is given as approx. 460 gm. This is premanufacturing estimate which will be helpful in reiterative design process. Some material options were unavailable in the software so similar materials were used whose densities are approximately equal to the densities for actual materials. After the completion of prototype, the actual measured mass was found to be 380 gm.

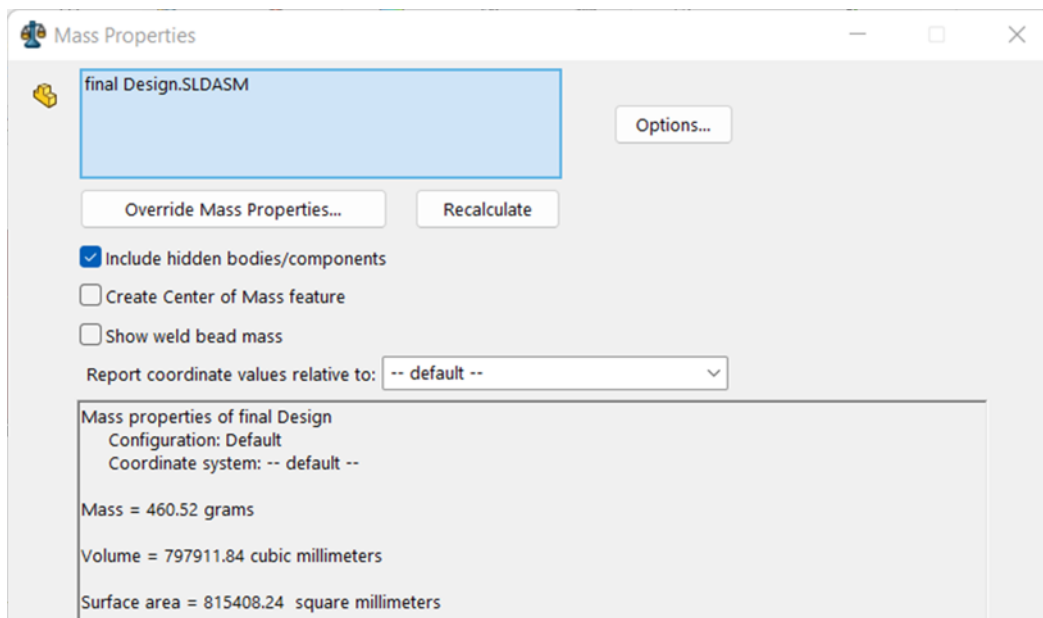


Figure 4.9: Solidworks Mass Properties

## Chapter 5

# Construction and Assembly

This chapter presents the selection of material and manufacturing method for several designed parts. Assembling the gearbox was the most difficult job during fabrication because it needed to be very precise. Any play in the gearbox could amplify the loads and vibrations. On the other hand, wing material was chosen purely by hit and trial method. Tail assembly was comparatively easier since all components were 3D printed. For body frame, I have used Styrofoam to sustain the impact in case of crash. However more aerodynamic and slick body covering will be needed for the complete product. Except servo, none of the joints uses mechanical fasteners. Obviously mechanical fasteners are better in terms of strength and reusability, but their weight is much more compared to glue or fevistick. Moreover, the strength provided by fevistick is more than sufficient for any joint in our model.

### 5.1 Gearbox

As mentioned before gearbox was the most difficult part to manufacture and assemble, as it required very high precision for smooth operation. Except BLDC motor, steel shafts and gears, everything else was manufactured in IIT Indore. Few parts were redesigned after assembling first gearbox prototype. CAD designs of only those parts are showed in this section.

#### 5.1.2 CAD Model of Parts

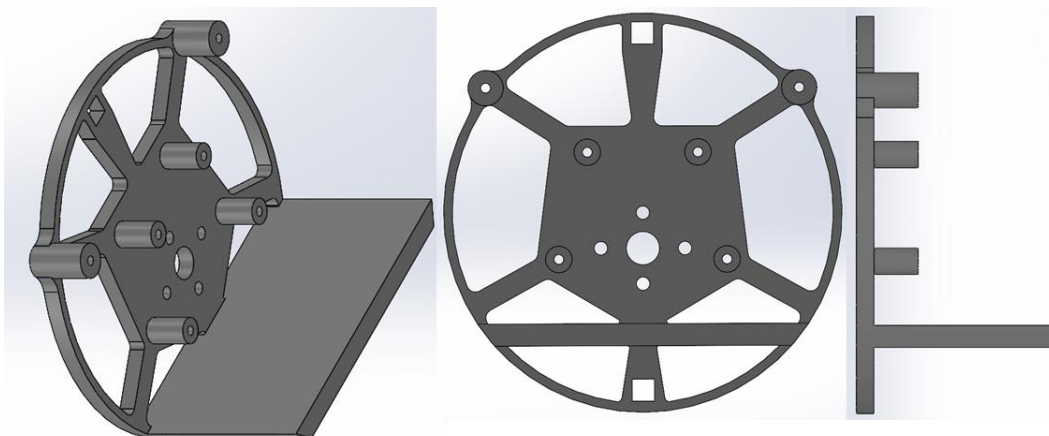


Figure 5.1: Mounting1: Isometric View, Front View, Side View

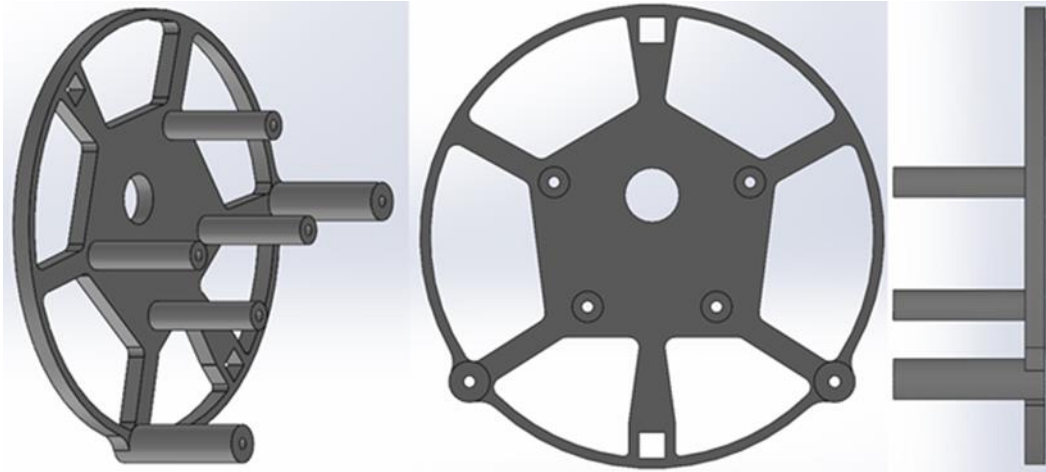


Figure 5.2: Mounting2: Isometric View, Front View, Side View

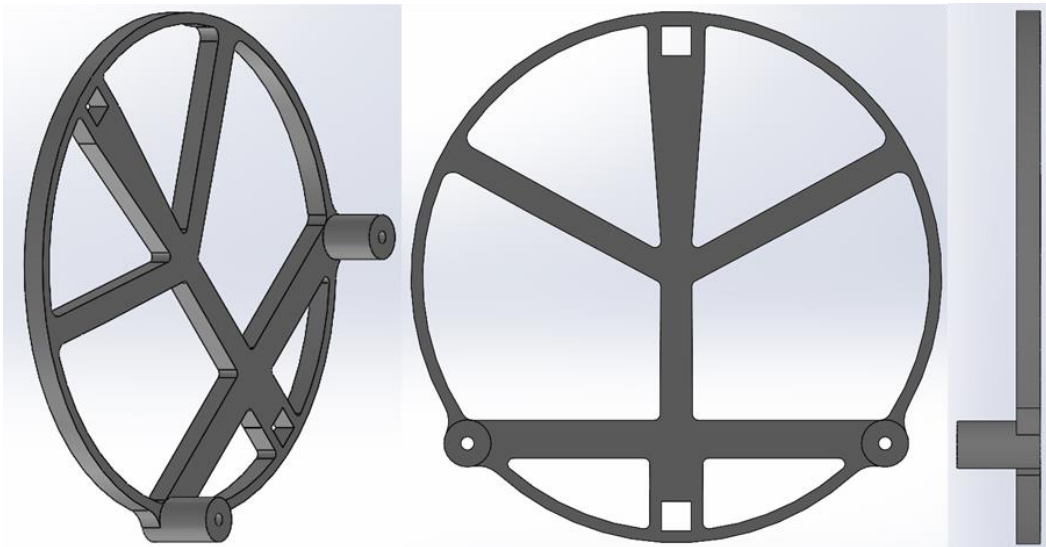


Figure 5.3: Mounting3: Isometric View, Front View, Side View

As shown above, all of these mountings have two square holes, of which one hosts the entire fuselage of 33 cm length, made out of 5 X 5 mm carbon fibre rod. The other square holes are meant for a support rod with same cross-sectional dimensions. Two circular holes on the outer rim are sleeves for the rods which will go through wingspars. All internal holes are sleeves for cantilever stainless steel shafts on which the gears will be mounted. Notice that the mounting1 has five holes arranged in the centre for the motor. Also, the extended part of mounting1 is made for supporting the battery. More details about these parts can be found in assembly subsection.

### 5.1.3 Materials and manufacturing method

The mountings of gearbox and various linkages were 3D printed using PLA at 60% infill density. The PLA is standard material used in 3D printing services which stands for Polylactic Acid. Stainless steel rods of 2 mm diameter are used for shafts. Along with these, two types of carbon fibre rods are used. 5 X 5 mm rod and 4 X 4 mm rod with circular go-through hole. According to the online store from where the gears were purchased, the material for gear was high density plastic.

### 5.1.4 Assembly

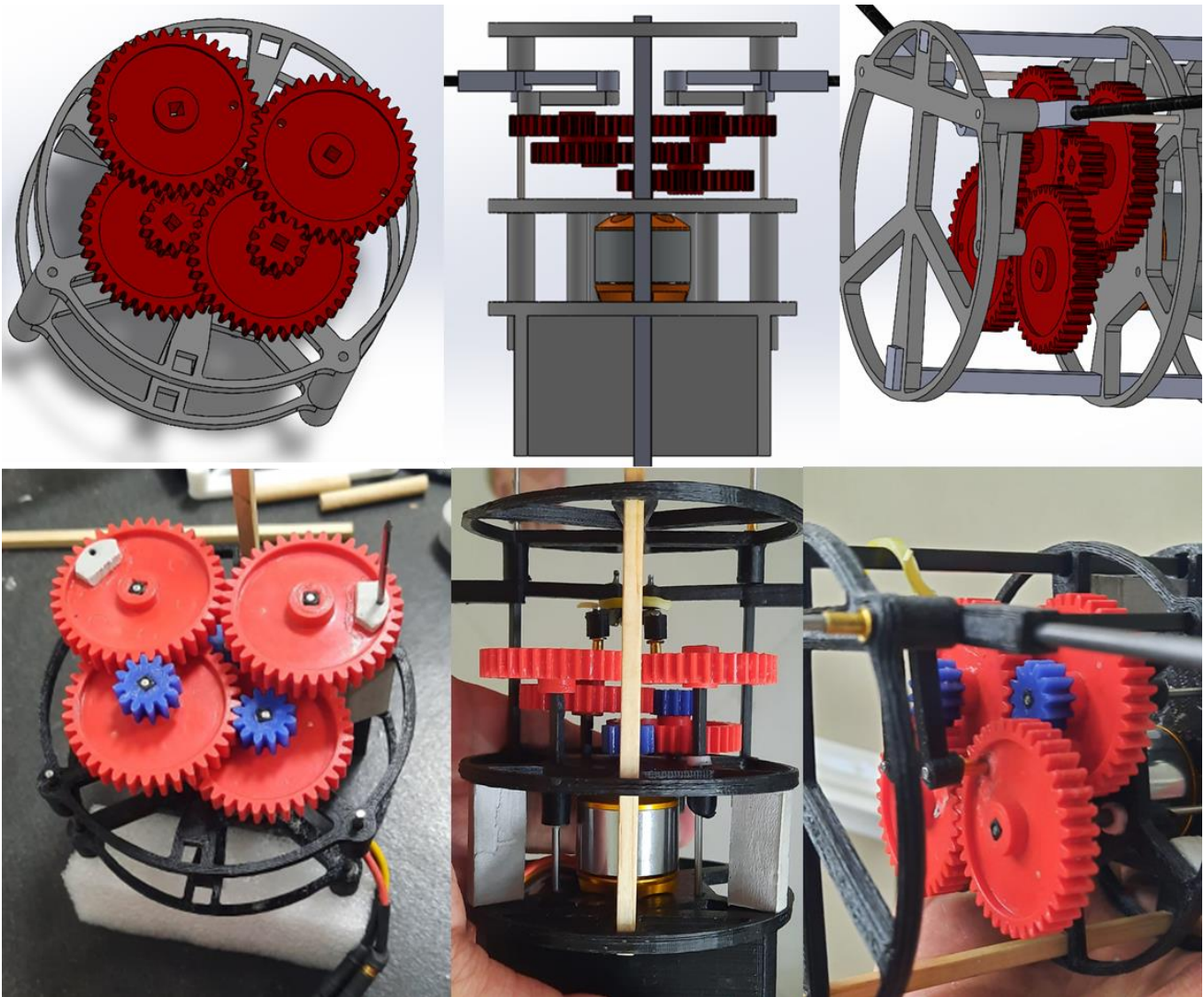


Figure 5.4: Complete Gear assembly

Since compound gears were required for the gearbox, we needed to join the spur gears. The first approach was gluing them together, but later it was discovered that more strength is required in this particular joint. Therefore, we decided to use half square – half circular shaft which will hold both gears together and the circular part can rotate freely in the sleeves of the mountings shown above. Figure 5.5 shows assembly of the compound gear.

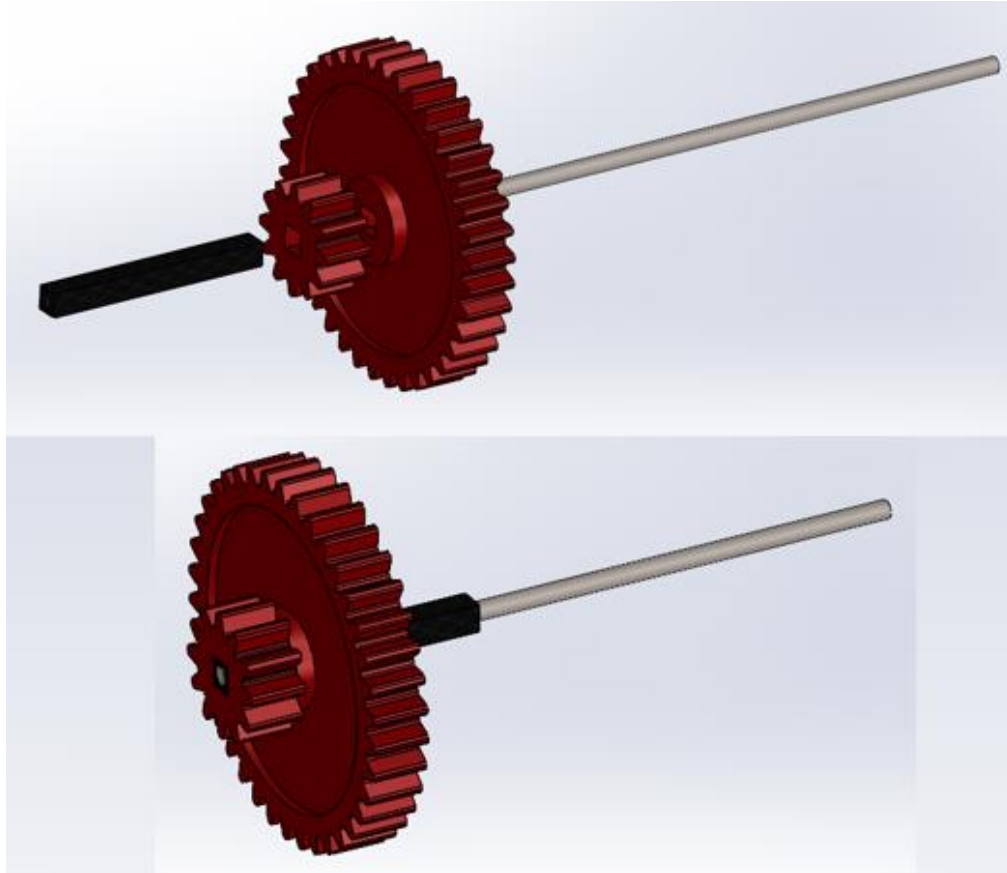


Figure 5.5: compound gear assembled through square shaft

## 5.2 Wings

The material selection of wings has much more importance than material selection of any other part. In all other cases, we only needed to check the strength and the density of the material, but for wings we also had to take elasticity into account. If material is very less elastic, then wings will eventually lose the initial tension. If wings were too elastic then the load on the gearbox will increase.

## 5.2.1 Dimensions

Figure 5.6 shows the final dimensions of the ornithopter's wing.

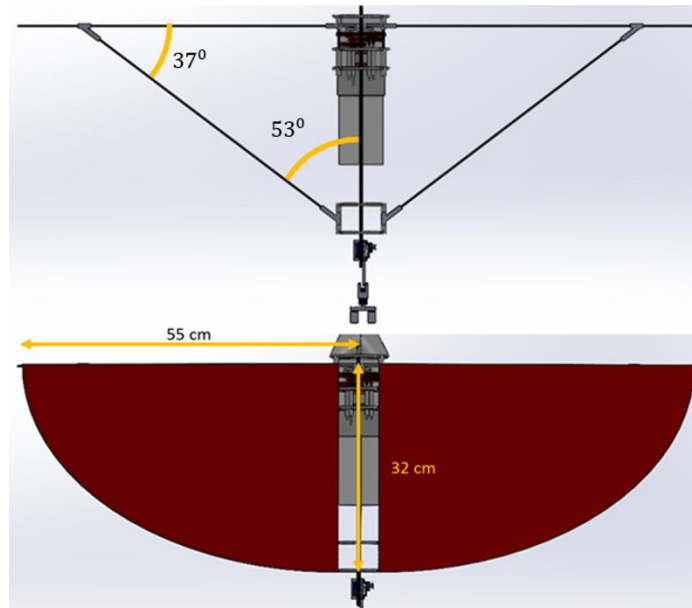


Figure 5.6: Dimensions of the wing

## 5.2.2 Wingspar and wingspar supports

Figure 5.7 shows the CAD models and assembly of the wingspars and wingspar supports.

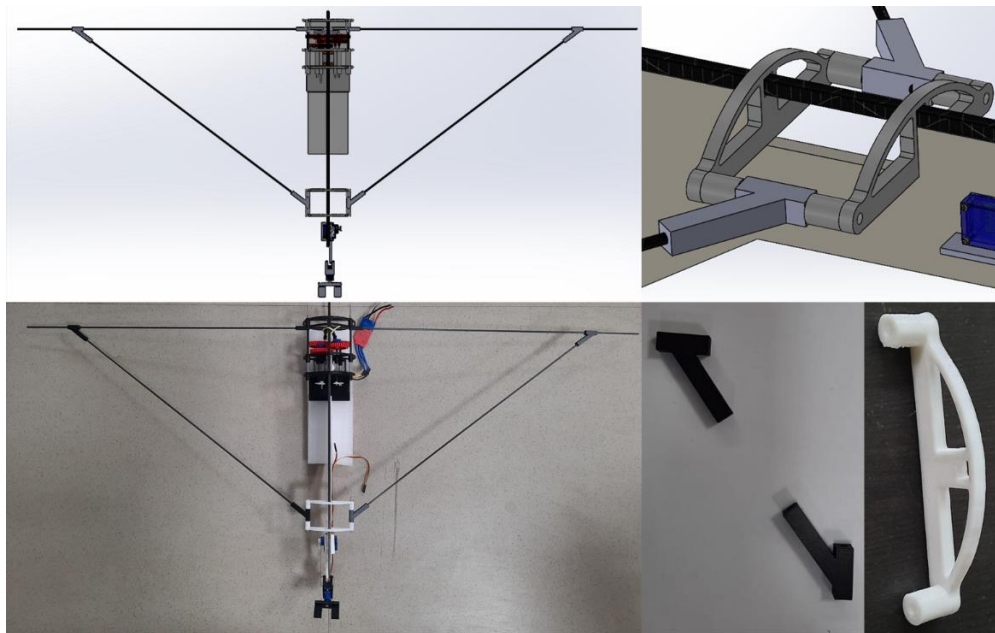


Figure 5.7: CAD Model and assembly of wingspar

### 5.1.3 Material

Three different kinds of wings material were tested. For wingspars or support rods, very light material with enough tensile strength to sustain bending was required. Balsa wood and carbon fibre were the recommended options. Both materials are sufficiently strong and light. Carbon fibre had better surface finish. Also, a lot of models in literature have used carbon fibre for wingspars, so we decided to do the same. The wing supports were again 3D printed with 60% infill density.



Figure 5.8: finely knit cotton fabric vs polythene plastic

For lamina of wing, we considered three options. Plastic from polythene bag, cloth from umbrella and lastly finely knitted cotton fabric. The latter two options were rejected because both of them were too heavy. Moreover, the umbrella cloth was tearing apart when we tried to sew it.

### 5.3 Tail Assembly

Tail assembly was inspired from previously built ornithopter model Phoenix [19]. Except the connecting rod, every other part was either purchase or 3D printed. So assembling the tail was easy job.

### 5.1.2 CAD Model of parts and assembly

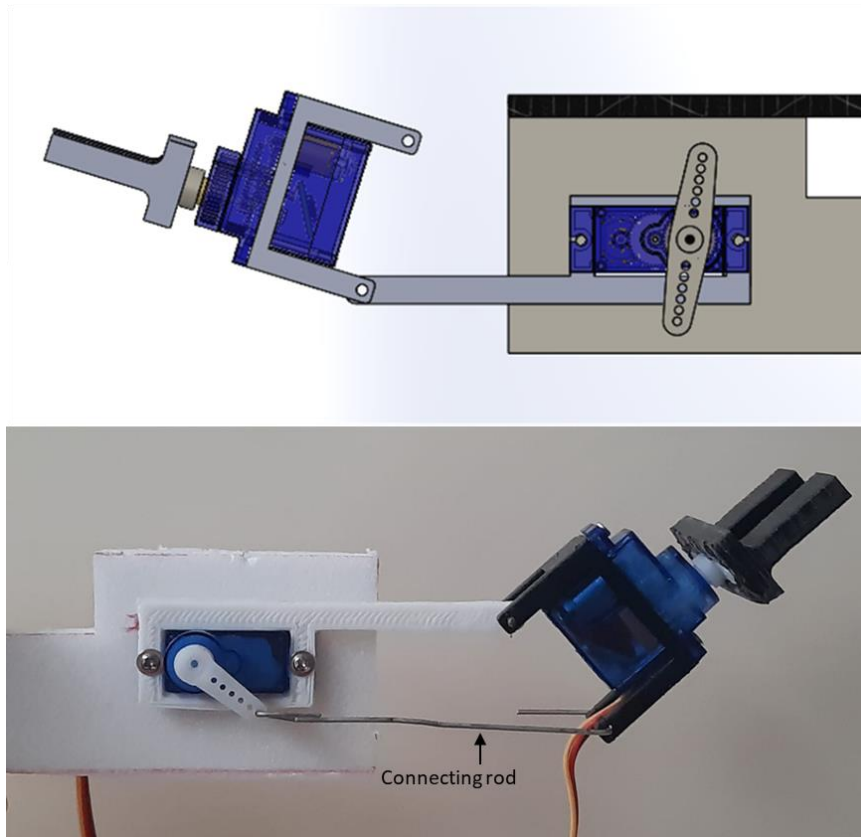


Figure 5.9: Tail Assembly

### 5.4 Complete Model

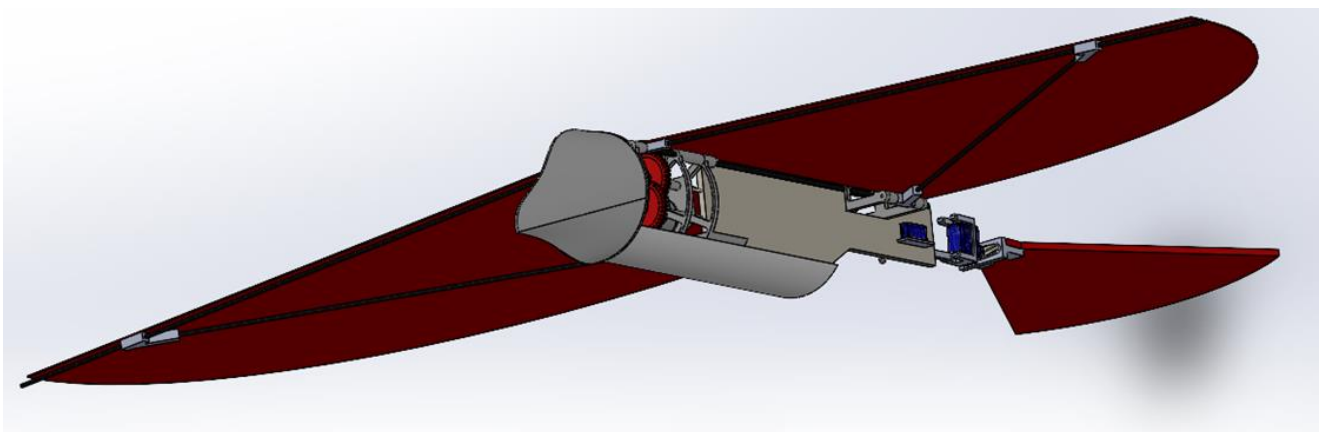


Figure 5.10: Complete CAD model



Figure 5.11: Completed Ornithopter

## Chapter 6

# Electronics

Electronics systems are essential part of any robot. In this chapter, we have explained the selection of various components and their integration into a circuit. Two circuits were used for this model. The first one uses manual remote control, which will be helpful for assisted flight tests. Other system has on board computer, IMU (inertial measurement unit) and two ways communication feature. The second system is provision for implementing fully fledge control system.

### 6.1 Actuators

There are three actuators used in this model: two servos and one BLDC motor. Specifically, Tower Pro SG90 servo and A2212 10T 1400KV BLDC motor. These actuators are chosen because of their low weight, cheap cost and easy availability in market. The BLDC motor is available in different RPM ratings so we had flexibility while designing the gearbox. Tower Pro SG90 servo are very small servos widely used in robotics application. The relevant details and pictures are shown in table 6.1.

Model	SG90	Model	A2212 10T
Weight(gm)	9	Motor KV (RPM/V)	1400
Operating Voltage (VDC)	3.0 ~ 7.2	Compatible LiPO Batteries	2S ~ 3S
Operating Speed @4.8V	0.10sec/60°	Shaft Diameter (mm)	3.17
Stall Torque @ 4.8V (Kg-Cm)	1.2	Current Handling Capacity (A)	16
Stall Torque @6.6V (Kg-Cm)	1.6	Max. Efficiency Current (A)	6 ~ 12
Gear Type	Glass Fiber	No-Load Current (mA)	700
Rotational Degree	180°	Maximum Efficiency	80%
Length (mm)	22.8	Length (mm)	27.5
Width (mm)	12.6	Weight (gm)	72
Height (mm)	34.5	Width (mm)	27
Shipment Weight	0.014 kg	Shipment Weight	0.078 kg

Table 6.1: Servo and Motor specifications

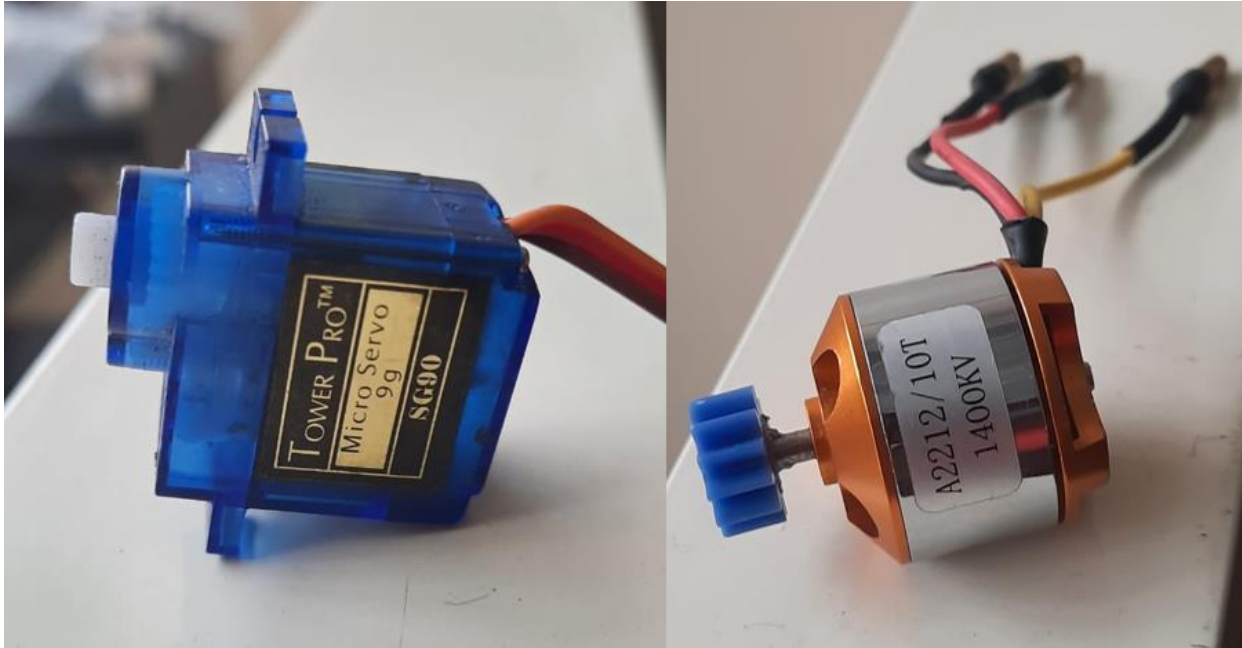


Figure 6.1: Tower Pro SG90 servo and BLDC motor

## 6.2 Electronic Speed controller (ESC)

For controlling BLDC motor, we need electronic speed controller. Simonk was chosen for this purpose. Since the lowest available current rating for these ESCs is 30A, the same was used in the model. As seen previously, maximum current handled by A2212 motor is 16A, so 30A ESC is more than sufficient.



Model	SIMONK 30A
Burst Current (A)	40
Constant Current (A)	30
BEC	Yes (5V/2A)
Dimensions (mm) LxWxH	45 × 24 × 9
Weight (gm)	23
Suitable Lipo Batteries	2 ~ 3S

Figure 6.2: Simonk 30A

## 6.3 Power Supply

Out of all power consuming components, BLDC motor draws most of the power. Therefore, we can neglect power consumption by other components. For power source, Lithium Polymer rechargeable batteries are used. The specification is decided by required runtime of the model. Since battery mass increases with battery capacity, runtime was reduced to only 2 minutes.

Referring to Table 6.1, we can assume that the motor continuously draws 12 A current at 80% efficiency. We will be using 3S rated batteries for which output voltage is approx. 11.5 volts.

Hence,

$$80\% \text{ of Battery capacity} = (12 \text{ A}) \times (2 \text{ minutes}) = 12000 \text{ mA} * 0.0333 \text{ h} = 400 \text{ mAh}$$

$$\text{Battery capacity} = 500 \text{ mAh.}$$

Note that, above calculations are conservative and actual runtime may be much longer due to the fact that, battery will not draw 12 A continuously. Considering the calculated estimate of battery capacity, *Bonka Ultra Light U2 Series Lipo Battery* with 460 mAh capacity was chosen. The battery is shown in figure 6.3.



Figure 6.3: Bonka Ultra Light U2 Series Lipo Battery

Above battery has discharge rating of 45C with very compact dimensions 6.5 X 3 X 1.5 cm. Overall weight of battery is 50 gm.

## 6.4 Computer (Arduino Nano)

Arduino is the most popular computer among roboticists. It is microcontroller based on ATmega328P. It can be easily programmed to implement simple control systems. Among various available versions of Arduino, Arduino nano is best fit for this project as it weighs only 7 grams and has very compact construction (18 X 45 mm). It can be easily used with MPU6050 and nrf24l01 transceiver module. Moreover, it has inbuilt voltage regulator which can take input voltage from 6 to 12 volts. It is more than sufficient to run a control system of an ornithopter, which is evident from its clock speed of 16MHz.



Figure 6.4: Arduino nano V3.0

## 6.5 Inertial measurement unit (MPU6050)

MPU6050 inertial measurement unit contains a 3 axis Accelerometer and Gyroscope in a single package. The 6 Degree of Freedom sensor breakout integrate with the MPU6050 sensor and the low noise 3.3v regulator and pull-up resistors for the I2C bus. So, it can be directly hooked up to an Arduino board.

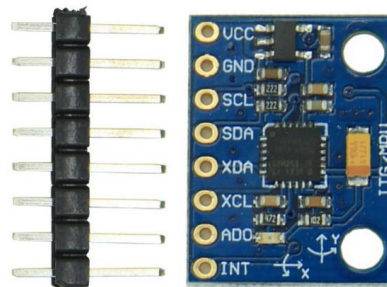


Figure 6.5: MPU6050

## 6.6 Radio communications

Radio communications can be one-way or two-way. The first one is usually used in remote controlled toys and planes whereas the later is used in fully fledged control systems where ground station requires sensor data from the vehicle. We have both types of Radio Frequency (RF) controls for our model. The Fly Sky FS-CT6B 6-Channel 2.4 GHz Transmitter and Receiver pair is one-way communication system and NRF24L01 2.4GHz Wireless Transceiver Modules are used to build two-way communication system.

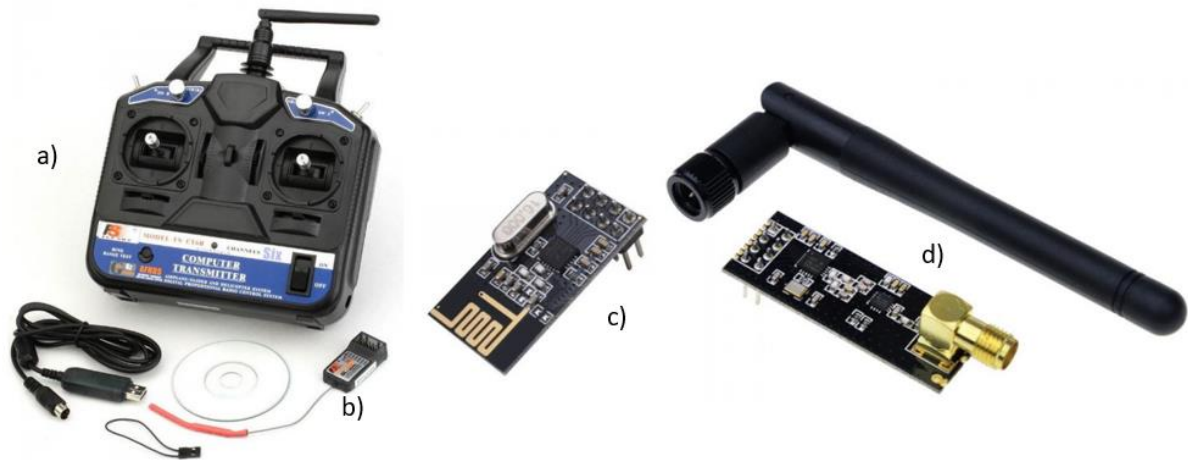


Figure 6.6: Radio Frequency Modules

a) Fly Sky transmitter; b) Fly Sky receiver; c) NRF24L01; d) NRF24L01 PA+LNA SMA;

The Fly Sky FS-CT6B Transmitter is programmable with several built-in settings for common UAVs such as Quadrotor and planes. On the other hand, NRF24L01 modules needs to be hooked up with Arduino, dedicated power line through voltage regulator and programming from scratch. Both versions C and D shown in figure 6.6 can be used as a replacement for each other. However, version C contains bare minimum to run the circuit whereas version D features a reverse polarized SMA connector for maximum RF range, and there is PA (power amplifier) and LNA (low noise amplifier) circuit on board, with the external antenna so it can reach longer distance than version C. NRF24L01 was clearly best choice because of lightweight design (10 gm), Long range ( up to 1000 m in open air), two-ways communication (i.e. it is transreceiver module) and up to 250 kbps communication speed.

## 6.7 Manual system

The purpose of manual system is to increase ease of experimenting with model, while it is still in design phase. The schematic is shown below.

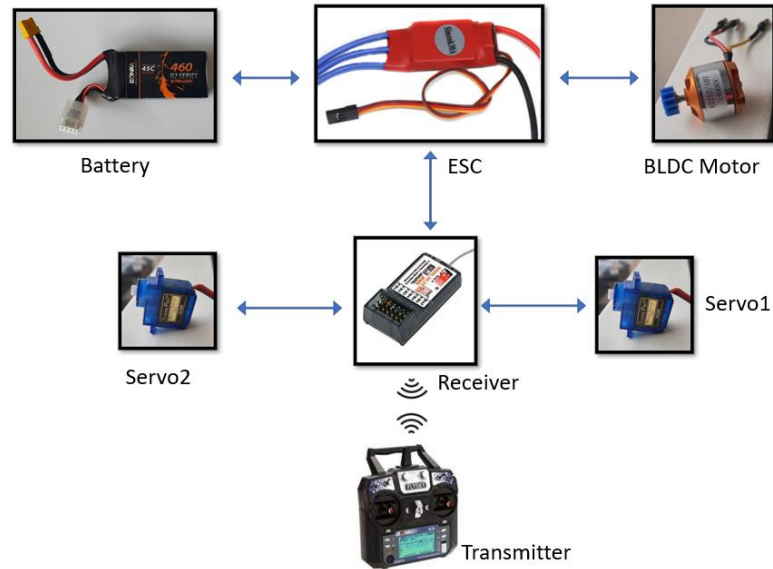


Figure 6.7: Manual System

## 6.8 Automatic system

As mentioned earlier, the purpose of automatic system is to make provision for implementation of control system. With following schematic, we can program the model to be fully autonomous or manually controlled or with hybrid control system. For example, the user can have directional control and onboard control system can be used for pitch stability.

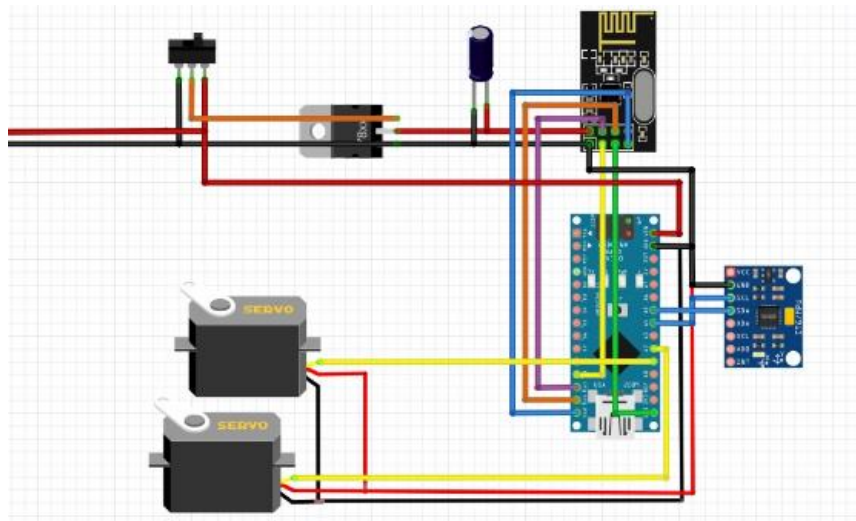


Figure 6.8: Schematic of automatic system

## Chapter 7

# Aerodynamic Model of flapping flight

This chapter presents mathematical model of flapping flight and its implementation in using MATLAB-Simulink. It is 6-DoF closed loop simulation model, where real time kinematics and dynamics of an ornithopter can be observed.

Purpose of this simulation is to get an insight of the control parameters and how they affect the motion of the ornithopter. Although I have taken a simplistic approach for modelling aerodynamic forces and moments, it serves its purpose quite well.

provisions are given in Simulink model so it can be developed further to include a fully-fledged control system. For now, we have simulated the dependence of control parameters such as flapping frequency controlled by throttle to BLDC motor and one of the tail angles controlled by independent servos.

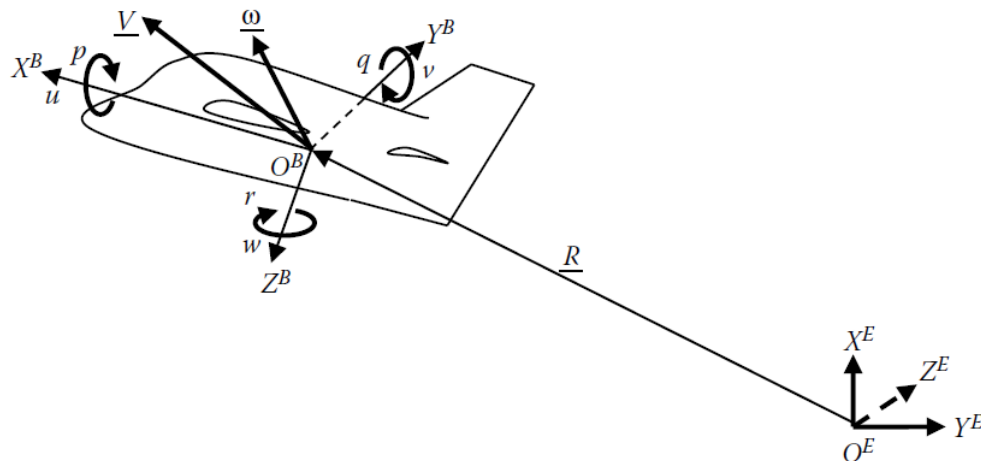


FIGURE 1.7 Sketch of an aircraft in flight with  $X^B Y^B Z^B$  axes fixed to its center of gravity (CG)  $O^B$ , velocity vector  $V$  at CG, and angular velocity vector  $\omega$  about the CG, axes  $X^E Y^E Z^E$  fixed to the Earth, position vector  $R$  from origin ( $O^E$ ) of  $X^E Y^E Z^E$  to aircraft CG ( $O^B$ ).

Figure 7.1: Frame of references used in aircraft dynamics [32]

Figure 7.1 shows the different frames of reference used in aerodynamics textbook. We have used same notation as in book [32].

## 7.1 Definitions and Nomenclature

Symbol / Representation	Description
$\langle X_E Y_E Z_E \rangle$	Position of Centre of Mass of model with respect to earth frame.
$\langle \dot{X}_E \dot{Y}_E \dot{Z}_E \rangle$	Velocity of Centre of Mass of model with respect to earth frame.
$\langle u v w \rangle$ or $V_B$	Velocity of Centre of Mass of model with respect to body frame.
$\langle p q r \rangle$ or $\omega_B$	Angular velocity of Centre of Mass of model with respect to body frame.
$\langle \phi \theta \psi \rangle$	Euler Angles
$\delta_e$	Tail-elevation angle
$\delta_r$	Tail-roll angle
$f$	Flapping Frequency in Hz
$\beta$	Angle between Chord of an airfoil strip and fuselage when both are projected on the plane of bilateral symmetry of the model.
$\gamma$	Flapping angle
$m$	Mass of the model
$\begin{bmatrix} I_{xx} & -I_{yx} & -I_{zx} \\ -I_{xy} & I_{yy} & -I_{zy} \\ -I_{xz} & -I_{yz} & I_{zz} \end{bmatrix}$	Inertia Matrix of the model along body frame axes.

Table 7.1: Important terms and their definitions

## 7.2 Mathematical Model

The ornithopter in this model has three major parts which move relative to each other, namely wings, tails and main body. For describing the complete model, we need different frames of reference which are attached to these moving parts. The locations of these frames of references are shown below:

## 7.2.1 Frames of Reference

All frames are in cartesian coordinate system following right hand rule. These are shown in figure 6.3.

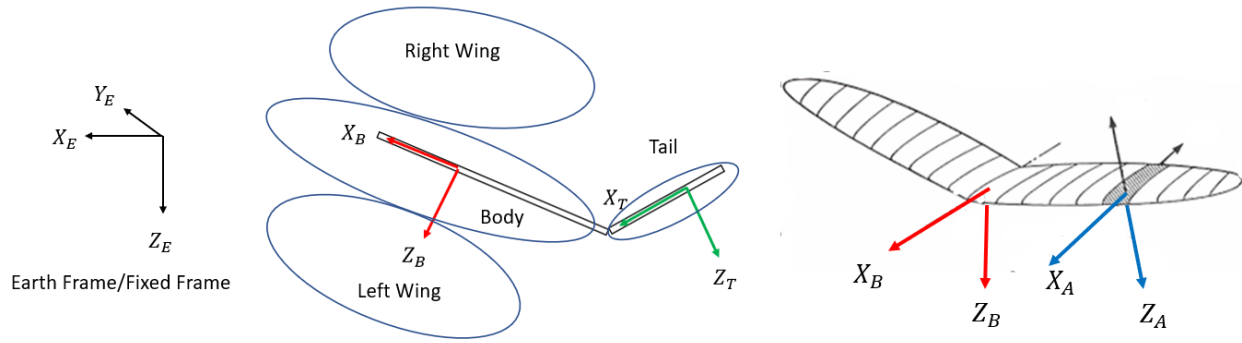


Figure 7.2: Frames of Reference

### 1) *Earth frame:* $\{X_E, Y_E, Z_E\}$

This is inertial frame of reference, whose origin is coincident on the ground. It is denoted by subscript E.

### 2) *Body frame:* $\{X_B, Y_B, Z_B\}$

This frame of reference's origin is attached to the centre of mass of the ornithopter. The X-axis points towards from head and Z-axis points towards legs. Since the model can accelerate, this is non-inertial frame of reference. It is denoted by subscript B.

### 3) *Tail frame:* $\{X_T, Y_T, Z_T\}$

This non-inertial frame's origin is attached to geometric centre of tail. The orientation of frame is obtained by rotating body frame, by tail elevation angle around body frame's Z-axis. It is denoted by subscript T.

### 4) *Airfoil frame:* $\{X_A, Y_A, Z_A\}$

We use this non-inertial frame in context of modified strip theory. Its origin is situated at quarter-chord location of the airfoil. It is denoted by subscript A.

## 7.2.2 Rotation Matrices

The rotation matrices will be defined here to convert vectors from one frame of reference to another. Earth frame to body frame conversion is done using Euler angles: Roll, pitch and Yaw denoted by  $(\phi, \theta, \psi)$  respectively. More detailed description can be found in aerospace engineering textbooks such as []. The 3-2-1 convention is followed as shown in figure 6.4.

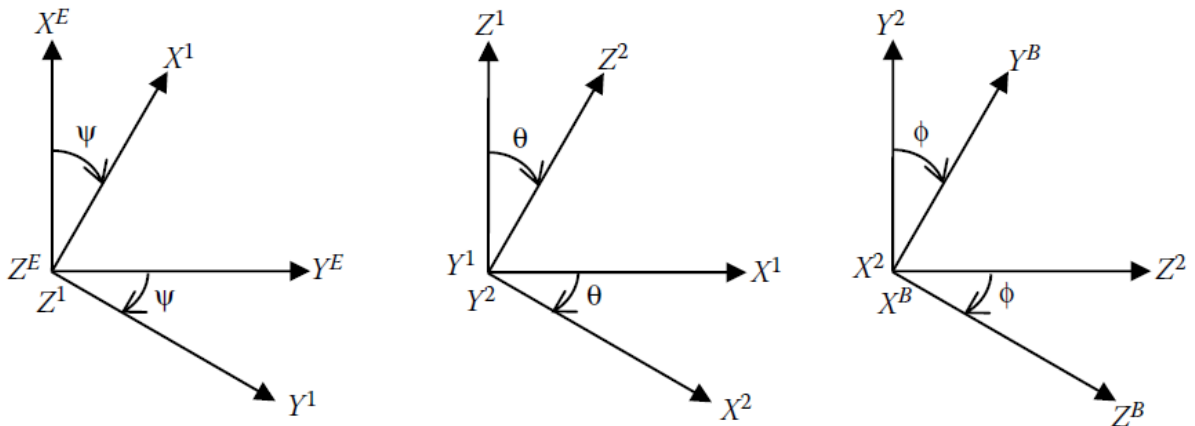


Figure 7.3: 3-2-1 convention of Euler angles

Any vector described in body frame can be described in earth frame by following equation. Here we adopt convention of denoting rotation matrices by R followed by subscripted angle.

$$\begin{bmatrix} X_B \\ Y_B \\ Z_B \end{bmatrix} = \begin{bmatrix} 1 & 0 & 0 \\ 0 & \cos \phi & \sin \phi \\ 0 & -\sin \phi & \cos \phi \end{bmatrix} \begin{bmatrix} \cos \theta & 0 & -\sin \theta \\ 0 & 1 & 0 \\ \sin \theta & 0 & \cos \theta \end{bmatrix} \begin{bmatrix} \cos \psi & \sin \psi & 0 \\ -\sin \psi & \cos \psi & 0 \\ 0 & 0 & 1 \end{bmatrix} \begin{bmatrix} X_E \\ Y_E \\ Z_E \end{bmatrix} = R_\psi R_\theta R_\phi \begin{bmatrix} X_E \\ Y_E \\ Z_E \end{bmatrix}$$

Similarly using properties  $R_\psi^T = R_\psi^{-1}$ ,  $R_\theta^T = R_\theta^{-1}$  and  $R_\phi^T = R_\phi^{-1}$ , we can write

$$\begin{bmatrix} X_E \\ Y_E \\ Z_E \end{bmatrix}^T = R_\phi^T R_\theta^T R_\psi^T \begin{bmatrix} X_B \\ Y_B \\ Z_B \end{bmatrix}^T$$

Similarly tail frame is linked with body frame by rotation matrices of tail angles. Firstly, the body frame is rotated about its Y-axis by tail elevation angle ( $\delta_e$ ) to get an intermediate frame of reference as shown in figure 7.4. Then the intermediate frame is rotated about its X-axis by tail-roll angle ( $\delta_r$ ) to get tail frame.

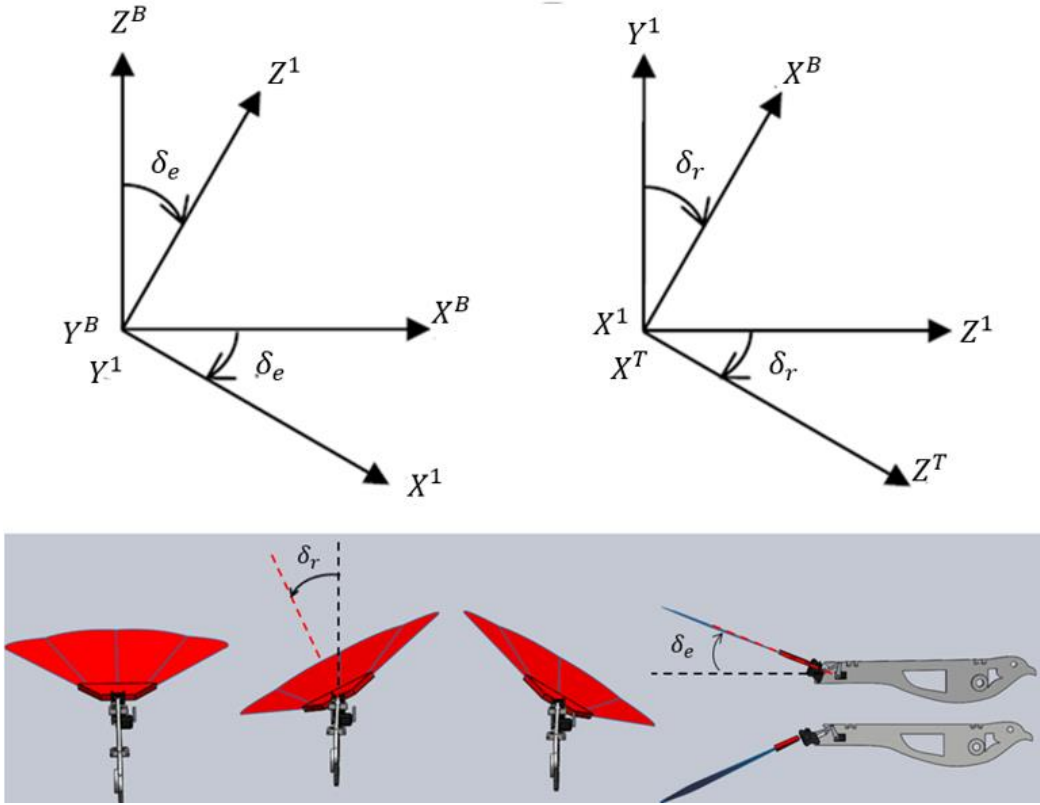


Figure 7.4: Convention for Tail angles

$$\begin{bmatrix} X_T \\ Y_T \\ Z_T \end{bmatrix} = \begin{bmatrix} 1 & 0 & 0 \\ 0 & \cos \delta_r & \sin \delta_r \\ 0 & -\sin \delta_r & \cos \delta_r \end{bmatrix} \begin{bmatrix} \cos \delta_e & 0 & -\sin \delta_e \\ 0 & 1 & 0 \\ \sin \delta_e & 0 & \cos \delta_e \end{bmatrix} \begin{bmatrix} X_B \\ Y_B \\ Z_B \end{bmatrix} = R_{\delta_r} R_{\delta_e} \begin{bmatrix} X_B \\ Y_B \\ Z_B \end{bmatrix}$$

Similarly, airfoil frame is linked with body frame by rotation matrices of flapping angle ( $\gamma$ ) and pitching angle ( $\beta$ ). Firstly, the body frame is rotated about its X-axis by flapping angle ( $\gamma$ ) to get an intermediate frame of reference. Then the intermediate frame is rotated about its Y-axis by pitching angle ( $\beta$ ) to get airfoil frame. This relation will be explained further in kinematics section.

$$\begin{bmatrix} X_A \\ Y_A \\ Z_A \end{bmatrix} = \begin{bmatrix} \cos \beta & 0 & -\sin \beta \\ 0 & 1 & 0 \\ \sin \beta & 0 & \cos \beta \end{bmatrix} \begin{bmatrix} 1 & 0 & 0 \\ 0 & \cos \gamma & \sin \gamma \\ 0 & -\sin \gamma & \cos \gamma \end{bmatrix} \begin{bmatrix} X_B \\ Y_B \\ Z_B \end{bmatrix} = R_{\beta} R_{\gamma} \begin{bmatrix} X_B \\ Y_B \\ Z_B \end{bmatrix}$$

## 7.3 Simulink model

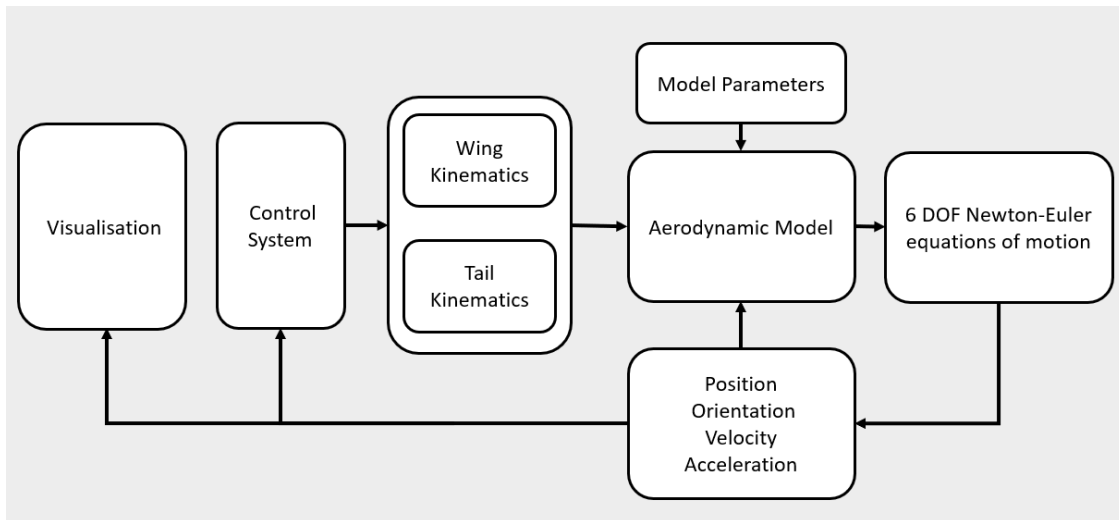


Figure 7.5: Simulink Model

The Simulink model have multiple blocks performing specific functions. The model runs in closed loop simulation as shown in figure 7.5. There are three control parameters: flapping frequency, tail-elevation angle and tail-roll angle, which are input signals in Simulink environment. These signals are given by user before running the simulation as a imitation to manual control of ornithopter. Wing and tail kinematics depend on these control parameters, which are used to calculate aerodynamic forces on the model. Then by integrating equations of motion, we get updated position, velocity and acceleration (i.e., kinematics of model). Hence the term close loop simulation is used to describe this model. The essential details of individual blocks are given below:

### 7.3.1 Wing and Tail kinematics

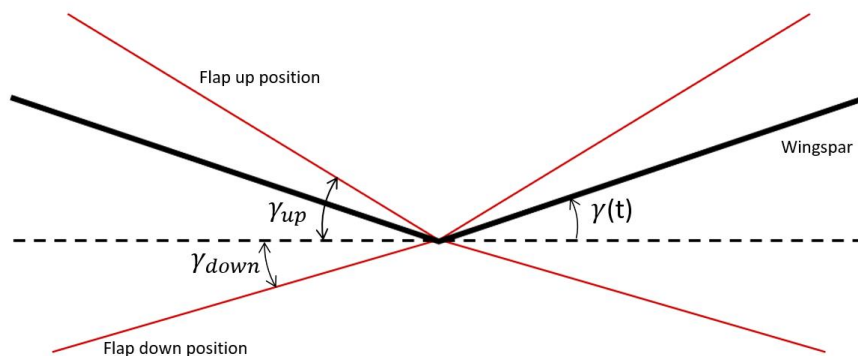


Figure 7.6: Definition of flapping angle

The flapping angle  $\gamma$  is shown in figure 7.6. It is directed angle between horizontal / neutral positions of wingspars (dotted line) and current time dependent position of wingspars (bold line). We assume sinusoidal flapping motion which is given by:

$$\gamma(t) = \left(\frac{\gamma_{up} + \gamma_{down}}{2}\right) \sin(2\pi ft) + \left(\frac{\gamma_{up} - \gamma_{down}}{2}\right)$$

Where  $f$  is the flapping frequency in Hz,  $\gamma_{up}$  and  $\gamma_{down}$  are respective magnitudes of upper and lower flapping angles shown above.

Pitching angle  $\beta$  is directed angle between chord line of a strip described in MST (Modified strip theory) and fuselage, when both are projected on bilateral symmetry plane of the ornithopter. ( $X_B Z_B$  plane in figure 7.7). The value of  $\beta$  depends on time as well as position of the strip from fuselage. We assume that pitching motion is linear across the wingspan and its value varies sinusoidally with respect to time. Its expression is given below:

$$\beta(t, y) = \frac{y}{L} (\beta_0 + \beta_{max} \sin(2\pi ft + \phi))$$

Where  $L$  is half of the wingspan,  $y$  is distance of the strip from the fuselage,  $\beta_0$  is offset in sinusoidal motion,  $\beta_{max}$  is amplitude,  $f$  is flapping frequency in Hz and  $\phi$  is phase difference between flapping motion and pitching motion. As per literature, both motions are out of phase so we consider  $\phi = 90^\circ$ .

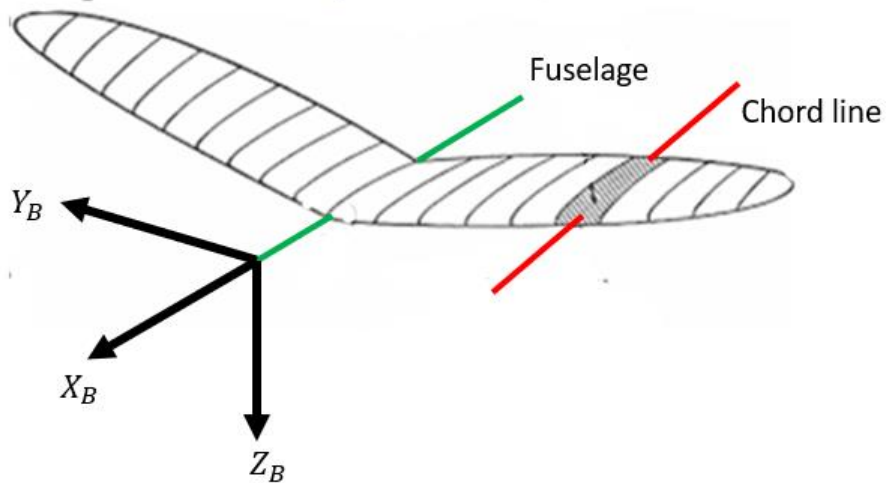


Figure 7.7: Definition of pitching angle

Tail kinematics are pretty straightforward as shown below. Tail elevation angle is directed angle about Y-axis of Tail frame whereas tail roll angle is directed angle about X-axis of tail frame.



Figure 7.8: Tail Angles

### 7.3.2 Equations of motion

The Newton-Euler equations of motion are derived in [32] , which are presented below.

*Translational Equations of motion in non-inertial frame:*

$$F_B = m \begin{bmatrix} \dot{u} \\ \dot{v} \\ \dot{w} \end{bmatrix} + m \begin{bmatrix} 0 & -r & q \\ r & 0 & -p \\ -q & p & 0 \end{bmatrix} \begin{bmatrix} u \\ v \\ w \end{bmatrix}$$

*Rotational Equations of motion in non-inertial frame:*

$$M_B = \begin{bmatrix} I_{xx} & -I_{yx} & -I_{zx} \\ -I_{xy} & I_{yy} & -I_{zy} \\ -I_{xz} & -I_{yz} & I_{zz} \end{bmatrix} \frac{d}{dt} \Big|_B \begin{bmatrix} p \\ q \\ r \end{bmatrix} + \omega_B \times \begin{bmatrix} I_{xx} & -I_{yx} & -I_{zx} \\ -I_{xy} & I_{yy} & -I_{zy} \\ -I_{xz} & -I_{yz} & I_{zz} \end{bmatrix} \begin{bmatrix} p \\ q \\ r \end{bmatrix}$$

### 7.3.3 Aerodynamic Model

We will be using following assumptions:

#### 1. *Quasi-steady approximation*

According to the quasi-steady assumption, the instantaneous aerodynamic forces on a flapping wing are equal to the forces during steady motion of the wing at an identical instantaneous velocity and angle of attack. The essence of a quasi-steady analysis is the assumption that the instantaneous forces on a wing are determined by its current motion and thus do not depend on the history.

#### 2. *Modified Strip Theory*

We divide the wing into finite number of strips (as shown in figure 7.9) and assume that airflow over each strip is chordwise. So, the aerodynamic forces on that strip can be calculated independently without considering influence of overall wing. i.e., Aerodynamic forces and moments on each strip are completely determined by flow over that strip. The MST was developed in Professor Delaurier's work which can be found here [1].

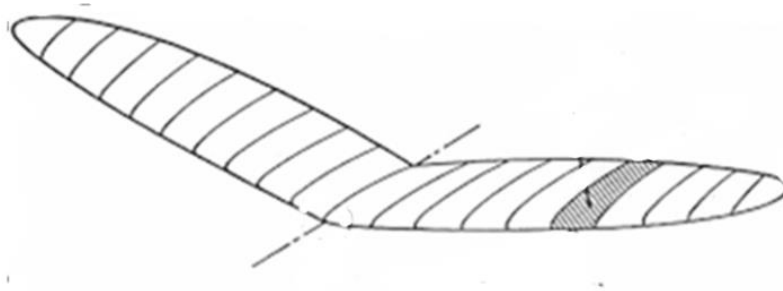


Figure 7.9: Modified Strip theory: breaking wing into chordwise elements

### 3. Point Mass Assumption

The model's overall mass is situated at its centre of mass. Wings and tails are massless.

### 4. Wing kinematics

As discussed in section 3.1, birds' wings exhibit complex motions. For sake of simplicity, we assume that our model exhibits flapping and passive pitching motion.

Now, since we have established the assumptions, the procedure for calculating instantaneous Force and Moment on the model can be explained. The total aerodynamic force and moment on model is vector sum of force and moment on individual strip of the wing.

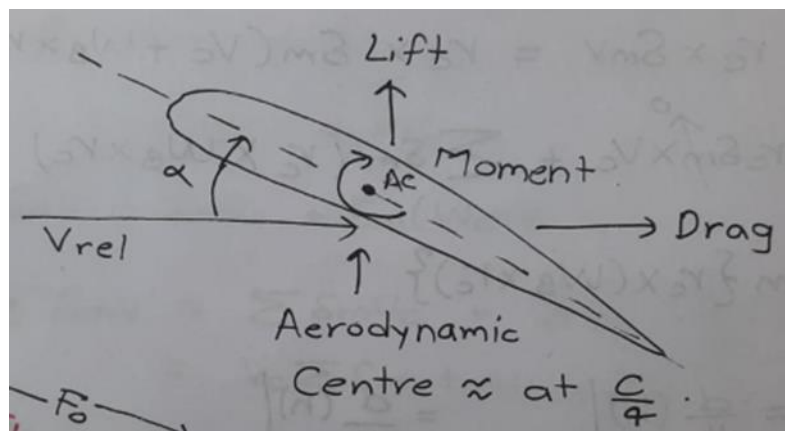


Figure 7.10: Forces on Airfoil

As shown in Figure 7.10, lift force is perpendicular to the direction of air flow and drag force is in its direction. We assume that aerodynamic centre of airfoil is at quarter-chord length which is the standard result of thin airfoil theory. Moreover, the expressions for these forces are given below:

$$L = \frac{1}{2} \rho A V_{rel}^2 C_L \quad \text{and} \quad D = \frac{1}{2} \rho A V_{rel}^2 C_D$$

From [citations] we assume that,

$$C_L = C_{L,MAX} \sin(2\alpha)$$

$$C_D = C_{D,90^\circ} \sin^2 \alpha + C_{D,0^\circ} \cos^2 \alpha$$

Where values of  $C_{L,MAX}$ ,  $C_{D,90^\circ}$  and  $C_{D,0^\circ}$  can be approximated from the graph in figure 7.11,

$C_{L,MAX} = 1.2$ ,  $C_{D,90^\circ} = 2$  and  $C_{D,0^\circ} = 0.2$ .

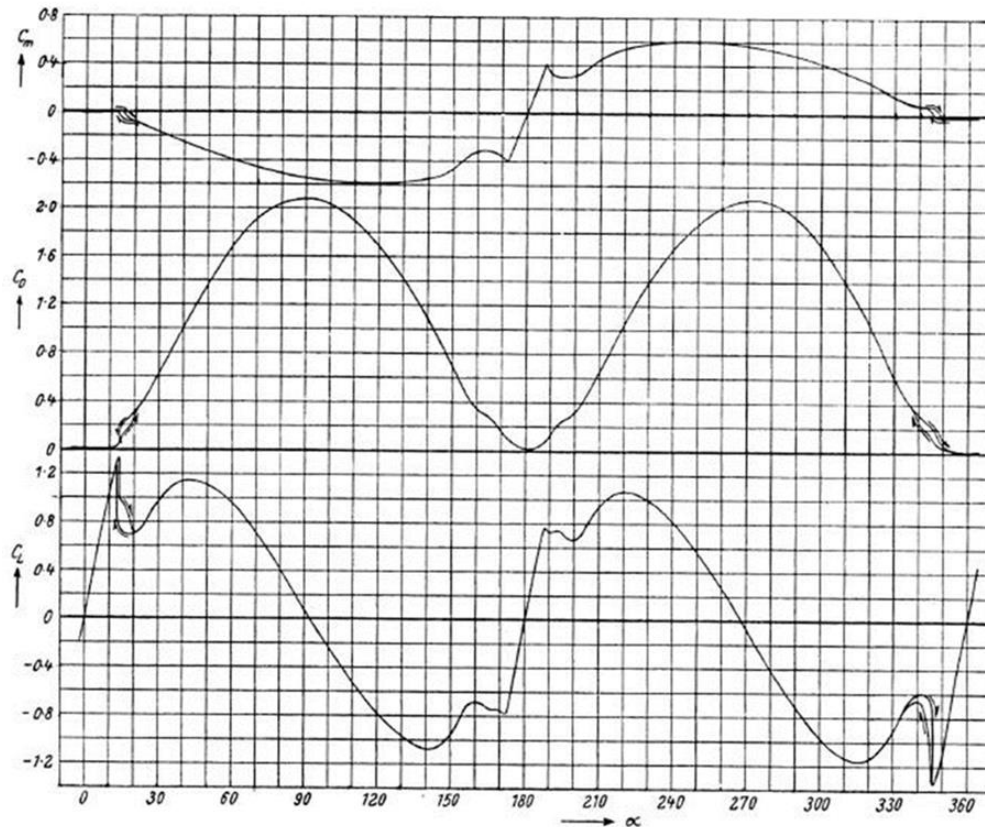


Fig. 12.105a. NACA 0012.  $R = 1.8 \cdot 10^6$ . Wind tunnel: TDT. (N 3361)

Figure 7.11: NACA 0012 Aerodynamic Coefficients

For calculating forces on a strip of the wing, we calculate the velocity of the aerodynamic centre of the strip (assumed at the quarter-chord length) in airfoil frame of reference ( $V_{rel}$ ). Note that this is absolute velocity of aerodynamic centre so it includes translation and rotation of whole bird along with flapping and pitching motion.

$$\text{i.e., } V_{rel} = V_c + \omega_c \times r_c + V_{flapping} + V_{pitching}$$

Then we calculate the directed angle from chord line to the direction of velocity which is angle of attack ( $\alpha$ ). Since we already know the area of the strip ( $A$ ) and density of the air ( $\rho$ ), we can calculate the lift and drag forces using above equations.

These lift and drag forces are applied at the aerodynamic centre of that particular strip. The vector sum of the forces from all such strips will give the total force on the centre of mass of the model. Note that, these forces also generate moment around the centre of mass, which will result into total moment after integrating. The process will become clearer by following image.

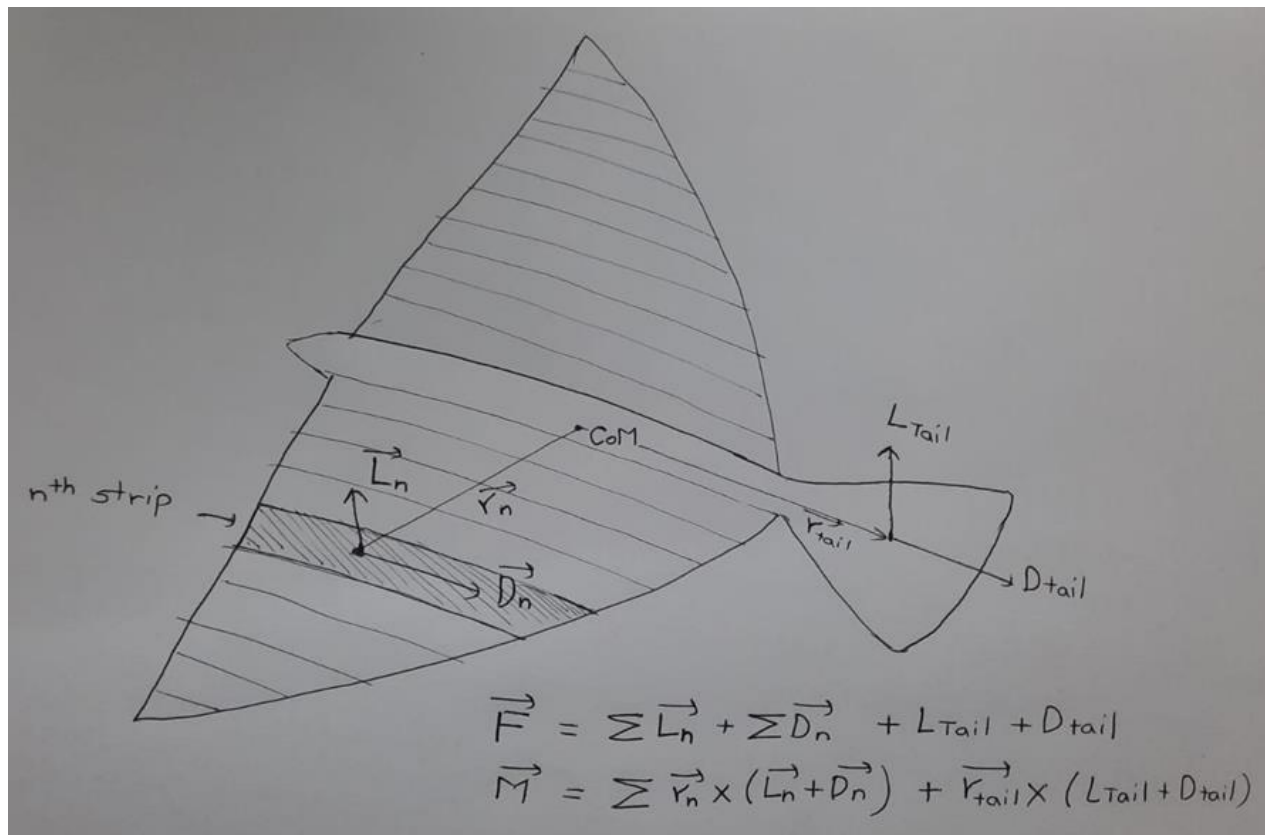


Figure 7.12: Total Force and Moment at Centre of Mass (CoM)

The aerodynamic model block outputs the total force and total moment to next block which is equations of motion.

### 7.3.4 Model Specific parameters

This block provides model specific parameters like wingspan, mass, inertia Matrix. We can simulate different models by changing parameters in this block.

Air Density	1.25 kg/m <sup>3</sup>	Calculated
BetaMax	10 deg.	Experimental
BetaNot	0 deg.	Experimental
Phase difference	90 deg.	Literature
Fuselage length	0.32	Model Specification
GammaUp	55.34	Model Specification
GammaDown	6.2	Model Specification
Inertia Matrix (Kgm <sup>2</sup> )	$\begin{bmatrix} 0.0283 & 0 & -0.000094 \\ 0 & 0.0546 & 0 \\ -0.000094 & 0 & 0.0437 \end{bmatrix}$	Measured in Solidworks CAD model
Mass	0.390 kg	Measured
Tail Area	0.3324 m <sup>2</sup>	Calculated
Tail Centre Distance	0.16 m	Calculated
Number of strips in MST	51	Experimental
Wing Length	55 cm	Model specification

Table 7.2: Model Specific Parameters

### 7.4 Simulation Results

Closed loop simulation of a physical scenario is simulated by varying flapping frequency with tail elevation angle to obtain the safe zone chart. The physical scenario was throwing the model with 9 m/s velocity at 10-degree angle from horizontal. Since we do not want any discontinuity in the simulation, we use exponential mask for flapping and pitching motion to increase them slowly from 0 to their maximum value in first few seconds of the simulation.

$$\gamma_{output} = (1 - e^{-0.5t})\gamma(t)$$

$$\beta_{output} = (1 - e^{-0.5t})\beta(t)$$

### 7.4.1 Safe Zone Chart

With initial velocity of 9 m/s and Initial pitch of 10 degrees, we simulated several cases by varying Flapping frequency from 0 to 12 Hz in steps of 2 and tail elevation angle from -20 degrees to 70 degrees in steps of 10 degrees. The safe cases are those where model either glided or climbed up. These cases are surrounded by unsafe cases (showed in red color), where the model flips upside-down or crashes or oscillates with dangerously high amplitude. Details of one of these cases are shown at the end of this chapter.

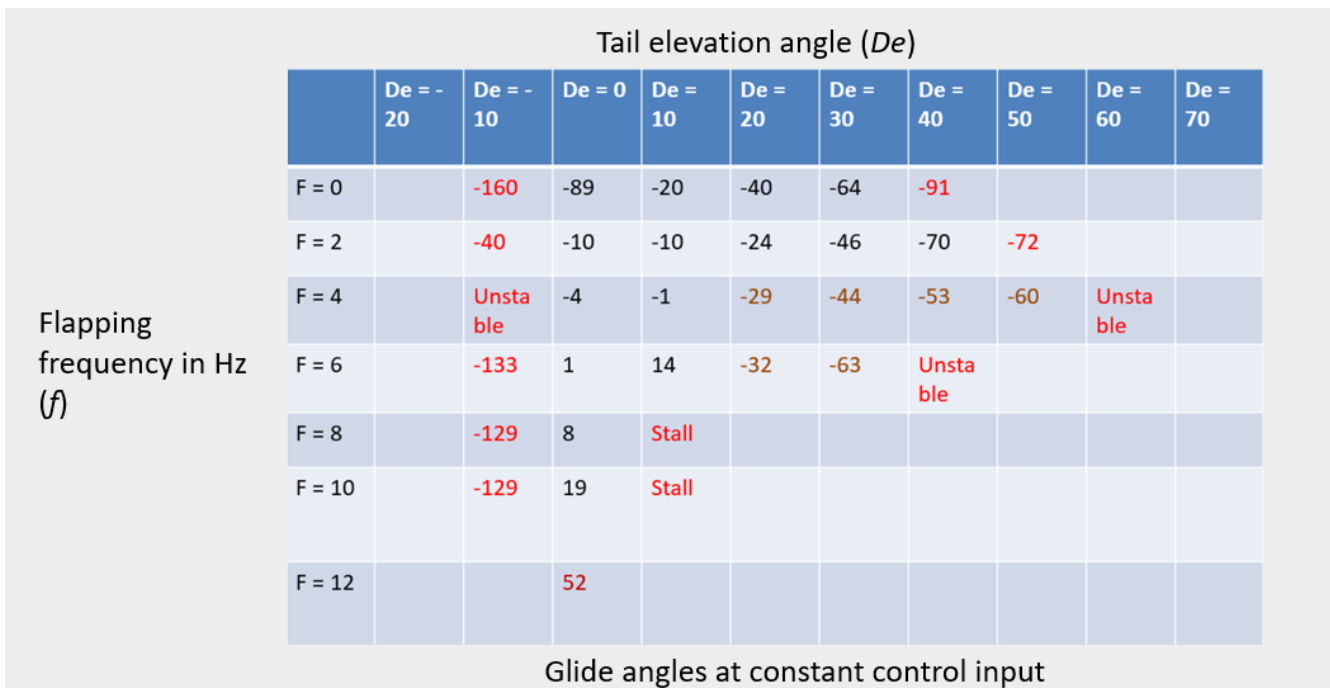


Figure 7.13: Gliding angles and different control parameters

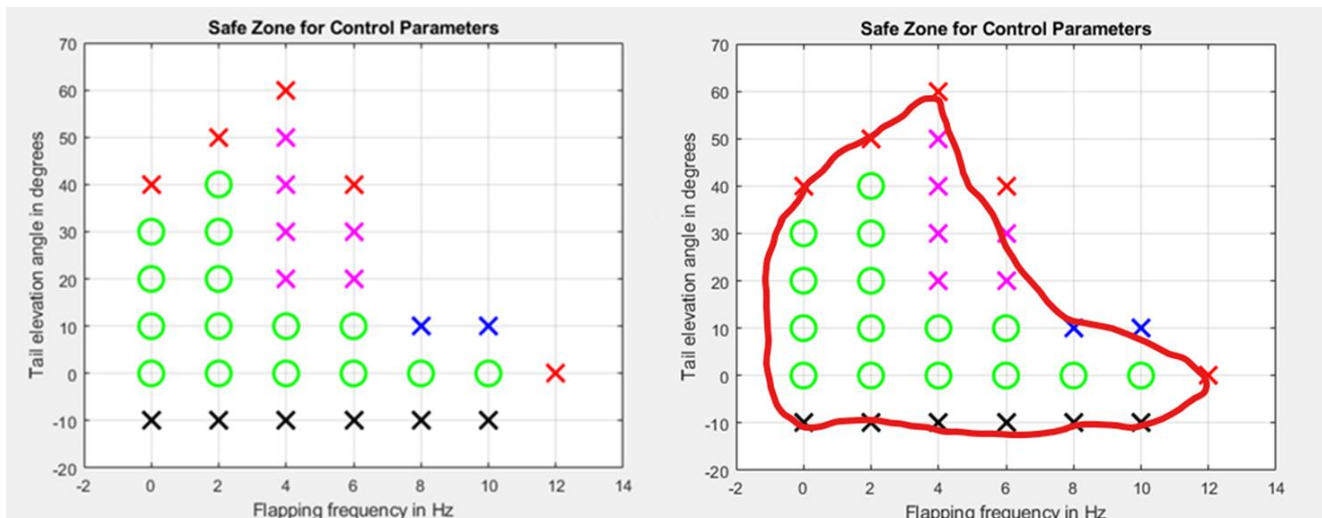


Figure 7.14: Safe zone charts

The green circles in figure 7.14, are safe conditions whereas the crosses represent unsafe conditions. The crosses are also color-coded indicating the reason of failure.

- Pink Cross = High amplitude oscillations in pitch
- Black Cross = Flipping
- Red Cross = Uncontrolled Crash

Although above safe zone chart was specific for our model, we hypothesize that the shape of the safe zone chart and relative positions of failure modes should remain same for all large scale ornithopters. This is an important insight in ornithopter research.

### 7.4.2 Example Simulations:

Simulation Results of one of the above cases is presented here in detailed manner. Initial velocity is 9 m/s with initial pitch angle 10 degree. Flapping frequency is  $f = 4$ , tail-elevation angle = 10 and tail-roll angle = 0 degrees.

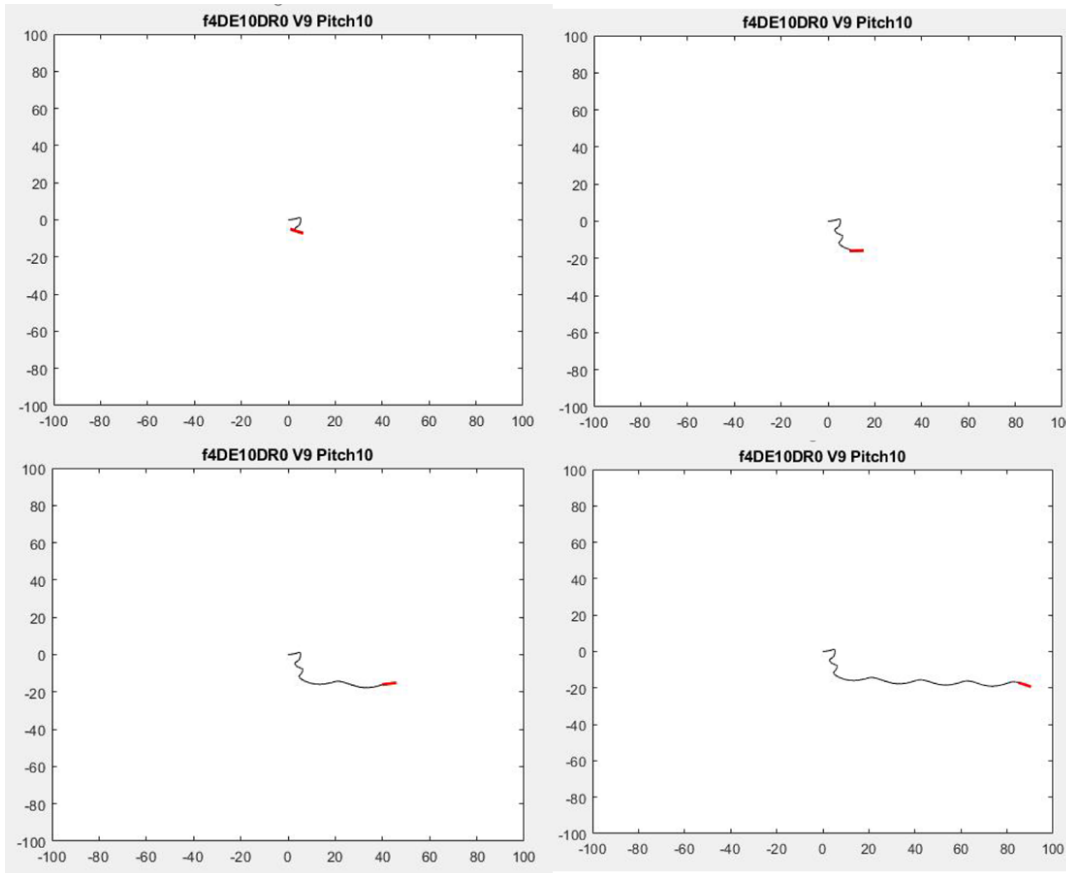


Figure 7.15: Snippets of video simulation

Figure 7.15 is combination of four screenshots taken from simulation video. The red line basically represents fuselage, the vertical axis represents height and the other one represents horizon. The inclination of the red line is instantaneous pitch of the model. We can see in above example, the model initially floats like a paper because of the exponential mask explained previously. Then it slowly picks up the pace and flies horizontally. Notice the small oscillations in trajectory. These oscillations are not because of the upstroke and downstroke wing motion. These types of oscillations we usually see with paper planes.



## Chapter 8

### Results & Discussions

This study was a cumulative work in three different domains, namely, flapping mechanisms, mechanical design of ornithopter and aerodynamic modelling. The results obtained from each of the sections have been listed with the conclusions.

In Chapter 3, I have analysed three flapping mechanisms based on their range of motion, loading, design compatibility and ease of manufacturing. For such analysis, I made few makeshift prototypes, solved some optimisation problems and designed the mechanisms in Linkage software. The observations are again presented here.

Different Aspects	Flapping Mechanisms		
	Single Crank	Dual Shaft	Dual Crank
Flapping Symmetry	Almost Symmetric	Exact Symmetric	Exact Symmetric with provision of folding motion
Bilateral Symmetry	Yes	*No	Yes
Weight	Lightweight	Heavy	Heavy
Complexity and ease of manufacturing	Simple	Complex	Complex
Loading	Locks up on low RPM	Locks up on low RPM	Do not lock

Table 8.1: Summary of results of chapter 3

In Chapter 4, I have determined preliminary parameters using empirical relations and reference data. I designed the gearbox completely from scratch. The designs of wings and tail mechanism were finalised and at the end we estimated the overall weight of the ornithopter. It was projected to be at most 460 gm. After complete design, the weight is 380 gm.

In Chapter 5, the complete assembling process is described and details of CAD models were given. The material selection procedure and logic behind the finalised materials is discussed.

In chapter 6, I have discussed the electronics systems needed and the reasoning behind the selection of the components. Two types of systems were designed. The manual system was

implemented in the model and used during testing phase. The automatic system was designed as a provision for implementing the control system in future.

In chapter 7, the details of mathematical model of flapping flight are explained and the implemented Simulink model is described in depth. The safe zone chart is constructed for our model by simulating a physical scenario. Based on those observations an important hypothesis was made. Also, the cause of failure in the unsafe zone and their relative position in the chart is given.

Using the theoretical background presented in all these chapters, I have constructed a physical prototype of an ornithopter and I was able to obtain following results.

1. The prototype was able to perform flapping motion in required frequency range and it was able to handle load of different types of wings. The kinematics of the prototype are in agreement with theoretical model.
2. The tail mechanism was sturdy and fast. It was able to produce articulated three-dimensional motion like a real bird.
3. In assisted flight test, where the model was hanged from the ceiling with threads, it was oscillating up and down. Which means the wings were able to produce lift and drag.
4. After testing it multiple times, we needed to repair the model. The model used temporary stoppers for shafts to hold them in their positions. Unfortunately, while replacing those stoppers we damaged the gearbox permanently. Due to limited time, we were unable to construct a second gearbox and continue testing.

## Chapter 9

# Conclusion & Scope for Further Investigations

This project was attempted with an objective designing an ornithopter which can be used for research in control systems and aerodynamics of birds.

From an undergraduate student's point of view, this project helped to acquire knowledge regarding design and manufacturing procedure, steps involved in the research methodology and aerodynamics involved with flapping flight. The project involved intensive use of software like MATLAB, Solidworks and Linkage. While optimising the parameters of flapping mechanism Python was used.

### 9.1 Future Scope

There are several major areas with a huge potential of future investigation, found during this project.

#### 9.1.1 More accurate mechanisms for biomimicry

Four major types of wing motions were identified from literature but only two of them were implemented. We need to develop more complex mechanisms to perfectly mimic the flight of bird.

#### 9.1.2 Refining Aerodynamic Model

Some aerodynamic effects were ignored for the sake of simplicity in presented simulation model. Also, approximations like point mass model made the programming easier. The model can be improved by making more generalized assumptions and including all known aerodynamic effects related to flapping flight like leading edge suction, vortex wake effects, etc.

#### 9.1.3 Experimental test bed setup

Some experimentation is necessary to determine the aerodynamic coefficients of flapping flight. Various data driven approaches can be used to model the flapping flight. Recent development in artificial intelligence, image processing can facilitate the ornithopter research is coupled with experimental setup. Also, the experimental data will increase our understanding of various aerodynamic effects.

### 9.1.4 Control System

Birds are extremely agile and have excellent manoeuvrability. To achieve that level of control, research in the field of control systems and dynamics is utmost needed.

## 9.2 Applications

### ➤ *Military:*

Can be used in military for surveillance and reconnaissance, as it can camouflage itself as a bird. Low altitude surveillance is possible without any problem of detection.

### ➤ *Bionic Research:*

Research and development in bionic robotic industry in an attempt to recreate nature identical robot, for more efficient and innovative way of flying.

### ➤ *Weather Forecast:*

Can be fitted with weather measuring instruments like temperature sensors, pressure sensors, Humidity sensors, etc. and can get low altitude weather information within seconds, which can be broadcasted locally.

### ➤ *Air Traffic Control:*

Flocks of birds are a hazard at airports, sometimes causing planes to crash. We can build a radio-controlled ornithopter that looks like a peregrine falcon. We can use it to chase away flocks of geese or seagulls that may appear on the runway. This method is far more eco-friendly than the current method in which High frequency ultra sound waves are used to scare away birds, which might damage the inner ear of the bird.

### ➤ *Wild Life Surveillance:*

It can be used to monitor wildlife without disturbing or spooking them. It can be used for get head count of endangered species, For example 'Tiger Census' in India. It can be also used to prevent poaching and smuggling of wild animals.

## 9.3 Conclusion

This project was an attempt to contribute to ornithopter research community. The field has made its mark, evident from ongoing research. The beauty and utility of this study lies in the fact that there is always a scope for further improvement and refinement. The ultimate goal is to develop a machine which can really compete with birds and insects, and surpass them if possible.

## References

- [1] S. Wei, L. Yongsheng, T. Jian, V. Dragos, and L. Hao, *Aerodynamics of Low Reynolds Number Flyers*. Cambridge University Press, 2008.
- [2] “Festo SmartBird.” [https://www.festo.com/net/SupportPortal/Files/46270/Brosch\\_SmartBird\\_en\\_8s\\_RZ\\_110311\\_lo.pdf](https://www.festo.com/net/SupportPortal/Files/46270/Brosch_SmartBird_en_8s_RZ_110311_lo.pdf)
- [3] “Aeriumanalytics.” <https://www.aeriumanalytics.com/>
- [4] FESTO, “Bionic Learning Network,” Festo Corporate, 2017. <https://www.festo.com/group/en/cms/10156.htm>
- [5] “Caltech Bat robot B2.” <https://www.caltech.edu/about/news/engineers-build-robot-drone-mimics-bat-flight-53794>
- [6] “Ro-bat.” <https://www.youtube.com/watch?v=R1iYXXaKvDE>
- [7] D. Harijono and R. Alif S. S., “An Assessment of a Linear Aerodynamic Modeling of a Generic Flapping Wing Ornithopter,” *Int. J. Astronaut. Aeronaut. Eng.*, vol. 3, no. 2, 2018, [doi: 10.35840/2631-5009/7517](https://doi.org/10.35840/2631-5009/7517).
- [8] T. Liu, K. Kuykendoll, R. Rhew, and S. Jones, “Avian wing geometry and kinematics,” *AIAA J.*, vol. 44, no. 5, pp. 954–963, 2006, [doi: 10.2514/1.16224](https://doi.org/10.2514/1.16224).
- [9] B. Parslew, “Predicting power-optimal kinematics of avian wings,” *J. R. Soc. Interface*, vol. 12, no. 102, 2015, [doi: 10.1098/rsif.2014.0953](https://doi.org/10.1098/rsif.2014.0953).
- [10] M. N. Rongfa, T. Pantuphag, and S. Srigrarom, “Analysis of kinematics of flapping wing UAV using OptiTrack systems,” *Aerospace*, vol. 3, no. 3, 2016, [doi: 10.3390/aerospace3030023](https://doi.org/10.3390/aerospace3030023).
- [11] M. Hassanalian and A. Abdelkefi, “Towards improved hybrid actuation mechanisms for flapping wing micro air vehicles: Analytical and experimental investigations,” *Drones*, vol. 3, no. 3, pp. 1–21, Sep. 2019, [doi: 10.3390/drones3030073](https://doi.org/10.3390/drones3030073).
- [12] L. Liu, Z. Fang, and Z. He, “Optimization design of flapping mechanism and wings for flapping-wing MAVs,” *Lect. Notes Comput. Sci. (including Subser. Lect. Notes Artif. Intell.*

- Lect. Notes Bioinformatics), vol. 5314 LNAI, no. PART 1, pp. 245–255, 2008, [doi: 10.1007/978-3-540-88513-9\\_27](https://doi.org/10.1007/978-3-540-88513-9_27).
- [13] Y. Zhang, X. Wang, G. Zhang, and J. Yang, “Design and analysis of single-degree-of-freedom flapping wing mechanism based on UG,” J. Phys. Conf. Ser., vol. 1629, no. 1, 2020, [doi: 10.1088/1742-6596/1629/1/012060](https://doi.org/10.1088/1742-6596/1629/1/012060).
- [14] Y. Nan, B. Peng, Y. Chen, Z. Feng, and D. McGlinchey, “Comparison study on flapping mechanisms of flapping wing micro air vehicle characterized on hovering flight,” ACM Int. Conf. Proceeding Ser., pp. 1–6, 2019, [doi: 10.1145/3325693.3325696](https://doi.org/10.1145/3325693.3325696).
- [15] B. Ji et al., “Design and experiment of a bionic flapping wing mechanism with flapping-twist-swing motion based on a single rotation,” AIP Adv., vol. 10, no. 6, 2020, [doi: 10.1063/5.0008792](https://doi.org/10.1063/5.0008792).
- [16] S. W. Ryu, J. G. Lee, and H. J. Kim, “Design, Fabrication, and Analysis of Flapping and Folding Wing Mechanism for a Robotic Bird,” J. Bionic Eng., vol. 17, no. 2, pp. 229–240, 2020, [doi: 10.1007/s42235-020-0018-3](https://doi.org/10.1007/s42235-020-0018-3).
- [17] H. Jiang, C. Zhou, and P. Xie, “Design and kinematic analysis of seagull inspired flapping wing robot,” 2016 IEEE Int. Conf. Inf. Autom. IEEE ICIA 2016, no. August, pp. 1382–1386, 2017, [doi: 10.1109/ICInfA.2016.7832035](https://doi.org/10.1109/ICInfA.2016.7832035).
- [18] M. Huang, “Optimization of flapping wing mechanism of bionic eagle,” Proc. Inst. Mech. Eng. Part G J. Aerosp. Eng., vol. 233, no. 9, pp. 3260–3272, 2019, [doi: 10.1177/0954410018794339](https://doi.org/10.1177/0954410018794339).
- [19] Z. Jackowski, “Design and construction of an autonomous ornithopter,” Thesis, 2009, [Online]. Available: [http://groups.csail.mit.edu/robotics-center/public\\_papers/Jackowski09.pdf](http://groups.csail.mit.edu/robotics-center/public_papers/Jackowski09.pdf)
- [20] Kinkade, “United States Patent Application Pub. No.: US 2002/0095146 A1,” vol. 1, no. 19, 2002.
- [21] “PigeonBot.” <https://spectrum.ieee.org/pigeonbot-uses-real-feathers-to-explore-how-birds-fly>.

- [22]J. D. DeLaurier, “An aerodynamic model for flapping-wing flight,” *Aeronaut. J.*, vol. 97, no. April 1993, pp. 125–130, 1993, [Online]. Available: <http://www.ornithopter.net/Publications/AnAerodynamicModelForFlapping-WingFlight.pdf>
- [23]S. P. Sane, “Review The aerodynamics of insect flight,” pp. 4191–4208, 2003, [doi: 10.1242/jeb.00663](https://doi.org/10.1242/jeb.00663).
- [24]Z. Yan, “Modeling and control of a flapping wing micro air vehicle at hover condition,” no. July, 2016, [Online]. Available: <http://hdl.handle.net/10057/12879>
- [25]Z. J. Wang, “Dissecting Insect light,” pp. 183–210, 2005, [doi: 10.1146/annurev.fluid.36.050802.121940](https://doi.org/10.1146/annurev.fluid.36.050802.121940).
- [26]Q. F. W. Micro-air-vehicle, H. Djojodihardjo, A. S. S. Ramli, S. Wiriadidjaja, A. Shakrine, and M. Rafie, “Kinematic and Aerodynamic Modelling of Bi- and,” pp. 83–101, 2016, [doi: 10.4236/aast.2016.13008](https://doi.org/10.4236/aast.2016.13008).
- [27]M. Khosravi and A. B. Novinzadeh, “A multi-body control approach for flapping wing micro aerial vehicles,” *Aerosp. Sci. Technol.*, vol. 112, p. 106525, 2021, [doi: 10.1016/j.ast.2021.106525](https://doi.org/10.1016/j.ast.2021.106525).
- [28]T. Reichert, “Kinematic Optimization in Birds, Bats and Ornithopters,” p. 396, 2011, [Online]. Available: <http://books.google.com/books?id=FmKkMwEACAAJ>
- [29]M. A. Malik and F. Ahmad, “[Effect of different design parameters on lift, thrust and drag of an ornithopter](#),” *WCE 2010 - World Congr. Eng. 2010*, vol. 2, pp. 1460–1465, 2010.
- [30]A. Mechanics, “Energy-minimizing kinematics in hovering insect flight,” vol. 582, pp. 153–168, 2007, [doi: 10.1017/S0022112007006209](https://doi.org/10.1017/S0022112007006209).
- [31]G. Ritchison, “Ornithology Lecture Notes 2 - Bird Flight I,” Department of Biological Sciences Eastern Kentucky University, 2003. <http://people.eku.edu/ritchisong/554notes2.html>
- [32]N. K. Sinha and N. Ananthkrishnan, “[Advanced Flight Dynamics with Elements of Flight Control](#)”.

